Playing with Marbles: Structural and Thermodynamic Properties of Hard-Sphere Systems

Andrés Santos

Abstract These lecture notes present an overview of equilibrium statistical mechanics of classical fluids, with special applications to the structural and thermodynamic properties of systems made of particles interacting via the hard-sphere potential or closely related model potentials. The exact statistical-mechanical properties of one-dimensional systems, the issue of thermodynamic (in)consistency among different routes in the context of several approximate theories, and the construction of analytical or semi-analytical approximations for the structural properties are also addressed.

1 Introduction

Hard-sphere systems represent a favorite playground in statistical mechanics, both in and out of equilibrium, as they represent the simplest models of many-body systems of interacting particles [1].

Apart from their academic or pedagogical values, hard-sphere models are also important from a more practical point of view. In real fluids, especially at high temperatures and moderate and high densities, the structural and thermodynamic properties are mainly governed by the repulsive forces among molecules and in this context hard-core fluids are very useful as reference systems [2, 3].

Moreover, the use of the hard-sphere model in the realm of soft condensed matter has become increasingly popular [4]. For instance, the effective interaction among (sterically stabilized) colloidal particles can be tuned to match almost perfectly the hard-sphere model [5].

As a very imperfect measure of the impact of the hard-sphere model on current research, Fig. 1.1 shows the number of papers per year published in the ten-year

Andrés Santos

Departamento de Física, Universidad de Extremadura, Badajoz, E-06071, Spain
e-mail: `andres@unex.es`

Fig. 1.1 Number of papers per year published in the ten-year period 2003–2012 that include the terms "hard" and "sphere" as a topic (hollow columns) or in the title (colored columns).
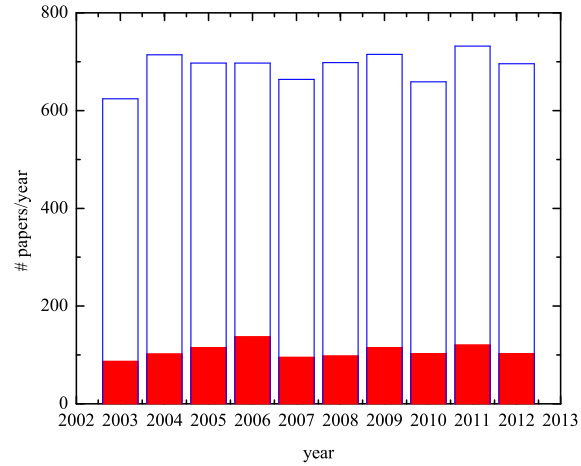
period 2003–2012 (according to Thomson Reuters' Web of Knowledge) that include the words "hard" *and* "sphere" as a topic (that is, in the title, in the abstract, or as a keyword). It can be observed that the number is rather stabilized, fluctuating around 700 papers/year. If one constrains the search criterion to papers including "hard" and "sphere" in the title, about 100 papers/year are found.

Despite the title of this work and the preceding paragraphs, the main aim of these lecture notes is neither restricted to hard-sphere fluids nor focused on the "state of the art" of the field. Instead, the notes attempt to present an introduction to the equilibrium statistical mechanics of liquids and non-ideal gases at a graduate-student textbook level, with emphasis on the basics and fundamentals of the topic. The treatment uses classical (i.e., non-quantum) mechanics and no special prerequisites are required, apart from standard statistical-mechanical ensembles. Most of the content applies to any (short-range) interaction potential, any dimensionality, and (in general) any number of components. On the other hand, some specific applications deal with the properties of fluids made of particles interacting via the hard-sphere potential or related potentials. The approach is unavoidably biased toward those aspects the author is more familiarized with. Thus, important topics such as inhomogeneous fluids and density functional theory [6, 7, 8, 9, 10, 11], metastable glassy states [12, 13, 14], and perturbation theories [2, 3] are not represented in these notes.

Apart from a brief concluding remark, the remainder of these lecture notes is split into the following sections:

- 2. A Brief Survey of Thermodynamic Potentials
- 3. A Brief Survey of Equilibrium Statistical Ensembles
- 4. Reduced Distribution Functions
- 5. Thermodynamics from the Radial Distribution Function

The core of the notes is made of Sects. 4, 5, 7, and 8. They start with the definition of the reduced distribution functions and, in particular, of the radial distribution function $g(r)$ (Sect. 4), and continues with the derivation of the main thermodynamic quantities in terms of $g(r)$ (Sect. 5). This includes the chemical-potential route, usually forgotten in textbooks. Sections 7 and 8 are more technical. They have to do with the expansion in powers of density of $g(r)$ and the pressure, the definition of the direct correlation function $c(r)$, and the construction of approximate equations of state and integral-equation theories. Both sections make extensive use of diagrams but several needed theorems and lemmas are justified by simple examples without formal proofs.

In addition to the four core sections mentioned above, there are five more sections that can be seen as optional. Sections 2 and 3 are included to make the notes as self-contained as possible and to unify the notation, but otherwise can be skipped by the knowledgeable reader. Sections 6, 9, and 10 are "side dishes." Whereas one-dimensional systems can be seen as rather artificial, it is undoubtedly important from pedagogical and illustrative perspectives to derive their exact structural and thermophysical quantities, and this is the purpose of Sect. 6. Section 9 presents three examples related to the problem of thermodynamic consistency among different routes when an approximate $g(r)$ is employed. Finally, Sect. 10 derives the exact solution of the Percus–Yevick integral equation for hard spheres as the simplest implementation of a more general class of approximations.

2 A Brief Survey of Thermodynamic Potentials

Just to fix the notation, this section provides a summary of some of the most important thermodynamic relations.

2.1 Isolated Systems. Entropy

In a reversible process, the first and second laws of thermodynamics in a fluid mixture can be combined as [15, 16]

$$\boxed{T\mathrm{d}S = \mathrm{d}E + p\mathrm{d}V - \sum_\nu \mu_\nu \mathrm{d}N_\nu}\,, \tag{2.1}$$

where S is the entropy, E is the internal energy, V is the volume of the fluid, and N_ν is the number of particles of species ν. All these quantities are *extensive*, i.e., they scale with the size of the system. The coefficients of the differentials in (2.1) are the conjugate *intensive* quantities: the absolute temperature (T), the pressure (p), and the chemical potentials (μ_ν).

Equation (2.1) shows that the *natural* variables of the entropy are E, V, and $\{N_\nu\}$, i.e., $S(E,V,\{N_\nu\})$. This implies that S is the right thermodynamic potential in *isolated* systems: at given E, V, and $\{N_\nu\}$, S is maximal in equilibrium. The respective partial derivatives give the intensive quantities:

$$\frac{1}{T} = \left(\frac{\partial S}{\partial E}\right)_{V,\{N_\nu\}}, \quad \frac{p}{T} = \left(\frac{\partial S}{\partial V}\right)_{E,\{N_\nu\}}, \quad \frac{\mu_\nu}{T} = -\left(\frac{\partial S}{\partial N_\nu}\right)_{E,V,\{N_{\gamma\neq\nu}\}}. \tag{2.2}$$

The extensive nature of S, E, V, and $\{N_\nu\}$ implies the extensivity condition $S(\lambda E, \lambda V, \{\lambda N_\nu\}) = \lambda S(E,V,\{N_\nu\})$. Application of Euler's homogeneous function theorem yields

$$S(E,V,\{N_\nu\}) = E\left(\frac{\partial S}{\partial E}\right)_{V,\{N_\nu\}} + V\left(\frac{\partial S}{\partial V}\right)_{E,\{N_\nu\}} + \sum_\nu N_\nu\left(\frac{\partial S}{\partial N_\nu}\right)_{E,V,\{N_{\gamma\neq\nu}\}}. \tag{2.3}$$

Using (2.2), we obtain the identity

$$\boxed{TS = E + pV - \sum_\nu \mu_\nu N_\nu}\,. \tag{2.4}$$

This is the so-called *fundamental equation of thermodynamics*. Differentiating (2.4) and subtracting (2.1) one arrives at the Gibbs–Duhem relation

$$S\mathrm{d}T - V\mathrm{d}p + \sum_\nu N_\nu \mathrm{d}\mu_\nu = 0\,. \tag{2.5}$$

Equation (2.1) also shows that S, V, and $\{N_\nu\}$, are the natural variables of the internal energy $E(S,V,\{N_\nu\})$, so that

$$T = \left(\frac{\partial E}{\partial S}\right)_{V,\{N_\nu\}}, \quad p = -\left(\frac{\partial E}{\partial V}\right)_{S,\{N_\nu\}}, \quad \mu_\nu = \left(\frac{\partial E}{\partial N_\nu}\right)_{S,V,\{N_{\gamma\neq\nu}\}}. \tag{2.6}$$

2.2 Closed Systems. Helmholtz Free Energy

From a practical point of view, it is usually more convenient to choose the temperature instead of the internal energy or the entropy as a control variable. In that case,

the adequate thermodynamic potential is no longer either the entropy or the internal energy, respectively, but the Helmholtz free energy F. It is defined from S or E through the Legendre transformation

$$F(T,V,\{N_v\}) = E - TS = -pV + \sum_v \mu_v N_v \, , \qquad (2.7)$$

where in the last step use has been made of (2.4). From (2.1) we obtain

$$\mathrm{d}F = -S\mathrm{d}T - p\mathrm{d}V + \sum_v \mu_v \mathrm{d}N_v \, , \qquad (2.8)$$

so that

$$S = -\left(\frac{\partial F}{\partial T}\right)_{V,\{N_v\}} \, , \quad p = -\left(\frac{\partial F}{\partial V}\right)_{T,\{N_v\}} \, , \quad \mu_v = \left(\frac{\partial F}{\partial N_v}\right)_{T,V,\{N_{\gamma \neq v}\}} \, . \quad (2.9)$$

The Helmholtz free energy is the adequate thermodynamic potential in a closed system, that is, a system that cannot exchange mass with the environment but can exchange energy. At fixed T, V, and $\{N_v\}$, F is minimal in equilibrium.

2.3 Isothermal-Isobaric Systems. Gibbs Free Energy

If, instead of the volume, the independent thermodynamic variable is pressure, we need to perform a Legendre transformation from F to define the Gibbs free energy (or free enthalpy) as

$$G(T,p,\{N_v\}) = F + pV = \sum_v \mu_v N_v \, . \qquad (2.10)$$

The second equality shows that the chemical potential μ_v can be interpreted as the contribution of each particle of species v to the total Gibbs free energy. The differential relations now become

$$\mathrm{d}G = -S\mathrm{d}T + V\mathrm{d}p + \sum_v \mu_v \mathrm{d}N_v \, , \qquad (2.11)$$

$$S = -\left(\frac{\partial G}{\partial T}\right)_{p,\{N_v\}} \, , \quad V = \left(\frac{\partial G}{\partial p}\right)_{T,\{N_v\}} \, , \quad \mu_v = \left(\frac{\partial G}{\partial N_v}\right)_{T,p,\{N_{\gamma \neq v}\}} \, . \quad (2.12)$$

Needless to say, G is minimal in equilibrium if one fixes T, p, and $\{N_v\}$.

2.4 Open Systems. Grand Potential

In an open system, not only energy but also particles can be exchanged with the environment. In that case, we need to replace $\{N_v\}$ by $\{\mu_v\}$ as independent variables and define the grand potential Ω from F via a new Legendre transformation:

$$\Omega(T,V,\{\mu_v\}) = F - \sum_v \mu_v N_v = -pV. \tag{2.13}$$

Interestingly, the second equality shows that $-\Omega/V$ is not but the pressure, except that it must be seen as a function of temperature and the chemical potentials. Now we have

$$d\Omega = -SdT - pdV - \sum_v N_v d\mu_v . \tag{2.14}$$

$$S = -\left(\frac{\partial \Omega}{\partial T}\right)_{V,\{\mu_v\}} , \quad p = -\left(\frac{\partial \Omega}{\partial V}\right)_{T,\{\mu_v\}} = -\frac{\Omega}{V} , \quad N_v = -\left(\frac{\partial \Omega}{\partial \mu_v}\right)_{T,p,\{\mu_{\gamma \neq v}\}} . \tag{2.15}$$

2.5 Response Functions

We have seen that the thermodynamic variables $E \leftrightarrow T$ (or $S \leftrightarrow T$), $V \leftrightarrow p$, and $N_v \leftrightarrow \mu_v$ appear as extensive $\leftrightarrow$ intensive conjugate pairs. Depending on the thermodynamic potential of interest, one of the members of the pair acts as independent variable and the other one is obtained by differentiation. If an additional derivative is taken one obtains the so-called *response* functions. For example, the heat capacities at constant volume and at constant pressure are defined as

$$C_V = \left(\frac{\partial E}{\partial T}\right)_{V,\{N_v\}} = T\left(\frac{\partial S}{\partial T}\right)_{V,\{N_v\}} = -T\left(\frac{\partial^2 F}{\partial T^2}\right)_{V,\{N_v\}} , \tag{2.16}$$

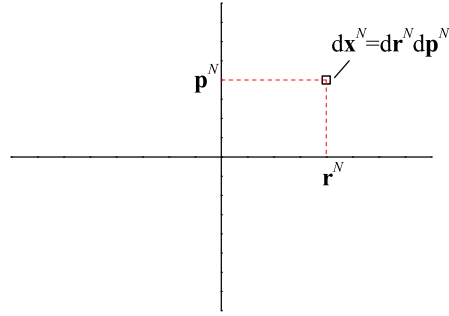$$C_p = T\left(\frac{\partial S}{\partial T}\right)_{p,\{N_v\}} = -T\left(\frac{\partial^2 G}{\partial T^2}\right)_{p,\{N_v\}} . \tag{2.17}$$

Analogously, it is convenient to define the isothermal compressibility

$$\kappa_T = -\frac{1}{V}\left(\frac{\partial V}{\partial p}\right)_{T,\{N_v\}} = -\frac{1}{V}\left(\frac{\partial^2 G}{\partial p^2}\right)_{T,\{N_v\}}$$

$$= -\left[V\left(\frac{\partial p}{\partial V}\right)_{T,\{N_v\}}\right]^{-1} = \left[V\left(\frac{\partial^2 F}{\partial V^2}\right)_{T,\{N_v\}}\right]^{-1} , \tag{2.18}$$

and the thermal expansivity

$$\alpha_p = \frac{1}{V}\left(\frac{\partial V}{\partial T}\right)_{p,\{N_v\}} = \frac{1}{V}\left(\frac{\partial^2 G}{\partial T \partial p}\right)_{\{N_v\}} = -\frac{1}{V}\left(\frac{\partial S}{\partial p}\right)_{T,\{N_v\}}. \tag{2.19}$$

The equivalence between the second and fourth terms in (2.19) is an example of a Maxwell relation.

3 A Brief Survey of Equilibrium Statistical Ensembles

In this section a summary of the main equilibrium ensembles is presented, essentially to fix part of the notation that will be needed later on. For simplicity, we will restrict this section to one-component systems, although the extension to mixtures is straightforward.

Let us consider a *classical* system made of *N identical* point particles in d dimensions. In classical mechanics, the dynamical state of the system is characterized by the N vector positions $\{\mathbf{r}_1, \mathbf{r}_2, \ldots, \mathbf{r}_N\}$ and the N vector momenta $\{\mathbf{p}_1, \mathbf{p}_2, \ldots, \mathbf{p}_N\}$. In what follows, we will employ the following short-hand notation

- $\mathbf{r}^N = \{\mathbf{r}_1, \mathbf{r}_2, \ldots, \mathbf{r}_N\}$, $\mathbf{dr}^N = \mathbf{dr}_1 \mathbf{dr}_2 \cdots \mathbf{dr}_N$,
- $\mathbf{p}^N = \{\mathbf{p}_1, \mathbf{p}_2, \ldots, \mathbf{p}_N\}$, $\mathbf{dp}^N = \mathbf{dp}_1 \mathbf{dp}_2 \cdots \mathbf{dp}_N$,
- $\mathbf{x}^N = \{\mathbf{r}^N, \mathbf{p}^N\}$, $\mathbf{dx}^N = \mathbf{dr}^N \mathbf{dp}^N$.

Thus, the whole *microscopic* state of the system (*microstate*) is represented by a single point $\mathbf{x}^N$ in the $(2d \times N)$-dimensional *phase space* (see Fig. 3.1). The time evolution of the microstate $\mathbf{x}^N$ is governed by the Hamiltonian of the system $H_N(\mathbf{x}^N)$ through the classical Hamilton's equations [17].

Given the practical impossibility of describing the system at a microscopic level, a statistical description is needed. Thus, we define the phase-space probability distribution function $\rho_N(\mathbf{x}^N)$ such that $\rho_N(\mathbf{x}^N)\mathbf{dx}^N$ is the probability that the microstate

of the system lies inside an infinitesimal (hyper)volume $d\mathbf{x}^N$ around the phase-space point $\mathbf{x}^N$.

3.1 Gibbs Entropy

The concept of a phase-space probability distribution function is valid both out of equilibrium (where, in general, it changes with time according to the Liouville theorem [18, 19]) and in equilibrium (where it is stationary). In the latter case $\rho_N(\mathbf{x}^N)$ can be obtained for isolated, closed, open, ... systems by following logical steps and starting from the *equal a priori probability postulate* for isolated systems. Here we follow an alternative (but equivalent) method based on information-theory arguments [19, 20, 21].

Let us define the Gibbs entropy *functional*

$$\boxed{S[\rho_N] = -k_B \int d\mathbf{x}^N \rho_N(\mathbf{x}^N) \ln\left[C_N \rho_N(\mathbf{x}^N)\right]} \, , \tag{3.1}$$

where k_B is the Boltzmann constant and

$$C_N \equiv N! h^{dN} \, . \tag{3.2}$$

In (3.2) the coefficient h^{dN} is introduced to comply with Heisenberg's uncertainty principle and preserve the non-dimensional character of the argument of the logarithm, while the factorial $N!$ accounts for the fact that two apparently different microstates which only differ on the particle labels are physically the same microstate (thus avoiding Gibbs's paradox).

Equation (3.1) applies to systems with a fixed number of particles N. On the other hand, if the system is allowed to exchange particles with the environment, microstates with different N exist, so that one needs to define a a phase-space density $\rho_N(\mathbf{x}^N)$ for each $N \geq 0$. In that case, the entropy functional becomes

$$S[\{\rho_N\}] = -k_B \sum_{N=0}^{\infty} \int d\mathbf{x}^N \rho_N(\mathbf{x}^N) \ln\left[C_N \rho_N(\mathbf{x}^N)\right] \, . \tag{3.3}$$

Now, the basic postulate consists of asserting that, out of all possible phase-space probability distribution functions ρ_N consistent with given *constraints* (which define the *ensemble* of accessible microstates), the *equilibrium* function ρ_N^{eq} is the one that *maximizes* the entropy functional $S[\rho_N]$. Once ρ_N^{eq} is known, connection with thermodynamics is made through the identification of $S^{\text{eq}} = S[\rho_N^{\text{eq}}]$ as the equilibrium entropy.

3.2 Microcanonical Ensemble (Isolated System)

The microcanical ensemble describes an isolated system and thus it is characterized by fixed values of V, N, E (the latter with a tolerance ΔE, in accordance with the uncertainty principle). Therefore, the basic constraint is the normalization condition

$$\int_{E \leq H_N(\mathbf{x}^N) \leq E + \Delta E} d\mathbf{x}^N \rho_N(\mathbf{x}^N) = 1 . \tag{3.4}$$

Maximization of the entropy functional just says that $\rho_N(\mathbf{x}^N) = \text{const}$ for all the accessible microstates $E \leq H_N(\mathbf{x}^N) \leq E + \Delta E$. Thus,

$$\rho_N(\mathbf{x}^N) = \begin{cases} \frac{1}{\omega_{\Delta E}(E,N,V)} , & E \leq H_N(\mathbf{x}^N) \leq E + \Delta E , \\ 0 , & \text{otherwise} . \end{cases} \tag{3.5}$$

The normalization function

$$\omega_{\Delta E}(E,N,V) = \int_{E \leq H_N(\mathbf{x}^N) \leq E + \Delta E} d\mathbf{x}^N \tag{3.6}$$

is the phase-space volume comprised between the hyper-surfaces $H_N(\mathbf{x}^N) = E$ and $H_N(\mathbf{x}^N) = E + \Delta E$. By insertion of (3.5) into (3.1) one immediately sees that $\omega_{\Delta E}(E,N,V)$ is directly related to the equilibrium entropy as

$$S(E,N,V) = k_B \ln \frac{\omega_{\Delta E}(E,N,V)}{N! h^{dN}} . \tag{3.7}$$

In this expression the specific value of ΔE becomes irrelevant in the thermodynamic limit (as long as $\Delta E \ll E$).

3.3 Canonical Ensemble (Closed System)

Now the system can have *any* value of the total energy E. However, we are free to prescribe a given value of the *average* energy $\langle E \rangle$. Therefore, the constraints in the canonical ensemble are

$$\int d\mathbf{x}^N \rho_N(\mathbf{x}^N) = 1 , \quad \int d\mathbf{x}^N H_N(\mathbf{x}^N) \rho_N(\mathbf{x}^N) = \langle E \rangle . \tag{3.8}$$

The maximization of the entropy functional subject to the constraints (3.8) can be carried out through the Lagrange multiplier method with the result

$$\rho_N(\mathbf{x}^N) = \frac{e^{-\beta H_N(\mathbf{x}^N)}}{N! h^{dN} \mathscr{Z}_N(\beta,V)} , \tag{3.9}$$

where β is the Lagrange multiplier associated with $\langle E \rangle$ and the *partition function* $\mathscr{Z}_N$ is determined from the normalization condition as

$$\mathscr{Z}_N(\beta,V) = \frac{1}{N!h^{dN}} \int d\mathbf{x}^N e^{-\beta H_N(\mathbf{x}^N)} . \qquad (3.10)$$

Substitution of (3.9) into (3.1) and use of (3.8) yields

$$S = k_B \left(\ln \mathscr{Z}_N + \beta \langle E \rangle \right) . \qquad (3.11)$$

Comparison with (2.7) (where now the internal energy is represented by $\langle E \rangle$) allows one to identify

$$\beta = \frac{1}{k_B T} , \quad F(T,N,V) = -k_B T \ln \mathscr{Z}_N(\beta,V) . \qquad (3.12)$$

Therefore, in the canonical ensemble the connection with thermodynamics is conveniently established via the Helmholtz free energy rather than via the entropy.

As an average of a phase-space dynamical variable, the internal energy can be directly obtained from $\ln \mathscr{Z}_N$ as

$$\langle E \rangle = -\frac{\partial \ln \mathscr{Z}_N}{\partial \beta} . \qquad (3.13)$$

Moreover, we can obtain the energy fluctuations:

$$\langle E^2 \rangle - \langle E \rangle^2 = \frac{\partial^2 \ln \mathscr{Z}_N}{\partial \beta^2} = k_B T^2 C_V . \qquad (3.14)$$

In the last step, use has been made of (2.16).

3.4 Grand Canonical Ensemble (Open System)

In an open system neither the energy nor the number of particles is determined but we can choose to fix their average values. As a consequence, the constraints are

$$\sum_{N=0}^{\infty} \int d\mathbf{x}^N \rho_N(\mathbf{x}^N) = 1 , \quad \sum_{N=0}^{\infty} \int d\mathbf{x}^N H_N(\mathbf{x}^N)\rho_N(\mathbf{x}^N) = \langle E \rangle , \qquad (3.15)$$

$$\sum_{N=0}^{\infty} N \int d\mathbf{x}^N \rho_N(\mathbf{x}^N) = \langle N \rangle . \qquad (3.16)$$

The solution to the maximization problem is

$$\rho_N(\mathbf{x}^N) = \frac{e^{-\alpha N} e^{-\beta H_N(\mathbf{x}^N)}}{N!h^{dN} \Xi(\beta,\alpha,V)} , \qquad (3.17)$$

where α and β are Lagrange multipliers and the *grand partition function* is

$$\Xi(\beta,\alpha,V) = \sum_{N=0}^{\infty} \frac{e^{-\alpha N}}{N! h^{dN}} \int d\mathbf{x}^N e^{-\beta H_N(\mathbf{x}^N)} = \sum_{N=0}^{\infty} e^{-\alpha N} \mathscr{Z}_N(\beta,V) . \qquad (3.18)$$

In this case the equilibrium entropy becomes

$$S = k_B \left(\ln \Xi + \beta \langle E \rangle T + \alpha \langle N \rangle \right) . \qquad (3.19)$$

From comparison with the first equality of (2.13) we can identify

$$\beta = \frac{1}{k_B T} , \quad \alpha = -\beta \mu , \quad \Omega(T,\mu,V) = -k_B T \ln \Xi(\beta,\alpha,V) . \qquad (3.20)$$

The average and fluctuation relations are

$$\langle E \rangle = -\frac{\partial \ln \Xi}{\partial \beta} , \quad \langle E^2 \rangle - \langle E \rangle^2 = \frac{\partial^2 \ln \Xi}{\partial \beta^2} = k_B T^2 C_V , \qquad (3.21)$$

$$\langle N \rangle = -\frac{\partial \ln \Xi}{\partial \alpha} , \qquad (3.22)$$

$$\langle N^2 \rangle - \langle N \rangle^2 = \frac{\partial^2 \ln \Xi}{\partial \alpha^2} = k_B T \frac{\langle N \rangle^2}{V} \kappa_T . \qquad (3.23)$$

The second equality of (3.23) requires the use of thermodynamic relations and mathematical properties of partial derivatives.

3.5 Isothermal-Isobaric Ensemble

In this ensemble the volume is a fluctuating quantity and only its average value is fixed. Thus, similarly to the grand canonical ensemble, the constraints are

$$\int_0^{\infty} dV \int d\mathbf{x}^N \rho_N(\mathbf{x}^N) = 1 , \quad \int_0^{\infty} dV \int d\mathbf{x}^N H_N(\mathbf{x}^N) \rho_N(\mathbf{x}^N) = \langle E \rangle , \qquad (3.24)$$

$$\int_0^{\infty} dV\, V \int d\mathbf{x}^N \rho_N(\mathbf{x}^N) = \langle V \rangle . \qquad (3.25)$$

Not surprisingly, the solution is

$$\rho_N(\mathbf{x}^N) = \frac{e^{-\gamma V} e^{-\beta H_N(\mathbf{x}^N)}}{V_0 N! h^{dN} \Delta_N(\beta,\gamma)} , \qquad (3.26)$$

where V_0 is an arbitrary volume scale factor (needed to keep the correct dimensions), γ and β are again Lagrange multipliers, and the isothermal-isobaric partition function is

$$\Delta_N(\beta,\gamma) = \frac{1}{V_0 N! h^{dN}} \int_0^\infty dV\, e^{-\gamma V} \int d\mathbf{x}^N e^{-\beta H_N(\mathbf{x}^N)} = \frac{1}{V_0} \int_0^\infty dV\, e^{-\gamma V}\, \mathscr{Z}_N(\beta,V)\,.$$

$$(3.27)$$

As expected, the entropy becomes

$$S = k_B \left(\ln \Delta_N + \beta \langle E \rangle + \gamma \langle V \rangle \right)\,. \tag{3.28}$$

From comparison with (2.10) we conclude that

$$\beta = \frac{1}{k_B T}\,, \quad \gamma = \beta p\,, \quad G(T,p,N) = -k_B T \ln \Delta_N(\beta,\gamma)\,. \tag{3.29}$$

The main average and fluctuation relations are

$$\langle E \rangle = -\frac{\partial \ln \Delta_N}{\partial \beta}\,, \quad \langle E^2 \rangle - \langle E \rangle^2 = \frac{\partial^2 \ln \Delta_N}{\partial \beta^2} = k_B T^2 C_V\,, \tag{3.30}$$

$$\langle V \rangle = -\frac{\partial \ln \Delta_N}{\partial \gamma}\,, \tag{3.31}$$

$$\langle V^2 \rangle - \langle V \rangle^2 = \frac{\partial^2 \ln \Delta_N}{\partial \gamma^2} = k_B T \langle V \rangle \kappa_T\,. \tag{3.32}$$

Equations (3.23) and (3.32) are equivalent. Both show that the density fluctuations are proportional to the isothermal compressibility and decrease as the size of the system increases. In (3.23) the volume is constant, so that the density fluctuations are due to fluctuations in the number of particles, while the opposite happens in (3.32).

3.6 Ideal Gas

The exact evaluation of the normalization functions (3.6), (3.10), (3.18), and (3.27) is in general a formidable task due to the involved dependence of the Hamiltonian on the coordinates of the particles. However, in the case of non-interacting particles (ideal gas), the Hamiltonian depends only on the momenta:

$$H_N(\mathbf{x}^N) \to H_N^{\mathrm{id}}(\mathbf{p}^N) = \sum_{i=1}^N \frac{p_i^2}{2m}\,, \tag{3.33}$$

where m is the mass of a particle. In this case the N-body Hamiltonian is just the sum over all the particles of the one-body Hamiltonian $p_i^2/2m$ and the exact statistical-mechanical results can be easily obtained. The expressions for the normalization function, the thermodynamic potential, and the first derivatives of the latter for each one of the four ensembles considered above are the following ones:

- *Microcanonical ensemble*

$$\ln \omega_{\Delta E}^{\mathrm{id}}(E,N,V) = N\left\{\frac{d}{2} + \ln\left[V\left(\frac{4\pi mE}{dN}\right)^{d/2}\right]\right\}, \qquad (3.34)$$

$$S^{\mathrm{id}}(E,N,V) = Nk_B\left\{\frac{d+2}{2} + \ln\left[\frac{V}{N}\left(\frac{4\pi mE}{dNh^2}\right)^{d/2}\right]\right\}, \qquad (3.35)$$

$$k_BT^{\mathrm{id}} = \frac{2}{d}\frac{E}{N}, \quad p^{\mathrm{id}} = \frac{2}{d}\frac{E}{V}, \quad \mu^{\mathrm{id}} = -\frac{2}{d}\frac{E}{N}\ln\left[\frac{V}{N}\left(\frac{4\pi mE}{dNh^2}\right)^{d/2}\right], \quad (3.36)$$

- *Canonical ensemble*

$$\mathscr{Z}_N^{\mathrm{id}}(\beta,V) = \frac{[\zeta(\beta,V)]^N}{N!}, \quad \zeta(\beta,V) = \frac{V}{[\Lambda(\beta)]^d}, \quad \Lambda(\beta) \equiv \frac{h}{\sqrt{2\pi mk_BT}}, \qquad (3.37)$$

$$F^{\mathrm{id}}(T,N,V) = Nk_BT\left[\ln\frac{\Lambda^d(\beta)}{V/N} - 1\right], \qquad (3.38)$$

$$\langle E\rangle^{\mathrm{id}} = \frac{d}{2}Nk_BT, \quad p^{\mathrm{id}} = \frac{N}{V}k_BT, \quad \mu^{\mathrm{id}} = k_BT\ln\left[\frac{\Lambda^d(\beta)}{V/N}\right], \qquad (3.39)$$

- *Grand canonical ensemble*

$$\Xi^{\mathrm{id}}(\beta,\alpha,V) = \sum_{N=0}^{\infty} \mathrm{e}^{-\alpha N}\frac{[\zeta(\beta,V)]^N}{N!} = \mathrm{e}^{z\zeta}, \quad z \equiv \mathrm{e}^{-\alpha} = \mathrm{e}^{\beta\mu}, \qquad (3.40)$$

$$\Omega^{\mathrm{id}}(\beta,\alpha,V) = -p^{\mathrm{id}}V = -k_BT\mathrm{e}^{-\alpha}\zeta(\beta,V), \qquad (3.41)$$

$$\langle E\rangle^{\mathrm{id}} = \frac{d}{2}k_BT\mathrm{e}^{-\alpha}\zeta(\beta,V), \quad \langle N\rangle^{\mathrm{id}} = \mathrm{e}^{-\alpha}\zeta(\beta,V), \qquad (3.42)$$

- *Isothermal-isobaric ensemble*

$$\Delta_N^{\mathrm{id}}(\beta,\gamma) = \frac{1}{V_0N![\Lambda(\beta)]^{dN}}\int_0^{\infty} \mathrm{d}V\, V^N\mathrm{e}^{-\gamma V} = \frac{\gamma^{-(N+1)}}{V_0[\Lambda(\beta)]^{dN}}. \qquad (3.43)$$

$$G^{\mathrm{id}}(N,p,T) = \mu^{\mathrm{id}}N = Nk_BT\ln\left[\beta p\Lambda^d(\beta)\right], \qquad (3.44)$$

$$\langle E\rangle^{\mathrm{id}} = \frac{d}{2}Nk_BT, \quad \langle V\rangle^{\mathrm{id}} = \frac{Nk_BT}{p}. \qquad (3.45)$$

In (3.37) ζ is the one-particle partition function and Λ is the thermal de Broglie wavelength. In (3.40) z is the *fugacity*. Note that (3.35), (3.38), (3.41), and (3.44) are equivalent. Likewise, (3.36), (3.39), (3.42), and (3.45) are also equivalent. This a manifestation of the ensemble equivalence in the thermodynamic limit, the only difference lying in the choice of independent and dependent variables.

3.7 Interacting Systems

Of course, particles do interact in real systems, so the Hamiltonian has the form

$$H_N(\mathbf{x}^N) = H_N^{\text{id}}(\mathbf{p}^N) + \Phi_N(\mathbf{r}^N) , \tag{3.46}$$

where Φ_N denotes the total potential energy. As a consequence, the partition function factorizes into its ideal and non-ideal parts:

$$\boxed{\mathscr{Z}_N(\beta,V) = \mathscr{Z}_N^{\text{id}}(\beta,V)Q_N(\beta,V) , \quad Q_N(\beta,V) = V^{-N}\int d\mathbf{r}^N e^{-\beta\Phi_N(\mathbf{r}^N)}} . \tag{3.47}$$

The non-ideal part Q_N is the *configuration integral*. In the canonical ensemble, Q_N is responsible for the *excess* contributions $\langle E\rangle^{\text{ex}} = \langle E\rangle - \langle E\rangle^{\text{id}}$, $p^{\text{ex}} = p - p^{\text{id}}$, $\mu^{\text{ex}} = \mu - \mu^{\text{id}}$:

$$\langle E\rangle^{\text{ex}} = -\frac{\partial \ln Q_N}{\partial \beta} , \quad p^{\text{ex}} = k_B T\frac{\partial \ln Q_N}{\partial V} , \quad \mu^{\text{ex}} = -k_B T\frac{\partial \ln Q_N}{\partial N} . \tag{3.48}$$

The grand partition function does not factorize but can be written as

$$\boxed{\Xi(\beta,\alpha,V) = 1 + \sum_{N=1}^{\infty}\frac{V^N Q_N(\beta,V)}{N!}[z_\Lambda(\beta,\alpha)]^N} , \tag{3.49}$$

where

$$z_\Lambda(\beta,\alpha) \equiv \frac{z(\alpha)}{[\Lambda(\beta)]^d} \tag{3.50}$$

is a sort of modified fugacity and we have taken into account that $Q_0 = 1$. Thus, the configuration integrals are related to the coefficients in the expansion of the grand partition function in powers of the quantity z_Λ.

4 Reduced Distribution Functions

The N-body probability distribution function $\rho_N(\mathbf{x}^N)$ contains all the statistical-mechanical information about the system. On the other hand, partial information embedded in *marginal* few-body distributions are usually enough for the most relevant quantities. Moreover, it is much simpler to introduce useful approximations at the level of the marginal distributions than at the N-body level.

Let us introduce the s-body *reduced distribution function* $f_s(\mathbf{x}^s)$ such that $f_s(\mathbf{x}^s)d\mathbf{x}^s$ is the (average) number of groups of s particles such that one particle lies inside a volume $d\mathbf{x}_1$ around the (1-body) phase-space point $\mathbf{x}_1$, other particle lies inside a volume $d\mathbf{x}_2$ around the (1-body) phase-space point $\mathbf{x}_2$, ...and so on (see Fig. 4.1 for $s = 3$). More explicitly,

Fig. 4.1 Sketch of the one-body phase space. The horizontal axis represents the d position coordinates, while the vertical axis represents the d momentum components. Three points ($\mathbf{x}_1$, $\mathbf{x}_2$, and $\mathbf{x}_3$) are represented.
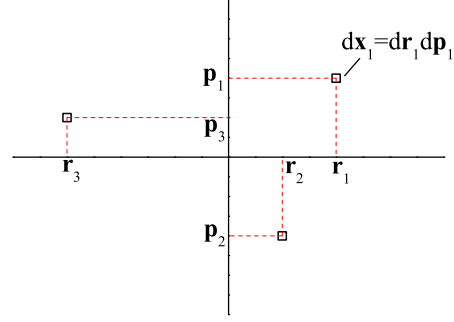
$$
f_s(\mathbf{x}^s) = \sum_{i_1 \neq i_2 \neq \cdots \neq i_s} \int d\mathbf{x}'^N \, \delta(\mathbf{x}'_{i_1} - \mathbf{x}_1) \cdots \delta(\mathbf{x}'_{i_s} - \mathbf{x}_s) \rho_N(\mathbf{x}'^N)
$$

$$
= \frac{N!}{(N-s)!} \int d\mathbf{x}_{s+1} \int d\mathbf{x}_{s+2} \cdots \int d\mathbf{x}_N \, \rho_N(\mathbf{x}^N) . \tag{4.1}
$$

In most situations it is enough to take $s = 2$ and integrate out the momenta. Thus, we define the *configurational* two-body distribution function as

$$
n_2(\mathbf{r}_1, \mathbf{r}_2) = \int d\mathbf{p}_1 \int d\mathbf{p}_2 \, f_2(\mathbf{x}_1, \mathbf{x}_2) . \tag{4.2}
$$

Obviously, its normalization condition is

$$
\int d\mathbf{r}_1 \int d\mathbf{r}_2 \, n_2(\mathbf{r}_1, \mathbf{r}_2) = N(N-1) . \tag{4.3}
$$

The importance of n_2 arises especially when one is interested in evaluating the average of a dynamical variable of the form

$$
A(\mathbf{r}^N) = \frac{1}{2} \sum_{i \neq j} A_2(\mathbf{r}_i, \mathbf{r}_j) . \tag{4.4}
$$

In that case, it is easy to obtain

$$
\langle A \rangle \equiv \int d\mathbf{x}^N A(\mathbf{r}^N) \rho_N(\mathbf{x}^N) = \frac{1}{2} \int d\mathbf{r}_1 \int d\mathbf{r}_2 A_2(\mathbf{r}_1, \mathbf{r}_2) n_2(\mathbf{r}_1, \mathbf{r}_2) . \tag{4.5}
$$

The quantities (4.1) and (4.2) can be defined both out of and in equilibrium. In the latter case, however, we can benefit from the (formal) knowledge of ρ_N. In particular, in the canonical ensemble [see (3.9) and (3.47)] one has

$$
n_2(\mathbf{r}_1, \mathbf{r}_2) = \frac{N(N-1)}{V^N Q_N} \int d\mathbf{r}_3 \cdots \int d\mathbf{r}_N e^{-\beta \Phi_N(\mathbf{r}^N)} . \tag{4.6}
$$

In the absence of interactions ($\Phi_N = 0$),

$$n_2^{\text{id}} = \frac{N(N-1)}{V^2} \approx n^2 , \quad n \equiv \frac{N}{V} . \tag{4.7}$$

In the grand canonical ensemble the equations equivalent to (4.3), (4.6), and (4.7) are

$$\int d\mathbf{r}_1 \int d\mathbf{r}_2 \, n_2(\mathbf{r}_1, \mathbf{r}_2) = \langle N(N-1) \rangle , \tag{4.8}$$

$$n_2(\mathbf{r}_1, \mathbf{r}_2) = \frac{1}{\Xi} \sum_{N=2}^{\infty} \frac{[z_\Lambda(\beta, \alpha)]^N}{N!} N(N-1) \int d\mathbf{r}_3 \cdots \int d\mathbf{r}_N e^{-\beta \Phi_N(\mathbf{r}^N)} , \tag{4.9}$$

$$n_2^{\text{id}} = \frac{\langle N(N-1) \rangle}{V^2} \approx n^2, \quad n \equiv \frac{\langle N \rangle}{V} . \tag{4.10}$$

4.1 Radial Distribution Function

Taking into account (4.7) and (4.10), we define the *pair* correlation function $g(\mathbf{r}_1, \mathbf{r}_2)$ by

$$n_2(\mathbf{r}_1, \mathbf{r}_2) = n^2 g(\mathbf{r}_1, \mathbf{r}_2) . \tag{4.11}$$

Thus, according to (4.6),

$$\boxed{g(\mathbf{r}_1, \mathbf{r}_2) = \frac{V^{-(N-2)}}{Q_N} \int d\mathbf{r}_3 \cdots \int d\mathbf{r}_N e^{-\beta \Phi_N(\mathbf{r}^N)}} \tag{4.12}$$

in the canonical ensemble.

Now, taking into account the translational invariance property of the system, one has $g(\mathbf{r}_1, \mathbf{r}_2) = g(\mathbf{r}_1 - \mathbf{r}_2)$. Moreover, a fluid is rotationally invariant, so that (assuming central forces), $g(\mathbf{r}_1 - \mathbf{r}_2) = g(r_{12})$, where $r_{12} \equiv |\mathbf{r}_1 - \mathbf{r}_2|$ is the distance between the points $\mathbf{r}_1$ and $\mathbf{r}_2$. In such a case, the function $g(r)$ is called *radial distribution function* and will play a very important role henceforth.

An interesting normalization relation holds in the grand canonical ensemble. Inserting (4.11) into (4.8) we get

$$\boxed{V^{-1} \int d\mathbf{r} \, g(r) = \frac{\langle N(N-1) \rangle}{\langle N \rangle^2} = \frac{\langle N^2 \rangle}{\langle N \rangle^2} - \frac{1}{\langle N \rangle}} . \tag{4.13}$$

In the thermodynamic limit ($\langle N \rangle \to \infty$ and $V \to \infty$ with $n = $ const), we know that $\langle N^2 \rangle / \langle N \rangle^2 \to 1$ [see (3.23)] (except near the critical point, where κ_T diverges). This implies that $V^{-1} \int d\mathbf{r} \, g(r) \approx 1$, meaning that $g(r) \approx 1$ for *macroscopic* distances r, which are those dominating the value of the integral. In other words, $\int d\mathbf{r} \, [g(r) - 1] \ll V$.

Apart from the formal definition provided by (4.11) and (4.12), it is important to have a more intuitive physical interpretation of $g(r)$. Two simple equivalent interpretations are:
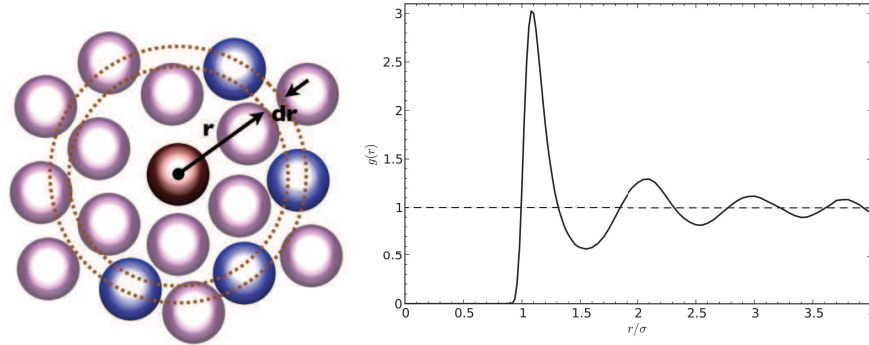
Fig. 4.2 Left panel: Schematic view of how $g(r)$ is determined. The red particle is the reference one and the blue particles are those whose centers are at a distance between r and $r + dr$. The average number of blue particles, divided by $n4\pi r^2 dr$ (in three dimensions) gives $g(r)$. Right panel: Radial distribution function for a Lennard-Jones fluid at a reduced temperature $T^* = 0.71$ and a reduced density $n^* = 0.844$, as obtained from Monte Carlo simulations. Source: http://en.wikipedia.org/wiki/Radial_distribution_function.

- $g(r)$ is the probability of finding a particle at a distance r away from a given reference particle, *relative* to the probability for an ideal gas.
- If a given reference particle is taken to be at the origin, then the *local* average density at a distance r from that particle is $ng(r)$.

Figure 4.2 illustrates the meaning of $g(r)$ and depicts the typical shape of the function for a (three-dimensional) fluid of particles interacting via the Lennard-Jones (LJ) potential

$$\phi(r) = 4\varepsilon \left[\left(\frac{\sigma}{r} \right)^{12} - \left(\frac{\sigma}{r} \right)^6 \right] \tag{4.14}$$

at the reduced temperature $T^* \equiv k_B T / \varepsilon = 0.71$ and the reduced density $n^* = n\sigma^3 = 0.844$. The Lennard-Jones potential is characterized by a scale distance σ and well depth ε, and is repulsive for $r < 2^{1/6}\sigma$ and attractive for $r > 2^{1/6}\sigma$. As we see from Fig. 4.2, $g(r)$ is practically zero in the region $0 \leq r \lesssim \sigma$ (due to the strongly repulsive force exerted by the reference particle at those distances), presents a very high peak at $r \approx \sigma$, oscillates thereafter, and eventually tends to unity for long distances as compared with σ. Thus, a liquid may present a strong structure captured by $g(r)$.

Some functions related to the radial distribution function $g(r)$ can be defined. The first one is simply the so-called *total correlation function*

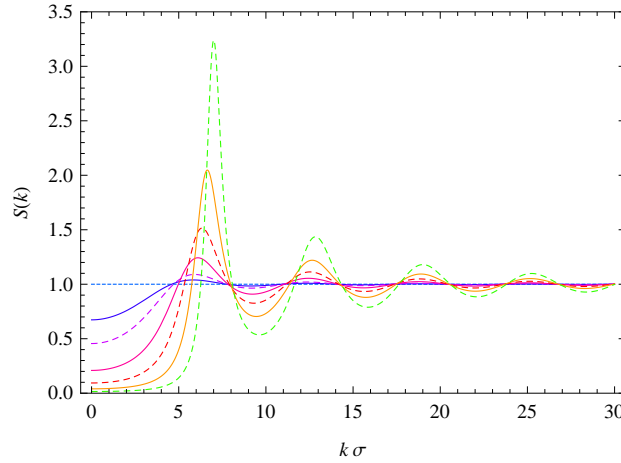$$\boxed{h(r) = g(r) - 1} . \tag{4.15}$$

Its Fourier transform

Fig. 4.3 Structure factor of a three-dimensional hard-sphere fluid (as obtained from the Percus–Yevick approximation) at several values of the packing fraction $\eta \equiv (\pi/6)n\sigma^3 = 0.05$, 0.1, 0.2, 0.3, 0.4, and 0.5, in increasing order of complexity.

$$\widetilde{h}(k) \equiv \int d\mathbf{r}\, e^{-i\mathbf{k}\cdot\mathbf{r}} h(r) \tag{4.16}$$

is directly connected to the (static) *structure factor*:

$$\boxed{S(k) = 1 + n\widetilde{h}(k)}. \tag{4.17}$$

The typical shape of $S(k)$ at several densities is illustrated in Fig. 4.3 for the hard-sphere (HS) potential [1]

$$\phi(r) = \begin{cases} \infty, & r < \sigma, \\ 0, & r > \sigma, \end{cases} \tag{4.18}$$

where σ is the diameter of the spheres.

The structure factor is a very important quantity because it is experimentally accessible by elastic scattering of radiation (x-rays or neutrons) by the fluid [18, 22]. Thus, while $g(r)$ can be measured directly in simulations (either Monte Carlo or molecular dynamics) [23, 24], it can be obtained indirectly in experiments from a numerical inverse Fourier transform of $S(k) - 1$.

5 Thermodynamics from the Radial Distribution Function

As shown by (3.7), (3.12), (3.20), and (3.29), the knowledge of any of the ensemble normalization functions allows one to obtain the full thermodynamic information about the system. But now imagine that instead of the normalization function (for

instance, the partition function in the canonical ensemble), we are given (from experimental measures, computer simulations, or a certain theory) the radial distribution function $g(r)$. Can we have access to thermodynamics directly from $g(r)$? As we will see in this section, the answer is affirmative in the case of pairwise interactions.

5.1 Compressibility Route

The most straightforward route to thermodynamics from $g(r)$ is provided by choosing the grand canonical ensemble and simply combining (3.23) and (4.13) to obtain

$$\boxed{\chi \equiv nk_BT\kappa_T = k_BT\left(\frac{\partial n}{\partial p}\right)_T = 1 + n\int d\mathbf{r}\,h(r) = S(0)}\,,\qquad (5.1)$$

where χ is the isothermal susceptibility and we recall that the total correlation function is defined by (4.15) and in the last step use has been made of (4.17). Therefore, the zero wavenumber limit of the structure factor (see Fig. 4.2) is directly related to the isothermal compressibility.

Equation (5.1) is usually known as the *compressibility equation of state* or the *compressibility route* to thermodynamics.

5.2 Energy Route

Equation (5.1) applies regardless of the specific form of the potential energy function $\Phi_N(\mathbf{r}^N)$. From now on, however, we assume that the interaction is *pairwise additive*, i.e., Φ_N can be expressed as a sum over all pairs of a certain function (interaction potential) ϕ that depends on the distance between the two particles of the pair. In mathematical terms,

$$\boxed{\Phi_N(\mathbf{r}^N) = \sum_{i=1}^{N-1}\sum_{j=i+1}^{N}\phi(r_{ij}) = \frac{1}{2}\sum_{i\neq j}\phi(r_{ij})}\,.\qquad (5.2)$$

We have previously encountered two particular examples [see (4.14) and (4.18)] of interaction potentials.

The pairwise additivity condition (5.2) implies that Φ_N is a dynamical variable of the form (4.4). As a consequence, we can apply the property (4.5) to the average potential energy:

$$\langle E\rangle^{\text{ex}} = \langle\Phi_N(\mathbf{r}^N)\rangle = \frac{1}{2}\int d\mathbf{r}_1\int d\mathbf{r}_2\,n_2(\mathbf{r}_1,\mathbf{r}_2)\phi(r_{12})\,.\qquad (5.3)$$

Fig. 5.1 Cavity function in
the overlapping region $r < \sigma$
for a hard-sphere fluid at three
different densities, as obtained
from Monte Carlo simulations
[25].
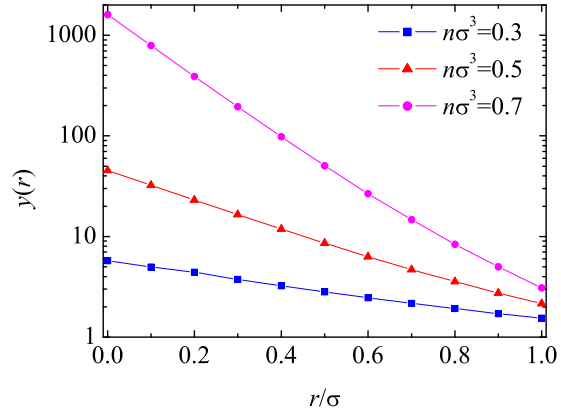
Adding the ideal-gas term [see (3.39)] and taking into account (4.11), we finally
obtain

$$\langle E \rangle = N \left[\frac{d}{2} k_B T + \frac{n}{2} \int d\mathbf{r}\, \phi(r) g(r) \right],$$ (5.4)

where we have used the general property $\int d\mathbf{r}_1 \int d\mathbf{r}_2\, \mathscr{F}(r_{12}) = V \int d\mathbf{r}\, \mathscr{F}(r)$, $\mathscr{F}(r)$
being an arbitrary function.

Equation (5.4) defines the *energy route* to thermodynamics. It can be equivalently
written in terms of the so-called *cavity function*

$$y(r) \equiv g(r) e^{\beta \phi(r)}.$$ (5.5)

The result is

$$\langle E \rangle = N \left[\frac{d}{2} k_B T + \frac{n}{2} \int d\mathbf{r}\, \phi(r) e^{-\beta \phi(r)} y(r) \right].$$ (5.6)

The cavity function $y(r)$ is much more regular than the radial distribution func-
tion $g(r)$. It is continuous even if the interaction potential is discontinuous or di-
verges. In the case of hard spheres, for instance, while $g(r) = 0$ if $r < \sigma$, $y(r)$ is well
defined in that region, as illustrated by Fig. 5.1.

5.3 Virial Route

Now we consider the pressure, which is the quantity more directly related to the
equation of state. In the canonical ensemble, the excess pressure is proportional to
$\partial \ln Q_N / \partial V$ [see (3.48)] and thus it is not the average of a dynamical variable of type
(4.5). To make things worse, the volume V appears in the configurational integral
[see (3.47)] both explicitly and *implicitly* through the integration limits. Let us make

this more evident by writing

$$Q_N(V) = V^{-N} \int_{V^N} d\mathbf{r}^N e^{-\beta \Phi_N(\mathbf{r}^N)} . \tag{5.7}$$

To get rid of this difficulty, we imagine now that the system is a sphere of volume V and the origin of coordinates is chosen at the center of the sphere. If the whole system is blown up by a factor λ [18], the volume changes from V to $\lambda^d V$ and the configurational integral changes from $Q_N(V)$ to $Q_N(\lambda^d V)$ with

$$Q_N(\lambda^d V) = (\lambda^d V)^{-N} \int_{(\lambda^d V)^N} d\mathbf{r}^N e^{-\beta \Phi_N(\mathbf{r}^N)} = V^{-N} \int_{V^N} d\mathbf{r}'^N e^{-\beta \Phi_N(\lambda^N \mathbf{r}'^N)} , \tag{5.8}$$

where in the last step the change $\mathbf{r}_i \to \mathbf{r}'_i = \mathbf{r}_i/\lambda$ has been performed. We see that $Q_N(\lambda^d V)$ depends on λ explicitly through the argument of the interaction potential. Next, taking into account the identity $\partial \ln Q_N(\lambda^d V)/\partial V = (\lambda/Vd)\partial \ln Q_N(\lambda^d V)/\partial \lambda$, we can write

$$\frac{\partial \ln Q_N(V)}{\partial V} = \frac{1}{Vd} \frac{\partial \ln Q_N(\lambda^d V)}{\partial \lambda}\bigg|_{\lambda=1} , \tag{5.9}$$

so that

$$\begin{aligned}
\frac{\partial \ln Q_N(\lambda^d V)}{\partial \lambda}\bigg|_{\lambda=1} &= -\beta \left\langle \frac{\partial \Phi_N(\lambda^N \mathbf{r}^N)}{\partial \lambda}\bigg|_{\lambda=1} \right\rangle \\
&= -\frac{\beta}{2} \int d\mathbf{r}_1 \int d\mathbf{r}_2 \, n_2(\mathbf{r}_1, \mathbf{r}_2) \frac{\partial \phi(\lambda r_{12})}{\partial \lambda}\bigg|_{\lambda=1} \\
&= -\frac{\beta}{2} n^2 V \int d\mathbf{r} \, g(r) \frac{\partial \phi(\lambda r)}{\partial \lambda}\bigg|_{\lambda=1} . \tag{5.10}
\end{aligned}$$

In the second equality use has been made of (4.5). Finally, a mathematical property similar to (5.9) is

$$\frac{\partial \phi(\lambda r)}{\partial \lambda}\bigg|_{\lambda=1} = r \frac{d\phi(r)}{dr} . \tag{5.11}$$

Inserting (5.11) into (5.10), and using (5.9), we obtain the sought result:

$$\boxed{Z \equiv \frac{p}{nk_B T} = 1 - \frac{n\beta}{2d} \int d\mathbf{r} \, r \frac{d\phi(r)}{dr} g(r)} . \tag{5.12}$$

This is known as the pressure route or *virial route* to the equation of state, where Z is the *compressibility factor*. Expressed in terms of the cavity function (5.5), the virial route becomes

$$\boxed{Z \equiv \frac{p}{nk_B T} = 1 + \frac{n}{2d} \int d\mathbf{r} \, y(r) r \frac{\partial e^{-\beta \phi(r)}}{\partial r}} . \tag{5.13}$$

5.4 Chemical-Potential Route

A look at (3.48) shows that we have already succeeded in expressing the first two derivatives of $\ln Q_N$ in terms of integrals involving the radial distribution function. The third derivative involves the chemical potential and is much more delicate. First, noting that N is actually a discrete variable, we can rewrite

$$\beta\mu^{\text{ex}} = -\frac{\partial \ln Q_N}{\partial N} \rightarrow \ln\frac{Q_N(\beta,V)}{Q_{N+1}(\beta,V)} \ . \tag{5.14}$$

Thus, the (excess) chemical potential is related to the response of the system to the addition of one more particle without changing either temperature or volume.

The N-body potential energy is expressed by (5.2). Now we add an extra particle (labeled as $i = 0$), so that the $(N+1)$-body potential energy becomes

$$\Phi_{N+1}(\mathbf{r}^{N+1}) = \sum_{i=1}^{N-1}\sum_{j=i+1}^{N}\phi(r_{ij}) + \sum_{j=1}^{N}\phi(r_{0j}) \ . \tag{5.15}$$

The trick now consists of introducing the extra particle (the "solute") little by little through a *charging process* [18, 19, 26, 27, 28, 29, 30, 31]. We do so by introducing a *coupling parameter* ξ such that its value $0 \le \xi \le 1$ controls the strength of the interaction of particle $i = 0$ to the rest of particles (the "solvent"):

$$\phi^{(\xi)}(r_{0j}) = \begin{cases} 0 \ , & \xi = 0 \ , \\ \phi(r_{0j}) \ , & \xi = 1 \ . \end{cases} \tag{5.16}$$

The associated total potential energy and configuration integral are

$$\Phi_{N+1}^{(\xi)}(\mathbf{r}^{N+1}) = \Phi_N(\mathbf{r}^N) + \sum_{j=1}^{N}\phi^{(\xi)}(r_{0j}) \ , \tag{5.17}$$

$$Q_{N+1}^{(\xi)}(\beta,V) = V^{-(N+1)}\int d\mathbf{r}^{N+1}\, e^{-\beta\Phi_{N+1}^{(\xi)}(\mathbf{r}^{N+1})} \ . \tag{5.18}$$

Thus, assuming that $Q_{N+1}^{(\xi)}$ is a smooth function of ξ, (5.14) becomes

$$\beta\mu^{\text{ex}} = -\int_0^1 d\xi\, \frac{\partial \ln Q_{N+1}^{(\xi)}(\beta,V)}{\partial \xi} \ . \tag{5.19}$$

Since the dependence of $Q_{N+1}^{(\xi)}$ on ξ takes place through the extra summation in (5.17) and all the solvent particles are assumed to be identical,

$$\frac{\partial \ln Q_{N+1}^{(\xi)}}{\partial \xi} = -\frac{n\beta V^{-N}}{Q_{N+1}^{(\xi)}}\int d\mathbf{r}^{N+1}\, e^{-\beta\Phi_{N+1}^{(\xi)}(\mathbf{r}^{N+1})}\frac{\partial\phi^{(\xi)}(r_{01})}{\partial\xi} \ . \tag{5.20}$$

Now we realize that, similarly to (4.12), the solute-solvent radial distribution function is defined as

$$g^{(\xi)}(r_{01}) = \frac{V^{-(N-1)}}{Q_{N+1}^{(\xi)}} \int d\mathbf{r}_2 \cdots \int d\mathbf{r}_N \, e^{-\beta \Phi_{N+1}^{(\xi)}(\mathbf{r}^{N+1})} . \tag{5.21}$$

This allows us to rewrite (5.20) in the form

$$\frac{\partial \ln Q_{N+1}^{(\xi)}}{\partial \xi} = -\frac{n\beta}{V} \int d\mathbf{r}_0 \int d\mathbf{r}_1 \, g^{(\xi)}(r_{01}) \frac{\partial \phi^{(\xi)}(r_{01})}{\partial \xi} . \tag{5.22}$$

Finally,

$$\boxed{\mu = k_B T \ln\left(n\Lambda^d\right) + n \int_0^1 d\xi \int d\mathbf{r} \, g^{(\xi)}(r) \frac{\partial \phi^{(\xi)}(r)}{\partial \xi}} , \tag{5.23}$$

or, equivalently,

$$\boxed{\beta\mu = \ln\left(n\Lambda^d\right) - n \int_0^1 d\xi \int d\mathbf{r} \, y^{(\xi)}(r) \frac{\partial e^{-\beta\phi^{(\xi)}(r)}}{\partial \xi}} . \tag{5.24}$$

In contrast to the other three conventional routes [see (5.1), (5.4), and (5.12)], the *chemical-potential route* (5.23) requires the knowledge of the solute-solvent correlation functions for all the values $0 \le \xi \le 1$ of the coupling parameter ξ.

5.5 *Extension to Mixtures*

In a multicomponent system the main quantities are

- Number of particles of species α: N_α.
- Total number of particles: $N = \sum_\alpha N_\alpha$.
- Mole fraction of species α: $x_\alpha = N_\alpha/N$, $\sum_\alpha x_\alpha = 1$.
- Interaction potential between a particle of species α and a particle of species γ: $\phi_{\alpha\gamma}(r)$.
- Radial distribution function for the pair $\alpha\gamma$: $g_{\alpha\gamma}(r)$

All the previous thermodynamic routes can be generalized to mixtures.

5.5.1 Compressibility Route

The generalization of (5.1) to mixtures is not trivial [32]. The result is

$$\chi^{-1} \equiv \left(\frac{\partial \beta p}{\partial n} \right)_T = \sum_{\alpha,\gamma} \sqrt{x_\alpha x_\gamma} \left(1 + \widehat{\mathsf{h}} \right)_{\alpha\gamma}^{-1}, \tag{5.25}$$

where the element $\widehat{h}_{\alpha\gamma}$ of the matrix $\widehat{\mathsf{h}}$ is proportional to the zero wavenumber limit of the Fourier transform of the total correlation function $h_{\alpha\gamma}(r) = g_{\alpha\gamma}(r) - 1$, namely

$$\widehat{h}_{\alpha\gamma} = n\sqrt{x_\alpha x_\gamma} \int \mathrm{d}\mathbf{r}\, h_{\alpha\gamma}(r) . \tag{5.26}$$

5.5.2 Energy Route

In this case, (5.6) is simply generalized as

$$\langle E \rangle = N \left[\frac{d}{2} k_B T + \frac{n}{2} \sum_{\alpha,\gamma} x_\alpha x_\gamma \int \mathrm{d}\mathbf{r}\, \phi_{\alpha\gamma}(r) \mathrm{e}^{-\beta\phi_{\alpha\gamma}(r)} y_{\alpha\gamma}(r) \right] . \tag{5.27}$$

5.5.3 Virial Route

Likewise, the generalization of (5.13) to mixtures reads

$$Z \equiv \frac{p}{nk_B T} = 1 + \frac{n}{2d} \sum_{\alpha,\gamma} x_\alpha x_\gamma \int \mathrm{d}\mathbf{r}\, y_{\alpha\gamma}(r) r \frac{\partial \mathrm{e}^{-\beta\phi_{\alpha\gamma}(r)}}{\partial r} . \tag{5.28}$$

5.5.4 Chemical-Potential Route

In this case, there exists a chemical potential associated with each species and the generalization of (5.24) is [31]

$$\beta\mu_v = \ln\left(n x_v \Lambda_v^d \right) - n \sum_\alpha x_\alpha \int_0^1 \mathrm{d}\xi \int \mathrm{d}\mathbf{r}\, y_{v\alpha}^{(\xi)}(r) \frac{\partial \mathrm{e}^{-\beta\phi_{v\alpha}^{(\xi)}(r)}}{\partial \xi} . \tag{5.29}$$

Here, the solute particle $i = 0$ is coupled to a particle of species α via an interaction potential $\phi_{v\alpha}^{(\xi)}(r)$ such that

$$\phi_{v\alpha}^{(\xi)}(r) = \begin{cases} 0 , & \xi = 0 , \\ \phi_{v\alpha}(r) , & \xi = 1 , \end{cases} \tag{5.30}$$

Fig. 5.2 Hard-sphere interaction potential. The potential is equal to infinity in the shaded region and zero otherwise.
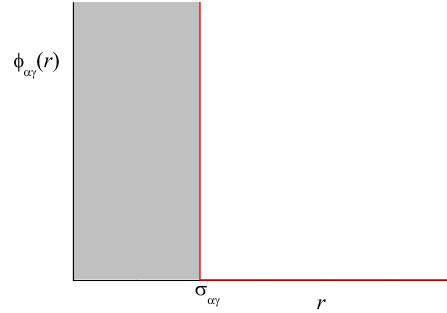
so that it becomes a particle of species v at the end of the charging process. The associated radial distribution and cavity functions are $g_{v\alpha}^{(\xi)}(r)$ and $y_{v\alpha}^{(\xi)}(r) = g_{v\alpha}^{(\xi)}(r)e^{\beta\phi_{v\alpha}^{(\xi)}(r)}$, respectively.

The Helmholtz and Gibbs free energies can be obtained from μ_v as [see (2.10)]

$$\sum_v \mu_v N_v = G = -V^2 \frac{\partial (F/V)}{\partial V} . \tag{5.31}$$

5.6 Hard Spheres

Let us now particularize the above expressions for multicomponent hard-sphere fluids [33]. The interaction potential function is given by the form (4.18) for any pair of species, namely (see Fig. 5.2)

$$\phi_{\alpha\gamma}(r) = \begin{cases} \infty, & r < \sigma_{\alpha\gamma} , \\ 0, & r > \sigma_{\alpha\gamma} . \end{cases} \tag{5.32}$$

Here, $\sigma_{\alpha\gamma}$ is the closest possible distance between the center of a sphere of species α and the center of a sphere of species γ. If we call $\sigma_\alpha = \sigma_{\alpha\alpha}$ to the closest distance between two spheres of the same species α, it is legitimate to refer to σ_α as the *diameter* of a sphere of species α. However, that does not necessarily mean that two spheres of different type repel each other with a distance equal to the sum of their radii. Depending on that, one can classify hard-sphere mixtures into additive or nonadditive:

- Additive mixtures: $\sigma_{\alpha\gamma} = \frac{1}{2}(\sigma_\alpha + \sigma_\gamma)$ for all pairs $\alpha\gamma$.
- Nonadditive mixtures: $\sigma_{\alpha\gamma} \neq \frac{1}{2}(\sigma_\alpha + \sigma_\gamma)$ for at least one pair $\alpha\gamma$.

As a consequence of (5.32),

$$e^{-\beta\phi_{\alpha\gamma}(r)} = \Theta(r - \sigma_{\alpha\gamma}) , \quad \frac{\partial e^{-\beta\phi_{\alpha\gamma}(r)}}{\partial r} = \delta(r - \sigma_{\alpha\gamma}) , \quad (5.33)$$

where $\Theta(x)$ and $\delta(x)$ are the Heaviside step function and the Dirac delta function, respectively.

The compressibility route (5.25) does not include the interaction potential explicitly and so it is not simplified in the hard-sphere case. As for the energy route, the integral (5.27) vanishes because $\phi_{\alpha\gamma}(r)e^{-\beta\phi_{\alpha\gamma}(r)} \to 0$ both for $r < \sigma_{\alpha\gamma}$ and $r > \sigma_{\alpha\gamma}$, while $y_{\alpha\gamma}(r)$ is finite even in the region $r < \sigma_{\alpha\gamma}$ (see Fig. 5.1). Therefore,

$$\langle E \rangle = N\frac{d}{2}k_B T . \quad (5.34)$$

But this is the ideal-gas internal energy! This is an expected result since the hard-sphere potential is only different from zero when two particles overlap but those configurations are forbidden by the Boltzmann factor $e^{-\beta\phi_{\alpha\gamma}(r)}$.

The generic virial route (5.28) is highly simplified for hard spheres. First, one changes to spherical coordinates and takes into account that the total d-dimensional solid angle (area of a d-dimensional sphere of unit radius) is

$$\int d\hat{\mathbf{r}} = d2^d v_d , \quad (5.35)$$

where

$$v_d = \frac{(\pi/4)^{d/2}}{\Gamma(1+d/2)} \quad (5.36)$$

is the volume of a d-dimensional sphere of unit diameter. Next, using the property (5.33), we obtain

$$\boxed{\frac{p}{nk_BT} = 1 + 2^{d-1}nv_d \sum_{\alpha,\gamma} x_\alpha x_\gamma \sigma_{\alpha\gamma}^d y_{\alpha\gamma}(\sigma_{\alpha\gamma})} . \quad (5.37)$$

The same method works for the chemical-potential route (5.29) with the choice

$$e^{-\beta\phi_{\nu\alpha}^{(\xi)}(\mathbf{r})} = \Theta(r - \sigma_{\nu\alpha}^{(\xi)}) , \quad (5.38)$$

where $\sigma_{\nu\alpha}^{(0)} = 0$ and $\sigma_{\nu\alpha}^{(1)} = \sigma_{\nu\alpha}$. Changing the integration variable in (5.29) from ξ to $\sigma_{\nu\alpha}^{(\xi)}$, one gets

$$\boxed{\beta\mu_\nu = \ln\left(nx_\nu\Lambda_\nu^d\right) + d2^d nv_d \sum_\alpha x_\alpha \int_0^{\sigma_{\nu\alpha}} d\sigma_{0\alpha}\, \sigma_{0\alpha}^{d-1} y_{0\alpha}(\sigma_{0\alpha})} , \quad (5.39)$$

where the notation has been simplified as $\sigma_{\nu\alpha}^{(\xi)} \to \sigma_{0\alpha}$ and $y_{\nu\alpha}^{(\xi)} \to y_{0\alpha}$.

If $\sigma_{\alpha\gamma} \geq \frac{1}{2}(\sigma_\alpha + \sigma_\gamma)$ (positive or zero *nonadditivity*), then it can be proved [31] that

Fig. 5.3 Schematic view of the thermodynamic inconsistency problem.

$$g(r) \quad \begin{array}{l} \text{energy route} \\ \text{virial route} \\ \text{compressibility route} \\ \text{chemical-potential route} \end{array}$$

$$\langle E \rangle = \frac{\partial(\beta F)}{\partial \beta} \longrightarrow F(T,V,N)$$

$$p = -\frac{\partial F}{\partial V} \longrightarrow F(T,V,N)$$

$$\kappa_T^{-1} = V\frac{\partial^2 F}{\partial V^2} \longrightarrow F(T,V,N)$$

$$\mu = \frac{\partial F}{\partial N} \longrightarrow F(T,V,N)$$

Same result?
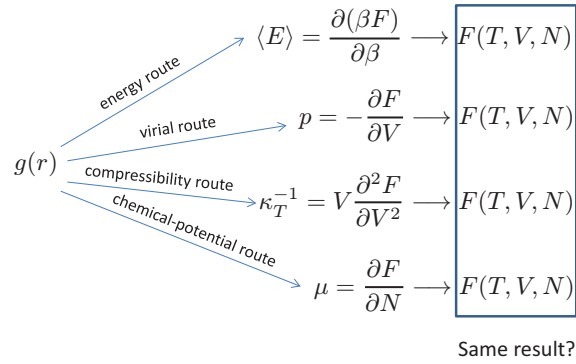
$$d2^d n v_d \sum_\alpha x_\alpha \int_0^{\frac{1}{2}\sigma_\alpha} \mathrm{d}\sigma_{0\alpha}\, \sigma_{0\alpha}^{d-1} y_{0\alpha}(\sigma_{0\alpha}) = -\ln(1-\eta)\,, \tag{5.40}$$

where

$$\eta \equiv n v_d \sum_\alpha x_\alpha \sigma_\alpha^d \tag{5.41}$$

is the total *packing* fraction. In that case, (5.39) can be rewritten as

$$\beta\mu_\nu = \ln\frac{nx_\nu\Lambda_\nu^d}{1-\eta} + d2^d n v_d \sum_\alpha x_\alpha \int_{\frac{1}{2}\sigma}^{\sigma_{\nu\alpha}} \mathrm{d}\sigma_{0\alpha}\, \sigma_{0\alpha}^{d-1} y_{0\alpha}(\sigma_{0\alpha})\,. \tag{5.42}$$

5.7 The Thermodynamic Inconsistency Problem

Going back to the case of an arbitrary interaction potential, we have seen that the knowledge of the radial distribution function $g(r)$ (where, for simplicity, we are using the one-component language) allows one to obtain four important thermodynamic quantities: the internal energy, the pressure, the isothermal compressibility, and the chemical potential. By integration, one could in principle derive the free energy of the system (except for functions playing the role of integration constants) from any of those routes, as sketched in Fig. 5.3. The important question is, would one obtain consistent results?

Since all the thermodynamic routes are derived from formally exact statistical-mechanical formulas, it is obvious that the use of the *exact* radial distribution function $g(r)$ must lead to the same exact free energy $F(T,V,N)$, regardless of the route followed. On the other hand, if an *approximate* $g(r)$ is used, one must be prepared to obtain (in general) a different approximate $F(T,V,N)$ from each separate route. This is known as the *thermodynamic (in)consistency problem*. Which route is more accurate, i.e., which route is more effective in concealing the deficiencies of an

approximate $g(r)$, depends on the approximation, the potential, and the thermody-namic state.

6 One-Dimensional Systems. Exact Solution for Nearest-Neighbor Interactions

As is apparent from (4.12), the evaluation of $g(r)$ is a formidable task, comparable to that of the evaluation of the configuration integral itself. However, in the case of one-dimensional systems ($d = 1$) of particles which only interact with their nearest neighbors, the problem can be exactly solved [34, 35, 36, 37, 38].

Let us consider a one-dimensional system of N particles in a box of length L (so the number density is $n = N/L$) subject to an interaction potential $\phi(r)$ such that

1. $\lim_{r \to 0} \phi(r) = \infty$. This implies that the *order* of the particles in the line does not change.
2. $\lim_{r \to \infty} \phi(r) = 0$. The interaction has a *finite* range.
3. Each particle interacts *only* with its two nearest neighbors.

The total potential energy is then

$$\Phi_N(\mathbf{r}^N) = \sum_{i=1}^{N-1} \phi(x_{i+1} - x_i) \,. \tag{6.1}$$

6.1 Nearest-Neighbor and Pair Correlation Functions

Given a particle at a certain position, let $p^{(1)}(r)\mathrm{d}r$ be the *conditional* probability of finding its (right) *nearest neighbor* at a distance between r and $r + \mathrm{d}r$ (see Fig. 6.1, top panel). More in general, we can define $p^{(\ell)}(r)\mathrm{d}r$ as the conditional probability of finding its (right) ℓth neighbor ($1 \leq \ell \leq N - 1$) at a distance between r and $r + \mathrm{d}r$ (see Fig. 6.1, middle panel). Since the ℓth neighbor must be somewhere, the normalization condition is

$$\int_0^\infty \mathrm{d}r \, p^{(\ell)}(r) = 1 \,. \tag{6.2}$$

In making the upper limit equal to infinity, we are implicitly assuming the thermo-dynamic limit ($L \to \infty$, $N \to \infty$, $n = $ const). Moreover, periodic boundary conditions are supposed to be applied when needed.

As illustrated by the bottom panel of Fig. 6.1, the following recurrence relation holds
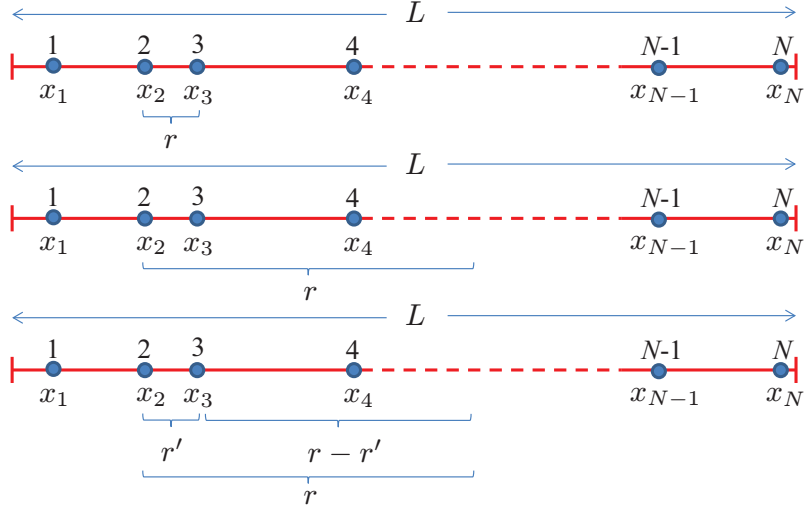
Fig. 6.1 Top panel: Two nearest-neighbor particles separated a distance r. Middle panel: Two ℓth-order neighbors separated a distance r. Bottom panel: Illustration of the convolution property.

$$p^{(\ell)}(r) = \int_0^r \mathrm{d}r'\, p^{(1)}(r')p^{(\ell-1)}(r-r') \,. \tag{6.3}$$

The convolution structure of the integral invites one to introduce the Laplace transform

$$P^{(\ell)}(s) = \int_0^\infty \mathrm{d}r\, \mathrm{e}^{-rs} p^{(\ell)}(r) \,, \tag{6.4}$$

so that (6.3) becomes

$$P^{(\ell)}(s) = P^{(1)}(s)P^{(\ell-1)}(s) \Rightarrow P^{(\ell)}(s) = \left[P^{(1)}(s)\right]^\ell \,. \tag{6.5}$$

The normalization condition (6.2) is equivalent to

$$P^{(\ell)}(0) = 1 \,. \tag{6.6}$$

Now, given a reference particle at a certain position, let $ng(r)\mathrm{d}r$ be the *number of particles* at a distance between r and $r+\mathrm{d}r$, regardless of whether those particles are the nearest neighbor, the next-nearest neighbor, ... of the reference particle. Thus,

$$ng(r) = \sum_{\ell=1}^{N-1} p^{(\ell)}(r) \overset{N\to\infty}{\longrightarrow} \sum_{\ell=1}^{\infty} p^{(\ell)}(r) \,. \tag{6.7}$$

Introducing the Laplace transform

$$G(s) = \int_0^\infty \mathrm{d}r\, \mathrm{e}^{-rs} g(r) \,, \tag{6.8}$$
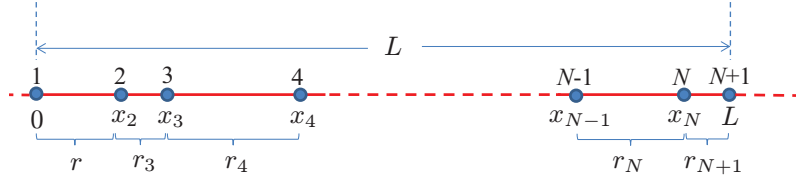
Fig. 6.2 Illustration of the evaluation of $p^{(1)}(r)$ in the isothermal-isobaric ensemble.

and using (6.5), we have

$$G(s) = \frac{1}{n} \sum_{\ell=1}^{\infty} \left[P^{(1)}(s) \right]^{\ell} = \frac{1}{n} \frac{P^{(1)}(s)}{1 - P^{(1)}(s)} . \qquad (6.9)$$

Thus, the determination of the radial distribution function $g(r)$ reduces to the determination of the nearest-neighbor distribution function $p^{(1)}(r)$. To that end, we take advantage of the ensemble equivalence in the thermodynamic limit and use the isothermal-isobaric ensemble.

6.2 Nearest-Neighbor Distribution. Isothermal-Isobaric Ensemble

The isothermal-isobaric ensemble is described by (3.26). The important point is that the N-body probability distribution function in configuration space is proportional to $e^{-\beta pV - \beta \Phi_N(\mathbf{r}^N)}$ Therefore, in this ensemble the one-dimensional nearest-neighbor probability distribution function is

$$p^{(1)}(r) \propto \int_r^{\infty} dL \, e^{-\beta pL} \int_{x_2}^{L} dx_3 \int_{x_3}^{L} dx_4 \cdots \int_{x_{N-1}}^{L} dx_N \, e^{-\beta \Phi_N(\mathbf{r}^N)} , \qquad (6.10)$$

where we have identified the volume V with the length L and have taken the particles $i = 1$ (at $x_1 = 0$) and $i = 2$ (at $x_2 = r$) as the canonical nearest-neighbor pair (see Fig. 6.2). Next, using (6.1) and applying periodic boundary conditions,

$$p^{(1)}(r) \propto e^{-\beta \phi(r)} \int_r^{\infty} dL \, e^{-\beta pL} \int_0^{L-r} dr_3 \, e^{-\beta \phi(r_3)} \int_0^{L-r-r_3} dr_4 \, e^{-\beta \phi(r_4)}$$

$$\times \cdots \int_0^{L-r-r_3-\cdots-r_{N-1}} dr_N \, e^{-\beta \phi(r_N)} e^{-\beta \phi(r_{N+1})} , \qquad (6.11)$$

where a change of variables $x_i \to r_i = x_i - x_{i-1}$ ($i = 3, \ldots, N$) has been carried out and $r_{N+1} = L - r - r_3 - r_4 - \cdots - r_N$. Finally, the change of variable $L \to L' = L - r$ shows that a factor $e^{-\beta pr}$ comes out of the integrals, the latter being independent of r. In summary,

$$p^{(1)}(r) = K e^{-\beta \phi(r)} e^{-\beta pr} , \qquad (6.12)$$

where the proportionality constant K will be determined by normalization. The Laplace transform of (6.12) is

$$P^{(1)}(s) = K\Omega(s + \beta p) \tag{6.13}$$

where

$$\Omega(s) \equiv \int_0^\infty dr\, e^{-rs} e^{-\beta\phi(r)} \tag{6.14}$$

is the Laplace transform of the Boltzmann factor $e^{-\beta\phi(r)}$. The normalization condition (6.6) yields

$$K = \frac{1}{\Omega(\beta p)} \ . \tag{6.15}$$

6.3 Exact Radial Distribution Function and Equation of State

Insertion of (6.15) into (6.9) gives the exact radial distribution function (in Laplace space):

$$G(s) = \frac{1}{n} \frac{\Omega(s + \beta p)}{\Omega(\beta p) - \Omega(s + \beta p)} \ . \tag{6.16}$$

To fully close the problem, it remains to relate the pressure p, the density n, and the temperature T (equation of state). To do that, we apply the consistency condition

$$\lim_{r \to \infty} g(r) = 1 \Rightarrow \lim_{s \to 0} sG(s) = 1 \ . \tag{6.17}$$

Expanding $\Omega(s + \beta p)$ in powers of s and imposing (6.17), we obtain

$$n(p, T) = -\frac{\Omega(\beta p)}{\Omega'(\beta p)} \ , \quad \Omega'(s) \equiv \frac{\partial \Omega(s)}{\partial s} \ . \tag{6.18}$$

As a consistency test, let us prove that the equation of state (6.18) is equivalent to the compressibility route (5.1). First, according to (6.18), the isothermal susceptibility is

$$\chi = \left(\frac{\partial n}{\partial \beta p}\right)_\beta = -1 + \frac{\Omega(\beta p)\Omega''(\beta p)}{[\Omega'(\beta p)]^2} \ . \tag{6.19}$$

Alternatively, the Laplace transform of $h(r)$ is $H(s) = G(s) - s^{-1}$, and thus the Fourier transform can be obtained as

$$\widetilde{h}(k) = [H(s) + H(-s)]_{s=ik} = [G(s) + G(-s)]_{s=ik} \ . \tag{6.20}$$

In particular, the zero wavenumber limit is

$$\int \mathrm{d}\mathbf{r}\, h(r) = 2\lim_{s\to 0}\left[G(s) - \frac{1}{s}\right] = \frac{\Omega'(\beta p)}{\Omega(\beta p)} - \frac{\Omega''(\beta p)}{2\Omega'(\beta p)} , \qquad (6.21)$$

so that

$$1 + n\int \mathrm{d}\mathbf{r}\, h(r) = 1 - 2\frac{\Omega(\beta p)}{\Omega'(\beta p)}\left[\frac{\Omega'(\beta p)}{\Omega(\beta p)} - \frac{\Omega''(\beta p)}{2\Omega'(\beta p)}\right]$$

$$= -1 + \frac{\Omega(\beta p)\Omega''(\beta p)}{[\Omega'(\beta p)]^2} . \qquad (6.22)$$

Comparison between (6.19) and (6.22) shows that (5.1) is indeed satisfied.

6.4 Extension to Mixtures

In the case of one-dimensional mixtures the arguments outlined above can be extended without special difficulties [36, 37, 38]. Now, instead of $p^{(\ell)}(r)\mathrm{d}r$ one defines $p_{\alpha\gamma}^{(\ell)}(r)\mathrm{d}r$ as the conditional probability that the ℓth neighbor to the right of a reference particle of species α is located at a distance between r and $r+\mathrm{d}r$ *and* belongs to species γ. The counterparts of (6.2), (6.3), and (6.7) are

$$\sum_{\gamma}\int_0^\infty \mathrm{d}r\, p_{\alpha\gamma}^{(\ell)}(r) = 1 , \qquad (6.23)$$

$$p_{\alpha\gamma}^{(\ell)}(r) = \sum_{\nu}\int_0^r \mathrm{d}r'\, p_{\alpha\nu}^{(1)}(r')p_{\nu\gamma}^{(\ell-1)}(r-r') , \qquad (6.24)$$

$$nx_\gamma g_{\alpha\gamma}(r) = \sum_{\ell=1}^\infty p_{\alpha\gamma}^{(\ell)}(r) . \qquad (6.25)$$

Next, by defining the Laplace transforms $P_{\alpha\gamma}^{(\ell)}(s)$ and $G_{\alpha\gamma}(s)$ of $p_{\alpha\gamma}^{(\ell)}(r)$ and $g_{\alpha\gamma}(r)$, respectively, one easily arrives at

$$G_{\alpha\gamma}(s) = \frac{1}{nx_\gamma}\left(\mathsf{P}^{(1)}(s)\cdot\left[\mathsf{I} - \mathsf{P}^{(1)}(s)\right]^{-1}\right)_{\alpha\gamma} , \qquad (6.26)$$

where $\mathsf{P}^{(1)}(s)$ is the matrix of elements $P_{\alpha\gamma}^{(1)}(s)$.

The nearest-neighbor probability distribution is again derived in the isothermal-isobaric ensemble with the result

$$p_{\alpha\gamma}^{(1)}(r) = x_\gamma K_{\alpha\gamma}\mathrm{e}^{-\beta\phi_{\alpha\gamma}(r)}\mathrm{e}^{-\beta pr} , \qquad (6.27)$$

so that

$$P_{\alpha\gamma}^{(1)}(s) = x_\gamma K_{\alpha\gamma}\Omega_{\alpha\gamma}(s + \beta p) , \qquad (6.28)$$

where $\Omega_{\alpha\gamma}(s)$ is the Laplace transform of $e^{-\beta\phi_{\alpha\gamma}(r)}$. The normalization condition (6.23) imposes the following relationship for the constants $K_{\alpha\gamma} = K_{\gamma\alpha}$:

$$\sum_\gamma x_\gamma K_{\alpha\gamma} \Omega_{\alpha\gamma}(\beta p) = 1 \ . \tag{6.29}$$

To complete the determination of $K_{\alpha\gamma}$, we can make use of the physical condition stating that $\lim_{r\to\infty} p_{\alpha\gamma}^{(1)}(r)/p_{\alpha\nu}^{(1)}(r)$ must be independent of the identity α of the species the reference particle belongs to, so that $K_{\alpha\gamma}/K_{\alpha\nu}$ is independent of α. It is easy to see that such a condition implies

$$K_{\alpha\gamma}^2 = K_{\alpha\alpha} K_{\gamma\gamma} \ . \tag{6.30}$$

Finally, the equation of state $n(p,T)$ is determined, as in the one-component case, from the condition $\lim_{r\to\infty} g_{\alpha\gamma}(r) = 1 \Rightarrow \lim_{s\to0} sG_{\alpha\gamma}(s) = 1$.

6.4.1 Binary Case

As a more explicit situation, here we particularize to a binary mixture. In that case, (6.26) yields

$$G_{11}(s) = \frac{Q_{11}(s)\left[1 - Q_{22}(s)\right] + Q_{12}^2(s)}{nx_1 D(s)} \ , \tag{6.31}$$

$$G_{22}(s) = \frac{Q_{22}(s)\left[1 - Q_{11}(s)\right] + Q_{12}^2(s)}{nx_2 D(s)} \ , \tag{6.32}$$

$$G_{12}(s) = \frac{Q_{12}(s)}{n\sqrt{x_1 x_2}D(s)} \ , \tag{6.33}$$

where

$$Q_{\alpha\gamma}(s) \equiv \sqrt{\frac{x_\alpha}{x_\gamma}} P_{\alpha\gamma}^{(1)}(s) = \sqrt{x_\alpha x_\gamma} K_{\alpha\gamma} \Omega_{\alpha\gamma}(s + \beta p) \ , \tag{6.34}$$

$$D(s) \equiv \left[1 - Q_{11}(s)\right]\left[1 - Q_{22}(s)\right] - Q_{12}^2(s) \ . \tag{6.35}$$

The parameters $K_{\alpha\gamma}$ are obtained from (6.29) and (6.30). First, K_{11} and K_{22} can be expressed in terms of K_{12} as

$$K_{11} = \frac{1 - x_2 K_{12}\Omega_{12}(\beta p)}{x_1 \Omega_{11}(\beta p)} \ , \quad K_{22} = \frac{1 - x_1 K_{12}\Omega_{12}(\beta p)}{x_2 \Omega_{22}(\beta p)} \ . \tag{6.36}$$

The remaining parameter K_{12} satisfies a quadratic equation whose solution is

$$K_{12} = \frac{1 - \sqrt{1 - 4x_1 x_2 R(\beta p)}}{2x_1 x_2 R(\beta p)\Omega_{12}(\beta p)} \ , \quad R(\beta p) \equiv 1 - \frac{\Omega_{11}(\beta p)\Omega_{22}(\beta p)}{\Omega_{12}^2(\beta p)} \ . \tag{6.37}$$

Finally, the equation of state becomes
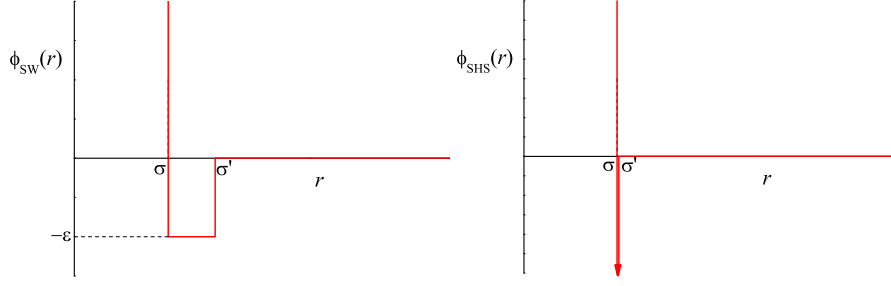
Fig. 6.3 Left panel: Square-well potential. Right panel: Sticky-hard-sphere potential.

$$n(p,T) = -\frac{1}{x_1^2 K_{11}\Omega'_{11}(\beta p) + x_2^2 K_{11}\Omega'_{11}(\beta p) + 2x_1 x_2 K_{12}\Omega'_{12}(\beta p)} \ . \tag{6.38}$$

6.5 Examples

6.5.1 Sticky Hard Rods

As an application, we consider here the sticky-hard-rod fluid, which is the one-dimensional version of the so-called sticky-hard-sphere (SHS) fluid. Let us first introduce the square-well (SW) potential (see Fig. 6.3, left panel)

$$\phi_{SW}(r) = \begin{cases} \infty, & r < \sigma, \\ -\varepsilon, & \sigma < r < \sigma', \\ 0, & r > \sigma'. \end{cases} \tag{6.39}$$

The associated Boltzmann factor is

$$e^{-\beta\phi_{SW}(r)} = \begin{cases} 0, & r < \sigma, \\ e^{\beta\varepsilon}, & \sigma < r < \sigma', \\ 1, & r > \sigma', \end{cases} \tag{6.40}$$

whose Laplace transform is

$$\Omega(s) = \frac{1}{s}\left[e^{\beta\varepsilon}\left(e^{-\sigma s} - e^{-\sigma' s}\right) + e^{-\sigma' s}\right] \ . \tag{6.41}$$

In order to apply the exact results for one-dimensional systems, we must prevent the square-well interaction from extending beyond nearest neighbors. This implies the constraint $\sigma' \le 2\sigma$.

Now we take the sticky-hard-sphere limit [39] (see Fig. 6.3, right panel)

$$\sigma' \to \sigma, \quad \varepsilon \to \infty, \quad \tau^{-1} \equiv (\sigma' - \sigma)e^{\beta\varepsilon} = \text{finite} , \tag{6.42}$$
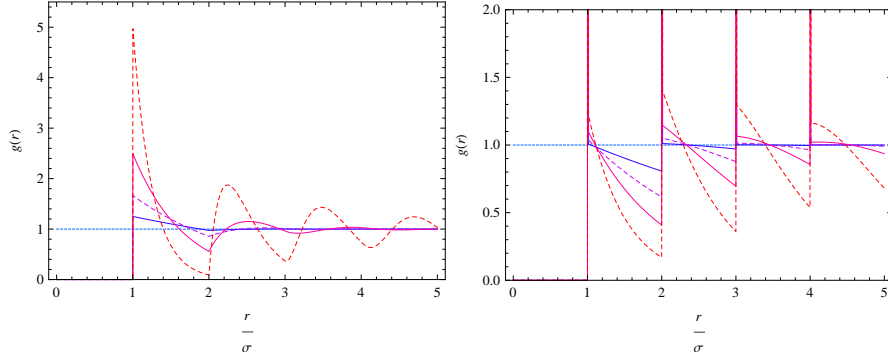
Fig. 6.4 Radial distribution function for hard rods ($\tau^{-1} = 0$, left panel) and sticky hard rods ($\tau^{-1}/\sigma = 0.5$, right panel) at several values of the packing fraction $\eta \equiv n\sigma = 0.2, 0.4, 0.6$, and 0.8, in increasing order of complexity.

where the temperature-dependent parameter τ^{-1} measures the "stickiness" of the interaction. In this limit, (6.40) and (6.41) become

$$e^{-\beta\phi(r)} = \Theta(r-\sigma) + \tau^{-1}\delta(r-\sigma) , \tag{6.43}$$

$$\Omega(s) = \left(\tau^{-1} + \frac{1}{s}\right)e^{-\sigma s} . \tag{6.44}$$

The equation of state (6.18) expresses the density as a function of temperature and pressure. Solving the resulting quadratic equation for the pressure one simply gets

$$Z \equiv \frac{\beta p}{n} = \frac{\sqrt{1 + 4\tau^{-1}n/(1-n\sigma)} - 1}{2\tau^{-1}n} . \tag{6.45}$$

In the hard-rod special case ($\tau^{-1} \to 0$), the equation of state becomes $Z = (1 - n\sigma)^{-1}$.

As for the radial distribution function, application of (6.16) gives

$$G(s) = \frac{1}{n}\frac{\left(\tau^{-1} + \frac{1}{s+\beta p}\right)e^{-\sigma s}}{\tau^{-1} + \frac{1}{\beta p} - \left(\tau^{-1} + \frac{1}{s+\beta p}\right)e^{-\sigma s}} = \frac{1}{n}\sum_{\ell=1}^{\infty}\frac{\left(\tau^{-1} + \frac{1}{s+\beta p}\right)^{\ell}}{\left(\tau^{-1} + \frac{1}{\beta p}\right)^{\ell}}e^{-\ell\sigma s} . \tag{6.46}$$

The last equality allows one to perform the inverse Laplace transform term by term with the result

$$g(r) = \sum_{\ell=1}^{\infty}\Psi_{\ell}(r-\ell\sigma)\Theta(r-\ell\sigma) , \tag{6.47}$$

where

Fig. 6.5 Threshold situation ($\sigma_{\alpha\omega} = \sigma_{\alpha\gamma} + \sigma_{\gamma\omega}$) for nearest-neighbor interaction.
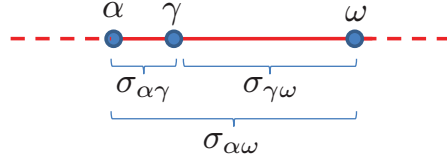
$$\Psi_\ell(r) = \frac{1}{n(\tau^{-1} + 1/\beta p)^\ell}\left[\tau^{-\ell}\delta(r) + \sum_{k=1}^{\ell}\binom{\ell}{k}\frac{\tau^{-(\ell-k)}}{(k-1)!}r^{k-1}e^{-\beta pr}\right]. \quad (6.48)$$

Note that, although an infinite number of terms formally appear in (6.47), only the first j terms are needed if one is interested in $g(r)$ in the range $1 \leq r/\sigma < j + 1$. Figure 6.4 shows $g(r)$ for hard rods ($\tau^{-1} = 0$) and a representative case of a sticky-hard-rod fluid ($\tau^{-1}/\sigma = 0.5$) at several densities [40].

Using (6.43), it is straightforward to see that the radial distribution function and the cavity functions are related by

$$g(r) = \tau^{-1}y(\sigma)\delta(r - \sigma) + y(r)\Theta(r - \sigma). \quad (6.49)$$

This, together with (6.47) and (6.48), implies the contact value

$$y(\sigma) = \frac{1}{n(\tau^{-1} + 1/\beta p)}. \quad (6.50)$$

This value is useful to obtain the mean potential energy per particle,

$$\frac{\langle E\rangle^{\text{ex}}}{N\varepsilon} = -n\tau^{-1}y(\sigma) = -\frac{1}{1 + \tau/\beta p}, \quad (6.51)$$

where the energy route (5.6) has been particularized to our system.

6.5.2 Mixtures of Nonadditive Hard Rods

As a representative example of a one-dimensional mixture, we consider here a non-additive hard-rod binary mixture [see (5.32) and Fig. 5.2]. The nearest-neighbor interaction condition requires $\sigma_{\alpha\omega} \leq \sigma_{\alpha\gamma} + \sigma_{\gamma\omega}$, $\forall(\alpha, \gamma, \omega)$, as illustrated by Fig. 6.5. In the binary case, this condition implies $2\sigma_{12} \geq \max(\sigma_1, \sigma_2)$.

The Laplace transform of $e^{-\beta\phi_{\alpha\gamma}(r)}$ is

$$\Omega_{\alpha\gamma}(s) = \frac{e^{-\sigma_{\alpha\gamma}s}}{s}. \quad (6.52)$$

The recipe described by (6.31)–(6.38) can be easily implemented. In order to obtain the pair correlation functions $g_{\alpha\gamma}(r)$ in real space, we first note that, according to (6.35),
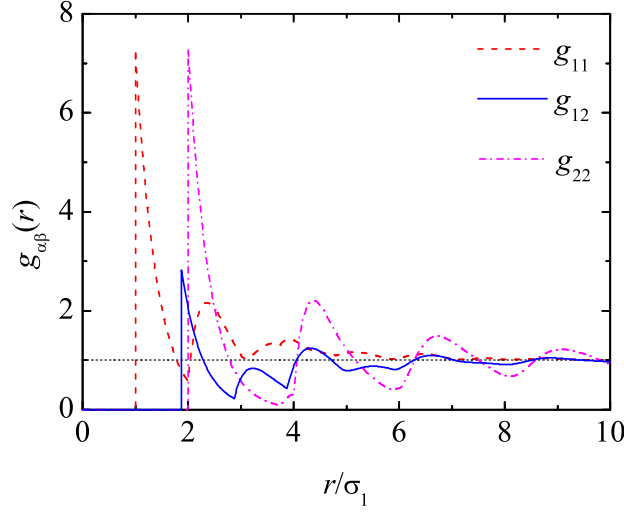
Fig. 6.6 Radial distribution functions for a one-dimensional hard-rod binary mixture with $x_1 = x_2 = \frac{1}{2}$, $\sigma_2 = 2\sigma_1$, $\sigma_{12} = \frac{15}{8}\sigma_1$, and $n\sigma_1 = \frac{1}{2}$.

$$\frac{1}{D(s)} = \sum_{m=0}^{\infty} \left[Q_{11}(s) + Q_{22}(s) + Q_{12}^2(s) - Q_{11}(s)Q_{22}(s) \right]^m . \qquad (6.53)$$

When this is inserted into (6.31)–(6.33), one can express $G_{\alpha\gamma}(s)$ as linear combinations of terms of the form

$$Q_{11}^{k_{11}}(s)Q_{22}^{k_{22}}(s)Q_{12}^{k_{12}}(s) = \frac{e^{-a(s+\beta p)}}{(s+\beta p)^k} \left(x_1 K_{11} \right)^{k_{11}+k_{12}/2} \left(x_2 K_{22} \right)^{k_{22}+k_{12}/2} , \qquad (6.54)$$

where $a \equiv k_{11}\sigma_1 + k_{22}\sigma_2 + k_{12}\sigma_{12}$ and $k \equiv k_{11} + k_{22} + k_{12}$. The inverse Laplace transforms $g_{\alpha\gamma}(r) = \mathscr{L}^{-1}\left[G_{\alpha\gamma}(s)\right]$ are readily evaluated by using the property

$$\mathscr{L}^{-1}\left[\frac{e^{-a(s+\beta p)}}{(s+\beta p)^k} \right] = e^{-\beta pr} \frac{(r-a)^{k-1}}{(k-1)!} \Theta(r-a) . \qquad (6.55)$$

Analogously to the case of (6.47), only the terms with $\{k_{11}, k_{22}, k_{12}\}$ such that $a < r_{\max}$ are needed if one is interested in distances $r < r_{\max}$. Figure 6.6 shows $g_{\alpha\gamma}(r)$ for a particular binary mixture [37].

7 Density Expansion of the Radial Distribution Function

Except for one-dimensional systems with nearest-neighbor interactions, the exact evaluation of the radial distribution function $g(r)$ or the equation of state $p(n,T)$ by

theoretical tools for arbitrary interaction potential $\phi(r)$, density n, and temperature T is simply not possible. However, the problem can be controlled if one gives up the "arbitrary density" requirement and is satisfied with the low-density regime. In such a case, a series expansion in powers of density is the adequate tool:

$$g(r) = g_0(r) + g_1(r)n + g_2(r)n^2 + \cdots , \tag{7.1}$$

$$Z \equiv \frac{p}{nk_BT} = 1 + B_2(T)n + B_3(T)n^2 + \cdots . \tag{7.2}$$

Therefore, our aim in this section is to derive expressions for the *virial* coefficients $g_k(r)$ and $B_k(T)$ as functions of T for any (short-range) interaction potential $\phi(r)$. First, a note of caution: although for an ideal gas one has $g^{\mathrm{id}}(r) = 1$ (and $Z^{\mathrm{id}} = B_1 = 1$), in a real gas $g_0(r) \neq 1$. This is because even, if the density is extremely small, interactions create correlations among particles. For instance, in a hard-sphere fluid, $g(r) = 0$ for $r < \sigma$, no matter how large or small the density is.

What is the basic idea behind the virial expansions? This is very clearly stated by E. G. D. Cohen in a recent work [41]:

The virial or density expansions reduce the intractable $N(\sim 10^{23})$–particle problem of a macroscopic gas in a volume V to a sum of an increasing number of tractable isolated few $(1, 2, 3, \ldots)$ particle problems, where each group of particles *moves alone* in the volume V of the system.

Density expansions will then appear, since the number of single particles, pairs of particles, triplets of particles, $\ldots$, in the system are proportional to n, n^2, n^3, $\ldots$, respectively, where $n = N/V$ is the number density of the particles.

In order to attain the goals (7.1) and (7.2), it is convenient to work with the grand canonical ensemble. This is because in that ensemble we already have a natural series power expansion for free: the grand canonical partition function is expressed as a series in powers of fugacity [see (3.49)]. Let us consider a generic quantity X that can be obtained from Ξ by taking its logarithm, by differentiation, etc. Then, from the expansion in (3.49) one could in principle obtain

$$X = \sum_{\ell=0}^{\infty} \bar{X}_\ell z_\Lambda^\ell , \tag{7.3}$$

where the coefficients $\bar{X}_\ell$ are related to the configuration integrals Q_N and depend on the choice of X. In particular, in the case of the average density $n = \langle N \rangle /V$, we can write

$$\boxed{n = \sum_{\ell=1}^{\infty} \ell \mathfrak{b}_\ell z_\Lambda^\ell} . \tag{7.4}$$

Now, eliminating the (modified) fugacity z_Λ between (7.3) and (7.4) one can express X in powers of n:
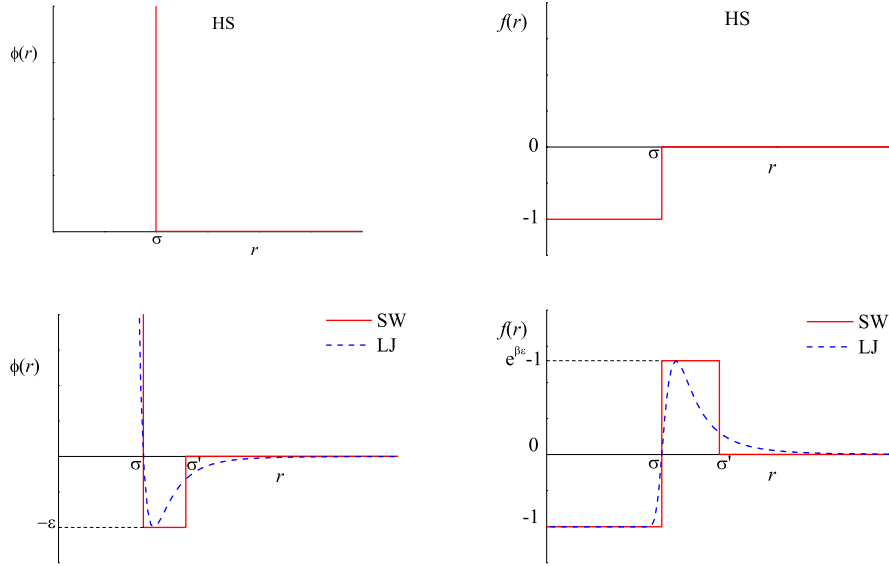
Fig. 7.1 Left panels: Hard-sphere, square-well, and Lennard-Jones potentials. Right panels: Respective Mayer functions.

$$X = \sum_{k=0}^{\infty} X_k n^k \ . \tag{7.5}$$

The first few relations are

$$X_0 = \bar{X}_0 \ , \quad X_1 = \frac{\bar{X}_1}{\mathfrak{b}_1} \ , \quad X_2 = \frac{\bar{X}_2}{\mathfrak{b}_1^2} - \frac{2\mathfrak{b}_2}{\mathfrak{b}_1^3} \bar{X}_1 \quad X_3 = \frac{\bar{X}_3}{\mathfrak{b}_1^3} - \frac{4\mathfrak{b}_2}{\mathfrak{b}_1^4} \bar{X}_2 - \left(\frac{3\mathfrak{b}_3}{\mathfrak{b}_1^4} - \frac{8\mathfrak{b}_2^2}{\mathfrak{b}_1^5} \right) \bar{X}_1 \ , \tag{7.6}$$

$$X_4 = \frac{\bar{X}_4}{\mathfrak{b}_1^4} - \frac{6\mathfrak{b}_2}{\mathfrak{b}_1^5} \bar{X}_3 - 2 \left(\frac{3\mathfrak{b}_3}{\mathfrak{b}_1^5} - \frac{10\mathfrak{b}_2^2}{\mathfrak{b}_1^6} \right) \bar{X}_2 - 2 \left(\frac{2\mathfrak{b}_4}{\mathfrak{b}_1^5} + \frac{20\mathfrak{b}_2^3}{\mathfrak{b}_1^7} - \frac{15\mathfrak{b}_2\mathfrak{b}_3}{\mathfrak{b}_1^6} \right) \bar{X}_1 \ . \tag{7.7}$$

7.1 Mayer Function and Diagrams

As we have seen many times before, the key quantity related to the interaction potential is the Boltzmann factor $e^{-\beta\phi(r)}$. Since it is equal to unity in the ideal-gas case, a convenient way of measuring deviations from the ideal gas is by means of the *Mayer function*

$$f(r) \equiv e^{-\beta\phi(r)} - 1 \ . \tag{7.8}$$

The shape of the Mayer function for the hard-sphere potential (4.18), the Lennard-Jones potential (4.14), and the square-well potential (6.39) is shown in Fig. 7.1.

Let us now rewrite (3.49) as

$$\Xi = 1 + \sum_{N=1}^{\infty} \frac{z_\Lambda^N}{N!} \int \mathrm{d}\mathbf{r}^N \, W_N(1,2,\ldots,N) \,, \qquad (7.9)$$

where

$$W_N(1,2,\ldots,N) \equiv W_N(\mathbf{r}^N) = \mathrm{e}^{-\beta \Phi_N(\mathbf{r}^N)} = \prod_{1 \le i < j \le N} (1 + f_{ij}) \,, \quad f_{ij} \equiv f(r_{ij}) \,, \quad (7.10)$$

and use has been made of (3.47) and of the pairwise additivity property (5.2). When expanding the product, $2^{N(N-1)/2}$ terms appear in W_N. To manage those terms, it is very convenient to represent them with diagrams. Each diagram contributing to W_N is made of N open circles (representing the N particles), some of them joined by a bond (representing a factor f_{ij}). The diagrams contributing to W_1–W_4 are

$$W_1(1) = 1 = \text{\Large o} \qquad , \qquad (7.11)$$

$$W_2(1,2) = 1 + f_{12} = \text{\Large o} \quad \text{\Large o} \; + \; \text{\Large o—o} \,, \qquad (7.12)$$

$$W_3(1,2,3) = (1 + f_{12})(1 + f_{13})(1 + f_{23})$$

$$= \quad + 3 \quad + 3 \quad + \quad , \qquad (7.13)$$

$$W_4(1,2,3,4) = (1 + f_{12})(1 + f_{13})(1 + f_{14})(1 + f_{23})(1 + f_{24})(1 + f_{34})$$

$$= \quad + 6 \quad + 12 \quad + 3 \quad + 4 \quad + 12$$

$$+ 4 \quad + 12 \quad + 3 \quad + 6 \quad + \quad . \qquad (7.14)$$

The numerical coefficients before some diagrams refer to the number of diagrams topologically equivalent, i.e., those that differ only in the particle labels associated with each circle. Some of the diagrams are *disconnected* (i.e., there exists at least one particle isolated from the remaining ones), while the other ones are *connected* diagrams or *clusters* (i.e., it is possible to go from any particle to any other particle by following a path made of bonds). Therefore, in general,

$$W_N(1,2,\ldots,N) = \sum \text{all (connected and disconnected) diagrams of } N \text{ particles.}$$

As we will see, in our goal of obtaining the coefficients in the expansions (7.1) and (7.2), we will follow a *distillation* process upon which we will get rid of the least

relevant diagrams at each stage, keeping only those containing more information. The first step consists of taking the logarithm of the grand partition function:

$$\ln \Xi = \sum_{\ell=1}^{\infty} \frac{z_\Lambda^\ell}{\ell!} \int d\mathbf{r}^\ell \, U_\ell(1,2,\ldots,\ell) \,, \tag{7.15}$$

where the functions $U_\ell(1,2,\ldots,\ell)$ are called *cluster* (or Ursell) functions. They are obviously related to the functions $W_N(1,2,\ldots,N)$. In fact, by comparing (7.9) and (7.15), one realizes that the relationship between $\{W_N\}$ and $\{U_\ell\}$ is exactly the same as that between *moments* and *cumulants* of a certain probability distribution [19]. In that analogy, Ξ plays the role of the *characteristic function* (or Fourier transform of the probability distribution) and $-iz_\Lambda$ plays the role of the Fourier variable. The first few relations are

$$W_1(1) = U_1(1) \,, \tag{7.16}$$

$$W_2(1,2) = U_1(1)U_1(2) + U_2(1,2) \,, \tag{7.17}$$

$$W_3(1,2,3) = U_1(1)U_1(2)U_1(3) + 3U_1(1)U_2(2,3) + U_3(1,2,3) \,, \tag{7.18}$$

$$W_4(1,2,3,4) = U_1(1)U_1(2)U_1(3)U_1(4) + 6U_1(1)U_1(2)U_2(3,4)$$
$$+ 3U_2(1,2)U_2(3,4) + 4U_1(1)U_3(2,3,4) + U_4(1,2,3,4) \,. \tag{7.19}$$

Again, each numerical factor represents the number of terms equivalent (except for particle labeling) to the indicated canonical term. Using (7.11)–(7.14), one finds

$$U_1(1) = 1 = \circ \qquad , \tag{7.20}$$

$$U_2(1,2) = f_{12} = \circ\!\!-\!\!\circ \,, \tag{7.21}$$

$$U_3(1,2,3) = 3 \; \triangle \; + \; \triangle \,, \tag{7.22}$$

$$U_4(1,2,3,4) = 12 \; \square \; + 4 \; \square \; + 12 \; \square \; + 3 \; \square$$
$$+ 6 \; \square \; + \; \square \,. \tag{7.23}$$

We observe that all the disconnected diagrams have gone away. In general,

$$U_\ell(1,2,\ldots,\ell) = \sum \text{all } \textit{connected} \text{ diagrams (i.e.,``clusters'') of } \ell \text{ particles.}$$

For later use, it is important to classify the clusters into *reducible* and *irreducible*. The first class is made of those clusters having at least one *articulation point*, i.e., a point that, if removed together with its bonds, the resulting diagram becomes disconnected. Examples of reducible clusters are

$$\text{(7.24)}$$

where the articulation points are surrounded by circles. Irreducible clusters (also called *stars*) are those clusters with no articulation point. For instance,

$$\text{(7.25)}$$

7.2 External Force. Functional Analysis

As can be seen from (3.21)–(3.23), the thermodynamic quantities can be obtained in the grand canonical ensemble from derivatives of $\ln \Xi$. On the other hand, the pair correlation function $n_2(\mathbf{r}_1, \mathbf{r}_2)$ is given by (4.9) and is not obvious at all how it can be related to a derivative of $\ln \Xi$. This is possible, however, by means of a trick consisting of assuming that an *external* potential $u(\mathbf{r})$ is added to the system. In that case,

$$\Phi_N(\mathbf{r}^N) \to \Phi_N(\mathbf{r}^N | u) = \Phi_N(\mathbf{r}^N) + \sum_{i=1}^{N} u(\mathbf{r}_i) \,, \tag{7.26}$$

$$U_\ell(\mathbf{r}^\ell | \theta) = U_\ell(\mathbf{r}^\ell) \prod_{i=1}^{\ell} \theta(\mathbf{r}_i) \,, \quad \theta(\mathbf{r}) \equiv e^{-\beta u(\mathbf{r})} \,, \tag{7.27}$$

$$\ln \Xi(\alpha, \beta, V | \theta) = \sum_{\ell=1}^{\infty} \frac{z_\Lambda^\ell}{\ell!} \int d\mathbf{r}^\ell \, U_\ell(1, 2, \dots, \ell | \theta) \,. \tag{7.28}$$

Thus, the quantities U_ℓ and $\ln \Xi$ become *functionals* of the free function $\theta(r)$.

To proceed, we will need a few simple functional derivatives:

$$\frac{\delta}{\delta \theta(\mathbf{r})} \theta(\mathbf{r}_1) = \delta(\mathbf{r}_1 - \mathbf{r}) \,, \tag{7.29}$$

$$\frac{\delta}{\delta \theta(\mathbf{r})} \prod_{k=1}^{N} \theta(\mathbf{r}_k) = \left[\prod_{k=1}^{N} \theta(\mathbf{r}_k) \right] \sum_{i=1}^{N} \frac{\delta(\mathbf{r}_i - \mathbf{r})}{\theta(\mathbf{r}_i)} \,, \tag{7.30}$$

$$\frac{\delta^2}{\delta \theta(\mathbf{r}) \delta \theta(\mathbf{r}')} \prod_{k=1}^{N} \theta(\mathbf{r}_k) = \left[\prod_{k=1}^{N} \theta(\mathbf{r}_k) \right] \sum_{i \neq j} \frac{\delta(\mathbf{r}_i - \mathbf{r}) \delta(\mathbf{r}_j - \mathbf{r}')}{\theta(\mathbf{r}_i) \theta(\mathbf{r}_j)} \,. \tag{7.31}$$

It is then straightforward to obtain the s-body reduced distribution function n_s in the absence of external force as the sth-order functional derivative of $\Xi(\theta)$ at $\theta = 1$, divided by Ξ. In particular,

$$n_1(\mathbf{r}_1) = \frac{1}{\Xi} \left. \frac{\delta \Xi(\theta)}{\delta \theta(\mathbf{r}_1)} \right|_{\theta=1} = \left. \frac{\delta \ln \Xi(\theta)}{\delta \theta(\mathbf{r}_1)} \right|_{\theta=1} , \tag{7.32}$$

$$\begin{aligned}
n_2(\mathbf{r}_1, \mathbf{r}_2) &= \frac{1}{\Xi} \left. \frac{\delta^2 \Xi(\theta)}{\delta \theta(\mathbf{r}_1) \delta \theta(\mathbf{r}_2)} \right|_{\theta=1} \\
&= \left. \frac{\delta^2 \ln \Xi(\theta)}{\delta \theta(\mathbf{r}_1) \delta \theta(\mathbf{r}_2)} \right|_{\theta=1} + \left. \frac{\delta \ln \Xi(\theta)}{\delta \theta(\mathbf{r}_1)} \frac{\delta \ln \Xi(\theta)}{\delta \theta(\mathbf{r}_2)} \right|_{\theta=1} \\
&= n_1(\mathbf{r}_1) n_1(\mathbf{r}_2) + \left. \frac{\delta^2 \ln \Xi(\theta)}{\delta \theta(\mathbf{r}_1) \delta \theta(\mathbf{r}_2)} \right|_{\theta=1} .
\end{aligned} \tag{7.33}$$

In (7.32) and (7.33), $n_1(\mathbf{r}) = n = \langle N \rangle / V$ is actually independent of the position $\mathbf{r}$ of the particle, but it is convenient to keep the notation $n_1(\mathbf{r})$ for the moment.

7.3 Root and Field Points

Taking into account (7.27), application of (7.30) and (7.31) yields

$$\left. \frac{\delta}{\delta \theta(\mathbf{r})} \int d\mathbf{r}^\ell U_\ell(\mathbf{r}^\ell|\theta) \right|_{\theta=1} = \ell \int d\mathbf{r}_2 \cdots d\mathbf{r}_\ell U_\ell(\mathbf{r}; \mathbf{r}_2, \ldots, \mathbf{r}_\ell) , \tag{7.34}$$

$$\left. \frac{\delta^2}{\delta \theta(\mathbf{r}) \delta \theta(\mathbf{r}')} \int d\mathbf{r}^\ell U_\ell(\mathbf{r}^\ell|\theta) \right|_{\theta=1} = \ell(\ell-1) \int d\mathbf{r}_3 \cdots d\mathbf{r}_\ell U_\ell(\mathbf{r}, \mathbf{r}'; \mathbf{r}_3, \ldots, \mathbf{r}_\ell) . \tag{7.35}$$

In the above two equations we have distinguished between position variables that are integrated out and those which are not. We will call *field* points to the former and *root* points to the latter. Thus,

$U_\ell(\mathbf{r}; \mathbf{r}_2, \ldots, \mathbf{r}_\ell)$: Ursell function with 1 root point and $\ell - 1$ field points ,

$U_\ell(\mathbf{r}, \mathbf{r}'; \mathbf{r}_3, \ldots, \mathbf{r}_\ell)$: Ursell function with 2 root points and $\ell - 2$ field points .

Therefore, using (7.28), (7.32), and (7.33), we have

$$n_1(\mathbf{r}_1) = z_\Lambda + \sum_{\ell=2}^{\infty} \frac{z_\Lambda^\ell}{(\ell-1)!} \int d\mathbf{r}_2 \cdots d\mathbf{r}_\ell U_\ell(1; 2, \ldots, \ell) , \tag{7.36}$$

$$n_2(\mathbf{r}_1,\mathbf{r}_2) = n_1(\mathbf{r}_1)n_1(\mathbf{r}_2) + z_\Lambda^2 U_2(1,2) + \sum_{\ell=3}^{\infty} \frac{z_\Lambda^\ell}{(\ell-2)!} \int d\mathbf{r}_3 \cdots d\mathbf{r}_\ell\, U_\ell(1,2;3,\ldots,\ell)\,.$$

(7.37)

From (7.20)–(7.23) we see that the first few one-root cluster diagrams are

$$\mathfrak{b}_1 \equiv U_1(1) = \circ \qquad,$$

(7.38)

$$2\mathfrak{b}_2 \equiv \int d\mathbf{r}_2\, U_2(1;2) = \circ\!\!-\!\!\bullet\ ,$$

(7.39)

$$6\mathfrak{b}_3 \equiv \int d\mathbf{r}_2 \int d\mathbf{r}_3\, U_3(1;2,3) = \ \wedge\ + 2\ \wedge\ +\ \triangle\ ,$$

(7.40)

$$24\mathfrak{b}_4 \equiv \int d\mathbf{r}_2 \int d\mathbf{r}_3 \int d\mathbf{r}_4\, U_4(1;2,3,4) = 6\ \sqcup\sqcup\ + 6\ \sqcup\sqcup\ +\ \bowtie\ + 3\ \bowtie$$

$$+ 3\ \boxtimes\ + 3\ \boxtimes\ + 6\ \boxtimes$$

$$+ 3\ \square\ + 3\ \boxtimes\ .$$

(7.41)

Now a filled circle means that the integration over that field point is carried out. As a consequence, some of the diagrams in (7.22) and (7.23) that were topologically equivalent need to be disentangled in (7.40) and (7.41) since the new diagrams are invariant under the permutation of two field points but not under the permutation root ↔ field. We observe from (7.36) that the expansion of density in powers of fugacity has the structure (7.4) with

$$\mathfrak{b}_\ell = \frac{1}{\ell!} \sum \text{all clusters with 1 root and } \ell-1 \text{ field points.}$$

Analogously, the first few two-root cluster diagrams are

$$U_2(1,2) = \circ\!\!-\!\!\circ\ ,$$

(7.42)

$$\int d\mathbf{r}_3\, U_3(1,2;3) = \ \wedge\ + 2\ \wedge\ +\ \triangle\ ,$$

(7.43)

$$\int d\mathbf{r}_3 \int d\mathbf{r}_4 \, U_4(1,2;3,4) = 2 \; \raisebox{-0.5em}{\includegraphics[height=2em]{d1}} \; + 4 \; \raisebox{-0.5em}{\includegraphics[height=2em]{d2}} \; + 2 \; \raisebox{-0.5em}{\includegraphics[height=2em]{d3}} \; + 4 \; \raisebox{-0.5em}{\includegraphics[height=2em]{d4}}$$

$$+ 2 \; \raisebox{-0.5em}{\includegraphics[height=2em]{d5}} \; + 2 \; \raisebox{-0.5em}{\includegraphics[height=2em]{d6}} \; + 2 \; \raisebox{-0.5em}{\includegraphics[height=2em]{d7}} \; + 4 \; \raisebox{-0.5em}{\includegraphics[height=2em]{d8}}$$

$$+ 4 \; \raisebox{-0.5em}{\includegraphics[height=2em]{d9}} \; + 2 \; \raisebox{-0.5em}{\includegraphics[height=2em]{d10}} \; + 2 \; \raisebox{-0.5em}{\includegraphics[height=2em]{d11}} \; + \; \raisebox{-0.5em}{\includegraphics[height=2em]{d12}}$$

$$+ 4 \; \raisebox{-0.5em}{\includegraphics[height=2em]{d13}} \; + \; \raisebox{-0.5em}{\includegraphics[height=2em]{d14}} \; + \; \raisebox{-0.5em}{\includegraphics[height=2em]{d15}} \; + \; \raisebox{-0.5em}{\includegraphics[height=2em]{d16}} \; . \tag{7.44}$$

In (7.42)–(7.44) we have colored those diagrams in which a direct bond between the root particles 1 and 2 exists. We will call them *closed* clusters. The other clusters in which the two root particles are not directly linked will be called *open* clusters.

Closed clusters factorize into $\circ\!\!-\!\!\circ$ times an *open* cluster. For instance,

$$\raisebox{-0.5em}{\includegraphics[height=2em]{e45}} \; = \; \circ\!\!-\!\!\circ \; \times \; \raisebox{-0.5em}{\includegraphics[height=2em]{e45b}} \; , \tag{7.45}$$

$$\raisebox{-0.5em}{\includegraphics[height=2em]{e46}} \; = \; \circ\!\!-\!\!\circ \; \times \; \raisebox{-0.5em}{\includegraphics[height=2em]{e46b}} \; , \tag{7.46}$$

$$\raisebox{-0.5em}{\includegraphics[height=2em]{e47}} \; = \; \circ\!\!-\!\!\circ \; \times \; \raisebox{-0.5em}{\includegraphics[height=2em]{e47b}} \; , \tag{7.47}$$

$$\raisebox{-0.5em}{\includegraphics[height=2em]{e48}} \; = \; \circ\!\!-\!\!\circ \; \times \; \raisebox{-0.5em}{\includegraphics[height=2em]{e48b}} \; . \tag{7.48}$$

In some cases, the root particles 1 and 2 become isolated *after* factorization.

7.4 Expansion of $n_2(\mathbf{r}_1, \mathbf{r}_2)$ in Powers of Fugacity

According to (7.37), the coefficients of the expansion of $n_2(1,2)$ come from two sources: the product $n_1(1)n_1(2)$ and the two-root clusters. The first class is represented by two-root diagrams where particles 1 and 2 are fully isolated. The second class includes open and closed clusters, the latter ones factorizing as in (7.45)–(7.48). Taking into account all of this, one realizes that the first few coefficients can be factorized as

$$z_\Lambda^2 : 1 + \circ\!\!-\!\!\circ \; = e^{-\beta \phi_{12}} \, , \tag{7.49}$$

$$z_\Lambda^3 : \ (1 + \text{о—о}) \underbrace{\left(2 \ \text{⊙} + \text{⩘} \right)}_{\alpha_3}, \tag{7.50}$$

$$z_\Lambda^4 : (1 + \text{о—о}) \ \frac{1}{2} \left(2 \ \text{⊙} + 2 \ \text{⊙} + 4 \ \text{⊙} + 2 \ \text{⊠} + 2 \ \text{⊔} \right.$$

$$\left. + 4 \ \text{⊔} + 2 \ \text{⊠} + 4 \ \text{⊠} + \text{☐} + \text{⊠} \right). \underbrace{\hspace{6cm}}_{\alpha_4} \tag{7.51}$$

It can be proved that this factorization scheme extends to all the orders. Thus, in general,

$$\boxed{n_2(\mathbf{r}_1, \mathbf{r}_2) = e^{-\beta\phi(\mathbf{r}_1, \mathbf{r}_2)} \sum_{\ell=2}^{\infty} \alpha_\ell(\mathbf{r}_1, \mathbf{r}_2) z_\Lambda^\ell}, \tag{7.52}$$

where

$$\alpha_\ell(\mathbf{r}_1, \mathbf{r}_2) = \frac{1}{(\ell - 2)!} \sum \text{all } open \text{ clusters with 2 root points and } \ell - 2 \text{ field points.}$$

A note of caution about the nomenclature employed is in order. We say that the diagrams in α_ℓ are *open* because the two root particles are not directly linked. But they are also *clusters* because either the group of ℓ particles are connected or they would be connected if we imagine a bond between the two roots. Having this in mind, we can classify the (open) clusters into (open) reducible clusters and (open) irreducible clusters (or stars), as done in (7.24) and (7.25). Of course, all open clusters with particles 1 and 2 isolated are reducible. The open reducible clusters factorize into products of open irreducible clusters. For instance,

$$\text{⊙} = \text{о—•} \ , \qquad \text{⊐} = (\text{о—•})^2 \ , \tag{7.53}$$

$$\text{⊔} = (\text{о—•})^2 \ , \qquad \text{⊔} = (\text{о—•})^2 \ , \tag{7.54}$$

$$\text{⊠} = \text{⩘} \ , \tag{7.55}$$

$$\text{(diagrams)} = \circ\!\!-\!\!\bullet \times \text{(diagram)} \quad , \quad \text{(diagram)} = \circ\!\!-\!\!\bullet \times \text{(diagram)} \quad . \qquad (7.56)$$

Examples of two-root open *irreducible* clusters ("stars") are

$$\text{(diagrams)} \quad . \qquad (7.57)$$

7.5 *Expansion in Powers of Density*

Equation (7.52) has the structure of (7.3) with $\bar{X}_0 = \bar{X}_1 = 0$ and $\bar{X}_\ell = e^{-\beta\phi}\alpha_\ell$. Elimination of fugacity in favor of density, as in (7.5), allows us to write

$$n_2(\mathbf{r}_1, \mathbf{r}_2) = e^{-\beta\phi(\mathbf{r}_1, \mathbf{r}_2)} \sum_{k=2}^{\infty} \gamma_k(\mathbf{r}_1, \mathbf{r}_2) n^k \,, \qquad (7.58)$$

where $X_0 = X_1 = 0$ and $X_k = e^{-\beta\phi}\gamma_k$. Using (7.6) and (7.7), we obtain

$$\gamma_2 = 1 \,, \qquad (7.59)$$

$$\gamma_3 = \alpha_3 - 4\mathfrak{b}_2 = \text{(diagram)} \quad , \qquad (7.60)$$

$$\gamma_4 = \alpha_4 - 6\alpha_3\mathfrak{b}_2 + 20\mathfrak{b}_2^2 - 6\mathfrak{b}_3$$

$$= \frac{1}{2}\left(2\,\text{(diagram)} + 4\,\text{(diagram)} + \text{(diagram)} + \text{(diagram)} \right). \qquad (7.61)$$

Here we have taken into account that $\mathfrak{b}_1 = \alpha_2 = 1$. The explicit diagrams displayed in (7.60) and (7.61) are the ones surviving after considering (7.39), (7.40), (7.50), (7.51), and the factorization properties (7.53)–(7.56). In general,

$$\gamma_k(\mathbf{r}_1, \mathbf{r}_2) = \frac{1}{(k-2)!} \sum \text{all open } \textit{stars} \text{ with 2 root points and } k-2 \text{ field points.}$$

A summary of the "distillation" process leading to (7.58) is presented in Table 7.1. Taking into account the definitions (4.11) and (5.5) of the radial distribution function and the cavity function, respectively, (7.58) can be rewritten as

Table 7.1 Summary of diagrams contributing to different quantities

Quantity	Expansion in powers of	Coefficient	Diagrams	Equation
Ξ	fugacity (z_Λ)	W_N	All (disconnected+clusters)	(7.9)
$\ln \Xi$	fugacity (z_Λ)	U_ℓ	Clusters (reducible+stars)	(7.15)
n_2	fugacity (z_Λ)	α_ℓ	Open clusters (reducible+stars)	(7.52)
n_2	density (n)	γ_k	Open stars	(7.58)

Fig. 7.2 Diagrams contributing to $\gamma_3(r)$, $\gamma_4(r)$, and $\gamma_5(r)$. Adapted from Table 8.3.1 of [18].
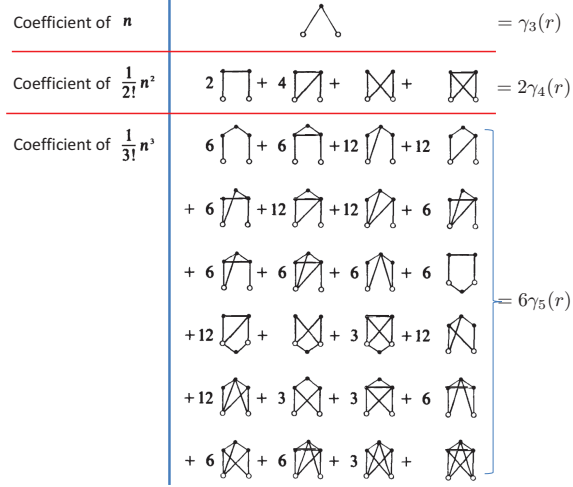
$$g(r) = e^{-\beta\phi(r)}\left[1 + \sum_{k=1}^{\infty} \gamma_{k+2}(r)n^k\right], \qquad y(r) = 1 + \sum_{k=1}^{\infty} \gamma_{k+2}(r)n^k. \qquad (7.62)$$

Thus, the functions $g_k(r)$ in (7.1) are given by $g_k(r) = e^{-\beta\phi(r)}\gamma_{k+2}(r)$. In particular, in the limit $n \to 0$, $g(r) \to g_0(r) = e^{-\beta\phi(r)}$, which differs from the ideal-gas function $g^{id}(r) = 1$, as anticipated. However, $\lim_{n\to 0} y(r) = 1$.

The formal extension of the result $g_0(r) = e^{-\beta\phi(r)}$ to any order in density *defines* the so-called *potential of mean force* $\psi(r)$ from

$$g(r) = e^{-\beta\psi(r)} \Rightarrow \psi(r) = -k_B T \ln g(r). \qquad (7.63)$$

Obviously, $\psi(r) \neq \phi(r)$, except in the limit $n \to 0$. In general,

$$\beta\psi(r) = \beta\phi(r) - \ln y(r). \qquad (7.64)$$

The diagrams representing the functions $\gamma_3(r)$ and $\gamma_4(r)$ are given by (7.60) and (7.61), respectively. As the order k increases, the number of diagrams and their complexity increase dramatically. This is illustrated by Fig. 7.2.

The simplest diagram (of course, apart from $\gamma_2 = 1$) is the one corresponding to γ_3. More explicitly,

$$\gamma_3(r_{12}) = \int d\mathbf{r}_3 \, f(r_{13})f(r_{23}) \, . \tag{7.65}$$

In the special case of hard spheres, where $f(r) = -\Theta(\sigma - r)$ (see Fig. 7.1), $\gamma_3(r)$ is the overlap volume of two spheres of radius σ whose centers are separated a distance r. In d dimensions, the result is [42]

$$\gamma_3(r) = \frac{2^{d-1} (\pi/4)^{(d-1)/2}}{\Gamma\left(\frac{d+1}{2}\right)} \sigma^d \Theta(2\sigma - r) B_{1-r^2/4\sigma^2}\left(\frac{d+1}{2}, \frac{1}{2}\right) , \tag{7.66}$$

where

$$B_x(a,b) = \int_0^x dt \, t^{a-1}(1-t)^{b-1} \tag{7.67}$$

is the incomplete beta function [43]. In particular, for three-dimensional systems,

$$\gamma_3(r) = \frac{\pi}{12}(2-r)^2(4+r)\Theta(2-r) , \tag{7.68}$$

where r is assumed to be measured in units of σ. For this system, each one of the diagrams contributing to $\gamma_4(r)$ has also been evaluated [44, 45, 46]. The results are

$$\begin{aligned} = \frac{\pi^2}{36}\frac{3}{35r}&(r-1)^4(r^3+4r^2-53r-162)\Theta(1-r) \\ & -\frac{\pi^2}{36}\frac{1}{35r}(r-3)^4(r^3+12r^2+27r-6)\Theta(3-r) , \end{aligned} \tag{7.69}$$

$$\begin{aligned} = -\frac{\pi^2}{36}\frac{2}{35r}&(r-1)^4(r^3+4r^2-53r-162)\Theta(1-r) + \frac{\pi^2}{36}\frac{1}{35r} \\ & \times(r-2)^2(r^5+4r^4-51r^3-10r^2+479r-81)\Theta(2-r) , \end{aligned} \tag{7.70}$$

$$= [\gamma_3(r)]^2 , \tag{7.71}$$

$$= \chi_A(r)\Theta(1-r) + \chi_B(r)\Theta(\sqrt{3}-r) - [\gamma_3(r)]^2 , \tag{7.72}$$

where

$$\begin{aligned} \chi_A(r) = \frac{\pi^2}{630}&(r-1)^4 \left(r^2+4r-53-162r^{-1}\right) \\ & -2\pi\left(\frac{3r^6}{560}-\frac{r^4}{15}+\frac{r^2}{2}-\frac{2r}{15}+\frac{9}{35r}\right)\cos^{-1}\frac{-r^2+r+3}{\sqrt{3(4-r^2)}} , \end{aligned} \tag{7.73}$$

$$\chi_B(r) = \pi \left[-r^2 \left(\frac{3r^2}{280} - \frac{41}{420} \right) \sqrt{3 - r^2} - \left(\frac{23}{15}r - \frac{36}{35r} \right) \cos^{-1} \frac{r}{\sqrt{3(4 - r^2)}} \right.$$

$$+ \left(\frac{3r^6}{560} - \frac{r^4}{15} + \frac{r^2}{2} + \frac{2r}{15} - \frac{9}{35r} \right) \cos^{-1} \frac{r^2 + r - 3}{\sqrt{3(4 - r^2)}}$$

$$\left. + \left(\frac{3r^6}{560} - \frac{r^4}{15} + \frac{r^2}{2} - \frac{2r}{15} + \frac{9}{35r} \right) \cos^{-1} \frac{-r^2 + r + 3}{\sqrt{3(4 - r^2)}} \right] , \qquad (7.74)$$

7.6 Equation of State. Virial Coefficients

The knowledge of the coefficients $\gamma_k(r)$ allows us to obtain the virial coefficients $B_k(T)$ defined in (7.2). As long as all the exact diagrams in $\gamma_k(r)$ are incorporated, it does not matter which route is employed to get the virial coefficients. The most straightforward route is the virial one [see (5.13)]. Therefore,

$$B_k(T) = \frac{1}{2d} \int d\mathbf{r}\, \gamma_k(r) r \frac{\partial f(r)}{\partial r} , \qquad (7.75)$$

where we have taken into account that $\partial e^{-\beta\phi(r)}/\partial r = \partial f(r)/\partial r$. In particular, the second virial coefficient is

$$B_2(T) = \frac{1}{2d} \int d\mathbf{r}\, r \frac{\partial f(r)}{\partial r} = 2^{d-1} v_d \int_0^\infty dr\, r^d \frac{\partial f(r)}{\partial r} = -d 2^{d-1} v_d \int_0^\infty dr\, r^{d-1} f(r) , \qquad (7.76)$$

where we have passed to spherical coordinates [see (5.35) and (5.36)] and have integrated by parts. Going back to a volume integral,

$$\boxed{ B_2(T) = -\frac{1}{2} \int d\mathbf{r}\, f(r) } . \qquad (7.77)$$

In general, it can be proved that [19]

$$B_k(T) = -\frac{k-1}{k!} \sum \text{all open } \textit{stars} \text{ with 1 root and } k-1 \text{ field points.}$$

The first few cases are

$$B_2(T) = -\frac{1}{2} \raisebox{-0.3em}{\input{graphic}} , \quad B_3(T) = -\frac{1}{3} \raisebox{-0.5em}{\input{graphic}} , \qquad (7.78)$$

$$B_4(T) = -\frac{1}{8}\left(3\ \blacksquare\ +6\ \blacksquare\ +\ \blacksquare\ \right).\qquad(7.79)$$

7.6.1 Second Virial Coefficient

For d-dimensional hard spheres, the second virial coefficient is simply

$$B_2 = 2^{d-1}v_d\sigma^d\ ,\qquad(7.80)$$

so that the equation of state truncated after B_2 is

$$Z \equiv \frac{p}{nk_BT} = 1 + 2^{d-1}\eta + \cdots\ ,\qquad(7.81)$$

where

$$\boxed{\eta \equiv nv_d\sigma^d}\qquad(7.82)$$

is the packing fraction [see (5.41) for its definition in the multicomponent case].

The hard-sphere Mayer function is independent of temperature (see Fig. 7.1) and so are the hard-sphere virial coefficients. On the other hand, in general $B_2(T)$ is a function of temperature. As a simple example, the result for the square-well potential [see (6.39) and Fig. 7.1] is

$$B_2(T) = 2^{d-1}v_d\sigma^d\left\{1 - \left(e^{\beta\varepsilon} - 1\right)\left[(\sigma'/\sigma)^d - 1\right]\right\}.\qquad(7.83)$$

The evaluation is less straightforward in the case of continuous potentials like the Lennard-Jones one [see (4.14)]. Let us consider the more general case of the Lennard-Jones (2s-s) potential (with $s > d$):

$$\phi(r) = 4\varepsilon\left[\left(\frac{\sigma}{r}\right)^{2s} - \left(\frac{\sigma}{r}\right)^s\right].\qquad(7.84)$$

Starting from the last equality in (7.76) and introducing the change of variable $r \to t \equiv \sqrt{8\beta\varepsilon}(\sigma/r)^s$, one has

$$B_2(T) = -2^{d-1}v_d\sigma^d\frac{d}{s}(8\beta\varepsilon)^{d/2s}\int_0^\infty dt\,t^{-d/s-1}\left(e^{-t^2/2+\sqrt{2\beta\varepsilon}t} - 1\right).\qquad(7.85)$$

The integral can be compared with the following integral representation of the parabolic cylinder function [43]:

$$D_a(z) = \frac{e^{-z^2/4}}{\Gamma(-a)}\int_0^\infty dt\,t^{-a-1}\left(e^{-t^2/2-zt} - 1\right),\quad 0 < \mathrm{Re}(a) < 1.\qquad(7.86)$$
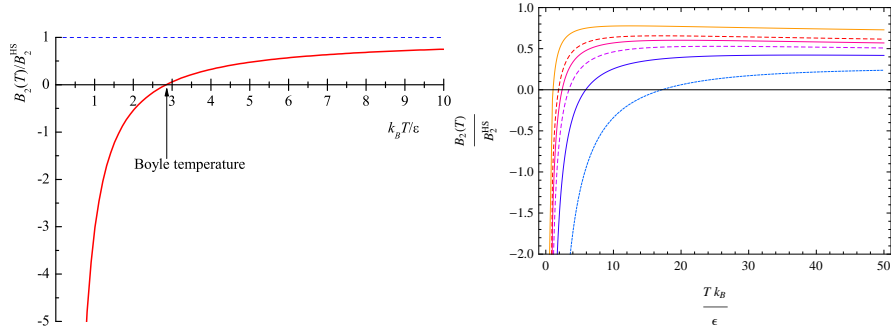
Thus, (7.85) becomes

Fig. 7.3 Left panel: $B_2(T)$ for a square-well fluid with $\sigma'/\sigma = 1.5$. Right panel: $B_2(T)$ for a Lennard-Jones ($2s$-s) fluid with $s = 4, 5, 6, 7, 8$, and 12, from bottom to top.

$$\frac{B_2(T)}{B_2^{\mathrm{HS}}} = \Gamma\left(1 - \frac{d}{s}\right)\left(\frac{8}{T^*}\right)^{d/2s} e^{1/2T^*} D_{d/s}\left(-\sqrt{\frac{2}{T^*}}\right), \qquad (7.87)$$

where $T^* \equiv k_B T/\varepsilon$ and B_2^{HS} is given by (7.80). To the best of the author's knowledge, the compact expression (7.87) has not been published before.

Figure 7.3 shows the temperature-dependence of B_2, relative to the hard-sphere value with the same σ, for (three-dimensional) square-well and Lennard-Jones fluids [47]. For low temperatures the attractive part of the potential dominates and thus $B_2 < 0$, meaning that in the low-density regime the pressure is smaller than that of an ideal gas at the same density. Reciprocally, $B_2 > 0$ for high temperatures, in which case the repulsive part of the potential prevails. The transition between both situations takes place at the so-called Boyle temperature T_B, where $B_2 = 0$. Note that, while the square-well second virial coefficient monotonically grows with temperature and asymptotically tends to the hard-sphere value, the Lennard-Jones coefficient reaches a maximum (smaller than the hard-sphere value corresponding to a diameter σ) and then decreases very slowly. This reflects the fact that for very high temperatures the system behaves practically as a hard-sphere system but with an *effective* diameter smaller than the nominal value σ.

7.6.2 Higher-Order Virial Coefficients for Hard Spheres

The evaluation of virial coefficients beyond B_2 becomes a formidable task as the order increases and it is necessary to resort to numerical Monte Carlo methods to perform the multiple integrals involved. Needless to say, the task is much more manageable in the case of hard spheres. In the one-component case, the third and fourth virial coefficients are analytically known [48, 49] and B_5–B_{12} have been numerically evaluated [50, 51, 52, 53, 54].

The third virial coefficient is [55]

Fig. 7.4 Second and third virial coefficients for d-dimensional hard spheres. Source: [50].

Table I.   The Second and Third Virial Coefficients as Functions of Dimension

D	B_2	B_3/B_2^2 Exact	B_3/B_2^2 Numerical
1	σ	1	1
2	$\pi\sigma^2/2$	$\dfrac{4}{3} - \dfrac{\sqrt{3}}{\pi}$	$0.782004\cdots$
3	$2\pi\sigma^3/3$	$5/8$	0.625
4	$\pi^2\sigma^4/4$	$\dfrac{4}{3} - \dfrac{\sqrt{3}}{\pi}\dfrac{3}{2}$	$0.506340\cdots$
5	$4\pi^2\sigma^5/15$	$53/2^7$	$0.414063\cdots$
6	$\pi^3\sigma^6/12$	$\dfrac{4}{3} - \dfrac{\sqrt{3}}{\pi}\dfrac{9}{5}$	$0.340941\cdots$
7	$8\pi^3\sigma^7/105$	$289/2^{10}$	$0.282227\cdots$
8	$\pi^4\sigma^8/48$	$\dfrac{4}{3} - \dfrac{\sqrt{3}}{\pi}\dfrac{279}{140}$	$0.234614\cdots$
9	$16\pi^4\sigma^9/945$	$6413/2^{15}$	$0.195709\cdots$
10	$\pi^5\sigma^{10}/240$	$\dfrac{4}{3} - \dfrac{\sqrt{3}}{\pi}\dfrac{297}{140}$	$0.163728\cdots$
11	$32\pi^5\sigma^{11}/10395$	$35995/2^{18}$	$0.137310\cdots$
12	$\pi^6\sigma^{12}/1440$	$\dfrac{4}{3} - \dfrac{\sqrt{3}}{\pi}\dfrac{243}{110}$	$0.115398\cdots$

Fig. 7.5 Fourth virial coefficient for d-dimensional hard spheres. Source: [49].

Table II.   Exact and Numerical Values of the Fourth Virial Coefficient

D	B_4/B_2^3	Decimal expansion
2	$2 - \frac{9}{2}\frac{\sqrt{3}}{\pi} + 10\frac{1}{\pi^2}$	$0.53223180\ldots$
3	$\frac{2707}{4480} + \frac{219}{2240}\frac{\sqrt{2}}{\pi} - \frac{4131}{4480}\frac{\arccos(1/3)}{\pi}$	$0.28694950598\ldots$
4	$2 - \frac{27}{4}\frac{\sqrt{3}}{\pi} + \frac{832}{45}\frac{1}{\pi^2}$	$0.15184606235\ldots$ $0.151846054(20)^{[9]}$ $0.15184(7)^{[13]}$
5	$\frac{25315393}{32800768} + \frac{3888425}{16400384}\frac{\sqrt{2}}{\pi} - \frac{67183425}{32800768}\frac{\arccos(1/3)}{\pi}$	$0.07597248028\ldots$ $0.075972512(4)^{[9]}$ $0.07592(6)^{[13]}$ $0.075978(4)^{[14]}$
6	$2 - \frac{81}{10}\frac{\sqrt{3}}{\pi} + \frac{38848}{1575}\frac{1}{\pi^2}$	$0.03336314\ldots$
7	$\frac{299189248759}{290596061184} + \frac{159966456685}{435894091776}\frac{\sqrt{2}}{\pi} - \frac{292926667005}{96865353728}\frac{\arccos(1/3)}{\pi}$	$0.00986494662\ldots$ $0.009873(3)^{[14]}$
8	$2 - \frac{2511}{280}\frac{\sqrt{3}}{\pi} + \frac{17605024}{606375}\frac{1}{\pi^2}$	$-0.00255768\ldots$
9	$\frac{2886207717678787}{2281372811001856} + \frac{2698457589952103}{5703432027504640}\frac{\sqrt{2}}{\pi} - \frac{8656066770083523}{2281372811001856}\frac{\arccos(1/3)}{\pi}$	$-0.00858079817\ldots$ $-0.008575(3)^{[14]}$
10	$2 - \frac{2673}{280}\frac{\sqrt{3}}{\pi} + \frac{49048616}{1528065}\frac{1}{\pi^2}$	$-0.01096248\ldots$
11	$\frac{17357449486516274011}{11932824186709344256} + \frac{16554115383300832799}{29832060466773360640}\frac{\sqrt{2}}{\pi}$ $- \frac{52251492946866520923}{11932824186709344256}\frac{\arccos(1/3)}{\pi}$	$-0.01133719858\ldots$ $-0.011333(3)^{[14]}$
12	$2 - \frac{2187}{220}\frac{\sqrt{3}}{\pi} + \frac{11565604768}{337702365}\frac{1}{\pi^2}$	$-0.010670281\ldots$

$$\frac{B_3}{B_2^2} = 2\mathrm{I}_{3/4}\left(\frac{d+1}{2}, \frac{1}{2}\right), \qquad (7.88)$$

where $\mathrm{I}_x(a,b) = \mathrm{B}_x(a,b)\Gamma(a+b)/\Gamma(a)\Gamma(b)$ is the *regularized* incomplete beta function [see (7.67)]. The explicit expressions of B_2 and B_3/B_2^2 for $d \leq 12$ can be found in Fig. 7.4. We note that B_3/B_2^2 is a rational number if $d =$ odd, while it is an

D	B_5/B_2^4	B_6/B_2^5	B_7/B_2^6	B_8/B_2^7	B_9/B_2^8	B_{10}/B_2^9
2	$0.33355604(1)^*$	0.1988425(42)	0.1148728(43)	0.0649930(34)	0.0362193(35)	0.0199537(80)
3	$0.110252(1)^*$	0.03888198(91)	0.01302354(91)	0.0041832(11)	0.0013094(13)	0.0004035(15)
4	0.0357041(17)	0.0077359(16)	0.0014303(19)	0.0002888(18)	0.0000441(22)	0.0000113(31)
5	0.0129551(13)	0.0009815(14)	0.0004162(19)	$-0.0001120(20)$	0.0000747(26)	$-0.0000492(48)$
6	0.0075231(11)	$-0.0017385(13)$	0.0013066(18)	$-0.0008950(30)$	0.0006673(45)	$-0.000525(16)$
7	0.0070724(10)	$-0.0035121(11)$	0.0025386(16)	$-0.0019937(28)$	0.0016869(41)	$-0.001514(14)$
8	0.00743092(93)	$-0.0045164(11)$	0.0034149(15)	$-0.0028624(26)$	0.0025969(38)	$-0.002511(13)$

Fig. 7.6 Fifth to tenth virial coefficient for d-dimensional hard spheres. The numbers in parentheses indicate the statistical error in the last significant digits. Source: [52].

irrational number (since it includes $\sqrt{3}/\pi$) if $d =$ even. The influence of the parity of d is also present in the exact evaluation of B_4, which has been carried out separately for $d =$ even [50] and $d =$ odd [49]. The results for $d \leq 12$ are shown in Fig. 7.5. We see that B_4/B_2^3 is always an irrational number that includes $\sqrt{3}/\pi$ and $1/\pi^2$ if $d =$ even, while it includes $\sqrt{2}/\pi$ and $\cos^{-1}(1/3)/\pi$ if $d =$ odd. Interestingly, the fourth virial coefficient becomes negative for $d \geq 8$.

The Monte Carlo numerical values of the virial coefficients B_5–B_{10} up to $d = 8$ [52, 53] are displayed in Fig. 7.6. While B_5, B_7, and B_9 remain positive (at least if $d \leq 8$), B_6, B_8, and B_{10} become negative if $d \geq 6$, $d \geq 5$, and $d \geq 5$, respectively. While the known first ten and twelve virial coefficients are positive if $d = 4$ and $d = 3$ [54], respectively, the behavior observed when $d \geq 5$ shows that this does not need to be necessarily the case for all the virial coefficients. It is then legitimate to speculate that, for three-dimensional hard-sphere systems, a certain high-order coefficient B_k (perhaps with $k =$ even) might become negative, alternating in sign thereafter. This scenario would be consistent with a singularity of the equation of state on the (density) negative real axis that would determine the radius of convergence of the virial series [52, 53, 56].
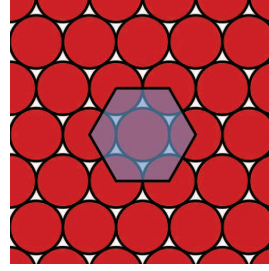
7.6.3 Simple Approximations

In terms of the packing fraction η, the virial series (7.2) becomes

$$Z = 1 + 2^{d-1}\eta + b_3\eta^2 + b_4\eta^3 + \cdots , \quad b_k \equiv B_k/(v_d\sigma^d)^{k-1} . \tag{7.89}$$

Although incomplete, the knowledge of the first few virial coefficients is practically the only access to exact information about the equation of state of the hard-sphere fluid. If the packing fraction η is low enough, the virial expansion truncated after a given order is an accurate representation of the exact equation of state. However, this tool is not practical at moderate or high values of η. In those cases, instead of truncating the series, it is far more convenient to construct an *approximant* which, while keeping a number of exact virial coefficients, includes all of orders in density [57]. The most popular class is made by Padé approximants [58], where the com-

Fig. 7.7 Close-packing configuration in a system of hard disks. The fraction of the total area occupied by the disks is $\eta_{cp} = \frac{\sqrt{3}\pi}{6}$. Source: http://en.wikipedia.org/wiki/Packing_problem.

pressibility factor Z is approximated by the ratio of two polynomials. Obviously, as the number of retained exact virial coefficients increases so does the complexity of the approximant. Here, however, we will deal with simpler, but yet accurate, approximations.

Hard disks ($d = 2$)

In the two-dimensional case, the virial series truncated after the third virial coefficient is

$$Z = 1 + 2\eta + b_3\eta^2 + \cdots, \quad \eta \equiv \frac{\pi}{4}n\sigma^2, \tag{7.90}$$

where

$$b_3 = 4\left(\frac{4}{3} - \sqrt{3}\pi\right) = 3.128\cdots \simeq \frac{25}{8}. \tag{7.91}$$

Henderson's approximation [59] consists of

$$\boxed{Z = \frac{1 + \eta^2/8}{(1-\eta)^2}} = 1 + 2\eta + \frac{25}{8}\eta^2 + \cdots. \tag{7.92}$$

As we see, it retains the exact second virial coefficient and a rational-number approximation of the third virial coefficient. On the other hand, (7.92) assumes that the pressure is finite for any $\eta < 1$, whereas by geometrical reasons the maximum conceivable packing fraction is the close-packing value $\eta_{cp} = \frac{\sqrt{3}\pi}{6} \simeq 0.907$ (see Fig. 7.7).

Another simple approximation [60, 61] exploits the second virial coefficient $b_2 = 2$ only but imposes a pole at η_{cp}. Thus, the constraints are

$$Z = \begin{cases} 1 + 2\eta + \cdots, & \eta \ll 1, \\ \infty, & \eta \to \eta_{cp}. \end{cases} \tag{7.93}$$

A simple approximation satisfying those requirements is

Fig. 7.8 Comparison between
computer-simulation values
of the equation of state of a
hard-disk fluid [62] and the
theoretical approximations
(7.92) (label H) and (7.94)
(label SHY).
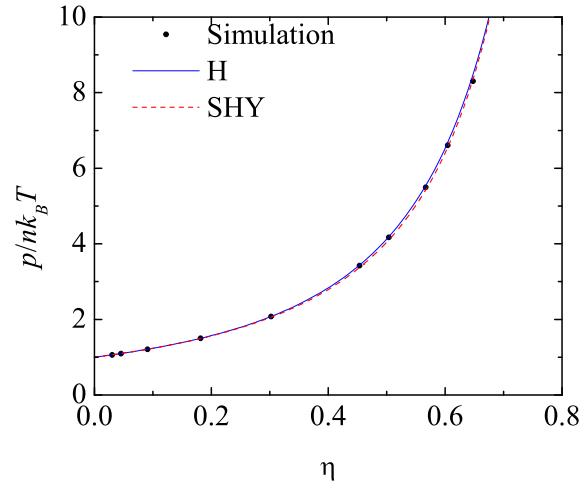
Table 7.2 The second row shows the round-off integer of the known first twelve reduced virial
coefficients b_k of a three-dimensional hard-sphere fluid. The third row gives the values obtained
from the formula $k^2 + k - 2$. Finally, the deviation Δb_k of the latter values from the true values of
b_k are shown in the fourth row.

k	2	3	4	5	6	7	8	9	10	11	12
Round-off	4	10	18	28	40	53	69	86	106	128(5)	111(30)
$k^2 + k - 2$	4	10	18	28	40	54	70	88	108	130	154
Δb_k	0	0	-0.36	-0.22	0.18	0.66	1.5	2.2	2.2(4)	2(5)	43(30)

$$Z = \frac{1}{1 - 2\eta + \frac{2\eta_{cp} - 1}{\eta_{cp}^2}\eta^2}. \tag{7.94}$$

Figure 7.8 compares the predictions of (7.92) and (7.94) against computer simu-
lations [62]. Despite their simplicity, both approximations exhibit an excellent per-
formance, even at packing fractions where the pressure is about ten times higher
than the ideal-gas one.

Hard spheres ($d = 3$)

In the three-dimensional case, $\eta = (\pi/6)n\sigma^3$ and the second and third reduced virial
coefficients are integer numbers: $b_2 = 4$ and $b_3 = 10$. The fourth virial coefficient,
however, is a transcendental number (see Fig. 7.11), namely $b_4 = 18.36476838\cdots$.
If we round off this coefficient ($b_4 \simeq 18$), we realize that $b_4 - b_3 = (b_3 - b_2) + 2$.
Interestingly, by continuing the rounding-off process, the relationship $b_k - b_{k-1} = (b_{k-1} - b_{k-2}) + 2$ extends up to $k = 6$, as shown in Table 7.2.

Fig. 7.9 Compressibility factor for three-dimensional hard spheres, as obtained from computer simulations [64] and from the Carnahan–Starling equation of state (7.96).
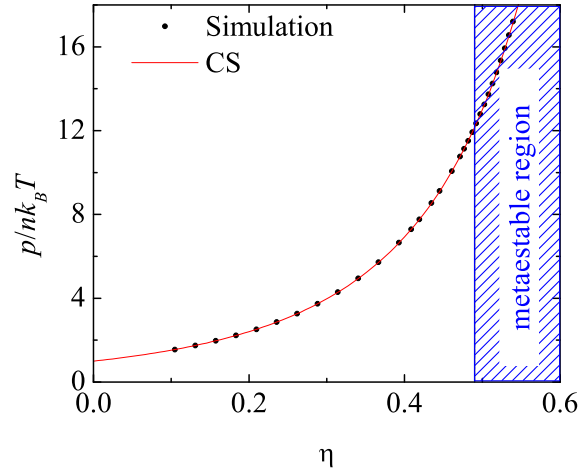
In the late sixties only the first six virial coefficients were accurately known and thus Carnahan and Starling [63] proposed to extrapolate the relationship $b_k - b_{k-1} = (b_{k-1} - b_{k-2}) + 2$ to any $k \geq 2$, what is equivalent to the approximation

$$b_k = k^2 + k - 2 . \tag{7.95}$$

By summing the virial series within that approximation, they obtained the famous Carnahan–Starling (CS) equation of state:

$$\boxed{Z_{\text{CS}} = \frac{1 + \eta + \eta^2 - \eta^3}{(1-\eta)^3}} . \tag{7.96}$$

The corresponding isothermal susceptibility is

$$\chi_{\text{CS}} = \left[\frac{\partial (\eta Z_{\text{CS}})}{\partial \eta} \right]^{-1} = \frac{(1-\eta)^4}{1 + 4\eta + 4\eta^2 - 4\eta^3 + \eta^4} . \tag{7.97}$$

Figure 7.9 shows that, despite its simplicity, the Carnahan–Starling equation exhibits an excellent performance over the whole fluid stable region and even in the metastable fluid region ($\eta \geq 0.492$ [65]), where the crystal is the stable phase. This is remarkable because, as shown in Table 7.2, the approximation $b_k = k^2 + k - 2$ fails to capture the rounding-off of the virial coefficient b_k for $k \geq 7$, the deviation Δb_k tending to increase with k. The explanation might partially lie in the fact that the Carnahan–Starling recipe underestimates b_4 and b_5 but this is compensated by an overestimate of the higher virial coefficients. Apart from that, and analogously to Henderson's equation (7.92), the Carnahan–Starling equation (7.96) provides finite values even for packing fractions higher than the close-packing value $\eta_{\text{cp}} = \pi \sqrt{2}/6 \simeq 0.7405$.

Fig. 8.1 Left panel: Leonard Salomon Ornstein (1880–1941). Right panel: Frits Zernike (1888–1966).

Fig. 8.2 Sketch of the meaning of the Ornstein–Zernike relation (8.1).
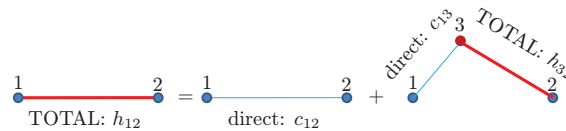
8 Ornstein–Zernike Relation and Approximate Integral Equation Theories

Similarly to what was said above in connection with the formal virial expansion (7.2) of the equation of state, the virial representation (7.62) of the radial distribution function is only practical in the low-density regime, in which case the expansion can be truncated after a certain low order. On the other hand, at moderate or high densities this strategy is not useful and in that case it is better to resort to approximations that include all the orders of density, in analogy to what was done in the hard-sphere equation-of-state case with (7.92), (7.94), and (7.96). In order to construct those approximations, a crucial quantity is the *direct correlation function* $c(r)$.

8.1 Direct Correlation Function

We recall that the total correlation function is defined by (4.15). This function owes its name to the fact that it measures the degree of spatial correlation between two particles separated a distance r due not only to their *direct* interaction but also *indirectly* through other intermediate or "messenger" particles. In fact, the range of $h(r)$ is usually much larger than that of the potential $\phi(r)$ itself, as illustrated by Figs. 4.2 and 6.4. In fluids with a gas-liquid phase transition, $h(r)$ decays algebraically at the *critical point*, so that the integral $\int d\mathbf{r}\, h(r)$ diverges and so does the isothermal compressibility κ_T [see (5.1)], a phenomenon known as *critical opalescence* [18, 22].

It is then important to disentangle from $h(r)$ its direct and indirect contributions. This aim was addressed in 1914 by the Dutch physicists L. S. Ornstein and F. Zernike (see Fig. 8.1). They defined the *direct* correlation function $c(r)$ by the

integral relation

$$h(r_{12}) = c(r_{12}) + n \int d\mathbf{r}_3 \, c(r_{13}) h(r_{32}) \, . \tag{8.1}$$

The idea behind the Ornstein–Zernike (OZ) relation (8.1) is sketched in Fig. 8.2: the total correlation function h_{12} between particles 1 and 2 can be decomposed into the direct correlation function c_{12} plus the indirect part, the latter being mediated by a messenger particle 3 that is directly correlated to 1 and totally correlated to 2.

Thanks to the convolution structure of the indirect part, the Ornstein–Zernike relation (8.1) becomes $\widetilde{h}(k) = \widetilde{c}(k) + n\widetilde{c}(k)\widetilde{h}(k)$ in Fourier space or, equivalently,

$$\widetilde{h}(k) = \frac{\widetilde{c}(k)}{1 - n\widetilde{c}(k)} \, , \quad \widetilde{c}(k) = \frac{\widetilde{h}(k)}{1 + n\widetilde{h}(k)} \, . \tag{8.2}$$

Thus, the compressibility route to the equation of state (5.1) can be rewritten as

$$\chi \equiv nk_B T \kappa_T = \frac{1}{1 - n\widetilde{c}(0)} \, . \tag{8.3}$$

Therefore, even if $\widetilde{h}(0) \to \infty$ (at the critical point), $\widetilde{c}(0) \to n^{-1} =$ finite, thus showing that $c(r)$ is much shorter ranged than $h(r)$, as expected.

It is important to bear in mind that the Ornstein–Zernike relation (8.1) *defines* $c(r)$. Therefore, it is *not* a closed equation. However, if an *approximate closure* of the form $c(r) = \mathscr{F}[h(r)]$ is assumed, one can obtain a *closed integral equation*:

$$h(r) = \mathscr{F}[h(r)] + n \int d\mathbf{r}' \, \mathscr{F}[h(r')] h(|\mathbf{r} - \mathbf{r}'|) \, . \tag{8.4}$$

In contrast to a truncated density expansion, a closure is applied to *all orders* in density.

Before addressing the *closure problem* let us first derive *formally exact* relations between $c(r)$, $h(r)$, and some other functions.

8.2 Classification of Diagrams

We recall from (7.62) (see also Fig. 7.2) that

$$y(r_{12}) = 1 + n \, \triangle + \frac{n^2}{2} \left(2 \, \square + 4 \, \boxtimes + \, \square + \, \boxtimes \right) + \cdots . \tag{8.5}$$

We now introduce the following classification of *open* stars:

- **"Chains" (or nodal diagrams), $\mathscr{C}(r)$:** Subset of *open* diagrams having at least one *node*. A node is a field particle which must be *necessarily* traversed when going from one root to the other one.

The first few terms in the expansion of $\mathscr{C}(r_{12})$ are

$$\mathscr{C}(r_{12}) = n \overset{\bullet}{\wedge} + \frac{n^2}{2} \left(2\, \square\!\square + 4\, \boxslash \right) + \cdots . \tag{8.6}$$

- **Open "parallel" diagrams (or open "bundles"), $\mathscr{P}(r)$:** Subset of *open* diagrams with no nodes, such that there are at least *two* totally independent ("parallel") paths to go from one root to the other one. The existence of parallel paths means that if the roots (together with their bonds) were removed, the resulting diagram would fall into two or more pieces.

The function $\mathscr{P}(r)$ is of second order in density:

$$\mathscr{P}(r_{12}) = \frac{n^2}{2}\, \square + \cdots . \tag{8.7}$$

- **"Bridge" (or "elementary") diagrams, $\mathscr{B}(r)$:** Subset of *open* diagrams with no nodes, such that there do *not* exist two totally independent ways to go from one root to the other one.

Analogously to $\mathscr{P}(r)$, the bridge function $\mathscr{B}(r)$ is of order n^2:

$$\mathscr{B}(r_{12}) = \frac{n^2}{2}\, \boxslash + \cdots . \tag{8.8}$$

Figure 8.3 shows the classification to order n^3. Since the three classes exhaust all the open stars, we can write

$$\boxed{y(r) = 1 + \mathscr{C}(r) + \mathscr{P}(r) + \mathscr{B}(r)} . \tag{8.9}$$

As for the total correlation function, the diagrams contributing to it are

Fig. 8.3 First few chain, open parallel, and bridge diagrams. Adapted from Table 8.3.1 of [18].

$$h(r_{12}) = (1 + \,\circ\!\!-\!\!\circ\,)y(r_{12}) - 1$$

$$= \circ\!\!-\!\!\circ\; + n \left(\triangle + \triangle \right) + \frac{n^2}{2} \left(2 \,\square\, + 4 \,\square\, + \square \right.$$

$$\left. + \square + 2 \,\square\, + 4 \,\square\, + \square + \square \right) + \cdots$$

$$= \sum_{k=0}^{\infty} \frac{n^k}{k!} \sum open \text{ and } closed \text{ stars with 2 roots and } k \text{ field points.} \qquad (8.10)$$

It is not worth classifying the closed diagrams. Instead, they join the open bundles to create an augmented class:

- **"Parallel" diagrams (or "bundles"), $\mathscr{P}^+(r)$:** All *closed* diagrams plus the *open* bundles.

The first few ones are

$$\mathscr{P}^+(r_{12}) = \circ\!\!-\!\!\circ\; + n \,\triangle\, + \frac{n^2}{2} \left(\square + 2\,\square\, + 4\,\square\, \right.$$

$$\left. + \square + \square \right) + \cdots . \qquad (8.11)$$

Obviously,

$$h(r) = \mathscr{C}(r) + \mathscr{P}^{+}(r) + \mathscr{B}(r). \tag{8.12}$$

Why this classification? There are two main reasons. First, open parallel diagrams ($\mathscr{P}$) factorize into products of chains ($\mathscr{C}$) and bridge diagrams ($\mathscr{B}$). For instance,

$$\boxed{\;} = \left(\bigwedge \right)^{2}. \tag{8.13}$$

As a consequence, it can be proved that

$$\mathscr{P} = \frac{1}{2}(\mathscr{C} + \mathscr{B})^{2} + \frac{1}{3!}(\mathscr{C} + \mathscr{B})^{3} + \cdots$$
$$= e^{\mathscr{C} + \mathscr{B}} - (1 + \mathscr{C} + \mathscr{B}) \Rightarrow \boxed{\mathscr{C} + \mathscr{B} = \ln(1 + \mathscr{C} + \mathscr{P} + \mathscr{B})}. \tag{8.14}$$

Making use of (8.14) in (8.9), we obtain $\ln y = \mathscr{C} + \mathscr{B}$ or, equivalently,

$$\boxed{\ln g(r) = -\beta \phi(r) + \mathscr{C}(r) + \mathscr{B}(r)}. \tag{8.15}$$

The second important reason for the classification of open stars is that, as we are about to see, the chains ($\mathscr{C}$) *do not* contribute to the direct correlation function $c(r)$.

Let us first rewrite (8.10) as

$$h(r_{12}) = \;\circ\!\!-\!\!\circ\; + n \left(\bigwedge + \bigwedge \right) + \frac{n^{2}}{2} \left(2\,\boxed{\;} + 4\,\boxed{\;} + \boxed{\;} \right.$$
$$\left. + \boxed{\;} + 2\,\boxed{\;} + 4\,\boxed{\;} + \boxed{\;} + \boxed{\;} \right) + \cdots, \tag{8.16}$$

where the chains are marked in blue. Next, the Ornstein–Zernike relation (8.1) or (8.2) can be iterated to yield

$$c = h - nh*h + n^{2}h*h*h - n^{3}h*h*h*h + \cdots, \tag{8.17}$$

where the asterisk denotes a convolution integral. The diagrams representing those convolutions are always chains. For instance,

$$h*h = \int d\mathbf{r}_{3}\, h(r_{13})h(r_{32}) = \bigwedge + 2n \left(\boxed{\;} + \boxed{\;} \right) + \cdots, \tag{8.18}$$

$$h*h*h = \int d\mathbf{r}_{3} \int d\mathbf{r}_{4}\, h(r_{13})h(r_{34})h(r_{42}) = \boxed{\;} + \cdots. \tag{8.19}$$

Inserting (8.16), (8.18), and (8.19) into (8.17), one obtains

$$c(r_{12}) = \text{[diagram]} + n \, \text{[diagram]} + \frac{n^2}{2} \left(\text{[diagram]} + \text{[diagram]} + 2 \, \text{[diagram]} + 4 \, \text{[diagram]} \right.$$

$$\left. + \text{[diagram]} + \text{[diagram]} \right) + \cdots . \tag{8.20}$$

Thus, as anticipated, all chain diagrams cancel out! This is not surprising after all since the chains are the open diagrams that more easily can be "stretched out", thus allowing particles 1 and 2 to be be correlated via intermediate particles, even if the distance r_{12} is much larger than the interaction range. Note, however, that the direct correlation function is not limited to closed diagrams but also includes the open diagrams with no nodes. Therefore,

$$\boxed{c(r) = \mathscr{P}^+(r) + \mathscr{B}(r)} . \tag{8.21}$$

From (8.9), (8.12), (8.15), and (8.21) we can extract the chain function in three alternative ways:

$$\mathscr{C}(r) = e^{\beta\phi(r)} g(r) - 1 - \mathscr{P}(r) - \mathscr{B}(r) , \tag{8.22}$$

$$\mathscr{C}(r) = \ln g(r) + \beta\phi(r) - \mathscr{B}(r) , \tag{8.23}$$

$$\mathscr{C}(r) = h(r) - c(r) . \tag{8.24}$$

Combination of (8.22) and (8.24) yields

$$\boxed{c(r) = g(r) \left[1 - e^{\beta\phi(r)} \right] + \mathscr{P}(r) + \mathscr{B}(r)} . \tag{8.25}$$

Similarly, combining (8.23) and (8.24) one gets

$$\boxed{c(r) = g(r) - 1 - \ln g(r) - \beta\phi(r) + \mathscr{B}(r)} . \tag{8.26}$$

8.3 Approximate Closures

Equations (8.25) and (8.26) are formally exact, but they are not closed since they have the structure $c(r) = \mathscr{F}[h(r), \mathscr{P}(r) + \mathscr{B}(r)]$ and $c(r) = \mathscr{F}[h(r), \mathscr{B}(r)]$, respectively.

In most of the cases, a closure $c(r) = \mathscr{F}[h(r)]$ [see (8.4)] is an *ad hoc* approximation whose usefulness must be judged *a posteriori*. The two prototype closures are

the hypernetted-chain (HNC) closure [66, 67] and the Percus–Yevick (PY) closure [68].

8.3.1 HNC and Percus–Yevick Integral Equations

The HNC closure consists of setting $\mathscr{B}(r) = 0$ in (8.26):

$$\boxed{c(r) = g(r) - 1 - \ln g(r) - \beta \phi(r)} \quad \text{(HNC)} . \qquad (8.27)$$

Similarly, the Percus–Yevick closure is obtained by setting $\mathscr{P}(r) + \mathscr{B}(r) = 0$ in (8.25), what results in

$$\boxed{c(r) = g(r) \left[1 - e^{\beta \phi(r)} \right]} \quad \text{(PY)} . \qquad (8.28)$$

By inserting the above closures into the Ornstein–Zernike relation (8.1) we obtain the HNC and Percus–Yevick integral equations, respectively:

$$\text{HNC} \Rightarrow \ln \left[g(r) e^{\beta \phi(r)} \right] = -n \int d\mathbf{r}' \left\{ \ln \left[g(r') e^{\beta \phi(r')} \right] - h(r') \right\} h(|\mathbf{r} - \mathbf{r}'|) , \quad (8.29)$$

$$\text{PY} \Rightarrow g(r) e^{\beta \phi(r)} - 1 = -n \int d\mathbf{r}' \left[g(r') e^{\beta \phi(r')} - 1 - h(r') \right] h(|\mathbf{r} - \mathbf{r}'|) . \qquad (8.30)$$

Interestingly, if one formally assumes that $y(r) \equiv g(r) e^{\beta \phi(r)} \approx 1$ and applies the linearization property $\ln \left[g(r) e^{\beta \phi(r)} \right] \to g(r) e^{\beta \phi(r)} - 1$, then the HNC integral equation (8.29) becomes the Percus–Yevick integral equation (8.30). On the other hand, the Percus–Yevick theory stands by itself, even if $y(r)$ is not close to 1.

A few comments are in order. First, the density expansion of $h_{\text{HNC}}(r)$ and $y_{\text{HNC}}(r)$ can be obtained from the closed integral equation by iteration. It turns out that not only the bridge diagrams disappear, but also *some* chain and open parallel diagrams are not retained either. This is because the neglect of $\mathscr{B}(r)$ at the level of (8.26) propagates to other non-bridge diagrams at the level of (8.9). For instance, while (8.14) is an identity, we cannot neglect $\mathscr{B}(r)$ on both sides, i.e., $\mathscr{C} \neq \ln(1 + \mathscr{C} + \mathscr{P})$. A similar comment applies to $h_{\text{PY}}(r)$ and $y_{\text{PY}}(r)$, in which case some chain diagrams disappear along with all the bridge and open parallel diagrams. This is illustrated by comparison between Figs. 8.3 and 8.4.

Another interesting feature is that all the diagrams neglected in the density expansion of $y_{\text{HNC}}(r)$ are neglected in the density expansion of $y_{\text{PY}}(r)$ as well. However, the latter neglects extra diagrams which are retained by $y_{\text{HNC}}(r)$. Thus, one could think that the HNC equation is *always* a better approximation than the Percus–Yevick equation. On the other hand, this is not necessarily the case, especially for hard-sphere-like systems. In those cases the diagrams neglected in the Percus–Yevick equation may cancel each other to a reasonable degree, so that adding more diagrams (as HNC does) may actually worsen the result. For instance, the combi-

Fig. 8.4 The colored diagrams are those neglected by the HNC and the Percus–Yevick approximations. Adapted from Table 8.3.1 of [18].

Fig. 8.5 Plot of ▭ (top curve), ◁ (bottom curve), and ▭ + ◁ (middle curve) for three-dimensional hard spheres.
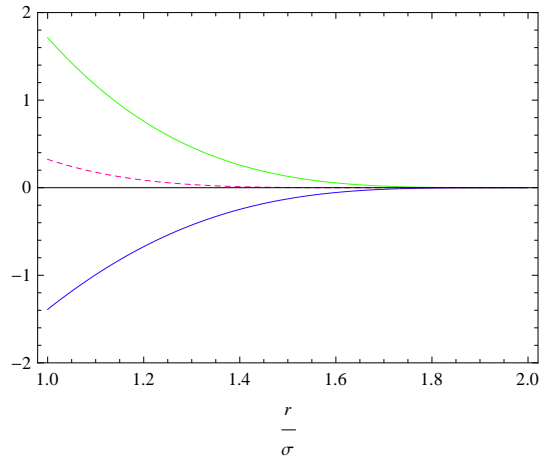
nation of the two diagrams neglected by the Percus–Yevick approximation to first order in density is

$$\text{▭} + \text{◁} = \text{◁} \quad , \qquad (8.31)$$

where the dotted line on the right-hand side means an e-bond between the field particles 3 and 4, i.e., a factor $1 + f(r_{34}) = e^{-\beta\phi(r_{34})}$. In the hard-sphere case the three diagrams in (8.31) vanish if $r_{12} > 2\sigma$ since in that case it is impossible that either particle 3 or particle 4 can be separated from both 1 and 2 a distance smaller than σ. If $r_{12} < 2\sigma$, the only configurations which contribute to the diagram on the right-hand side of (8.31) are those where $r_{13} < \sigma$, $r_{23} < \sigma$, $r_{14} < \sigma$, and $r_{24} < \sigma$ *but* $r_{34} > \sigma$. It is obvious that those configurations represent a smaller volume than

the ones contributing to any of the two diagrams on the left-hand side of (8.31), especially if $r_{12} > \sigma$. In fact, as can be seen from (7.71) and (7.72), the right-hand side of (8.31) vanishes if $r > \sqrt{3}\sigma$ in the three-dimensional case. The three diagrams in (8.31) are plotted in Fig. 8.5 in the range $1 \leq r_{12}/\sigma \leq 2$.

Being approximate, the $g(r)$ obtained from either the Percus–Yevick or the HNC theory is *not* thermodynamically consistent, i.e., virial route$\neq$chemical-potential route$\neq$compressibility route$\neq$energy route. However, it can be proved that the virial and energy routes are equivalent in the HNC approximation for any interaction potential [2, 69].

What makes the Percus–Yevick integral equation particularly appealing is that it admits a non-trivial *exact* solution for three-dimensional hard-sphere liquids [70, 71, 72], sticky hard spheres [39], additive hard-sphere mixtures [73], additive sticky-hard-sphere mixtures [74, 75], and their generalizations to $d =$ odd dimensions [76, 77, 78, 79].

8.3.2 A Few Other Closures

Apart from the classical Percus–Yevick and HNC approximations, many other ones have been proposed in the literature [2, 22]. Most of them as formulated as closing the formally *exact* relation (8.26) with an *approximation* of the form $\mathscr{B}(r) = \mathscr{F}[\gamma(r)]$, where

$$\boxed{\gamma(r) \equiv h(r) - c(r)} \tag{8.32}$$

is the *indirect* correlation function. In particular,

$$\text{HNC} \Rightarrow \mathscr{B}(r) = 0,$$
$$\text{PY} \Rightarrow \mathscr{B}(r) = \ln\left[1 + \gamma(r)\right] - \gamma(r) - 1. \tag{8.33}$$

In several cases the closure contains an *adjustable* parameter fitted to guarantee the thermodynamic consistency between two routes (usually virial and compressibility). A few examples are

- Verlet (modified) [80]

$$\mathscr{B}(r) = -\frac{1}{2}\frac{[\gamma(r)]^2}{1 + a_1\gamma(r)}, \quad a_1 = \frac{4}{5}, \tag{8.34}$$

- Martynov–Sarkisov [81]

$$\mathscr{B}(r) = \sqrt{1 + 2\gamma(r)} - \gamma(r) - 1, \tag{8.35}$$

- Rogers–Young [82]

$$\mathscr{B}(r) = \ln\left\{1 + \frac{\exp\left[(1 - e^{-a_2 r})\gamma(r)\right] - 1}{1 - e^{-a_2 r}}\right\} - \gamma(r), \quad a_2 = 0.160, \tag{8.36}$$

- Ballone–Pastore–Galli–Gazzillo [83]

$$\mathscr{B}(r) = [1 + a_3 \gamma(r)]^{1/a_3} - \gamma(r) - 1 , \quad a_3 = \frac{15}{8} . \tag{8.37}$$

8.3.3 Linearized Debye–Hückel and Mean Spherical Approximations

We end this section with two more simple approximate theories. First, the linearized Debye–Hückel (LDH) theory consists of retaining only the *linear* chain diagrams in the expansion of $y(r)$ [see (8.5)]:

$$w(r) \equiv y(r) - 1 = n\circ\!\!-\!\!\bullet\!\!-\!\!\circ + n^2 \circ\!\!-\!\!\bullet\!\!-\!\!\bullet\!\!-\!\!\circ + n^3 \circ\!\!-\!\!\bullet\!\!-\!\!\bullet\!\!-\!\!\bullet\!\!-\!\!\circ + \cdots . \tag{8.38}$$

This apparently crude approximation is justified in the case of *long-range* interactions (like Coulomb's) since the linear chains are the most divergent diagrams but their sum gives a convergent result [22]. The approximation (8.38) is also valid for *bounded* potentials in the high-temperature limit [84]. For those potentials $|f(r)|$ can be made arbitrarily small by increasing the temperature and thus, at any order in density, the linear chains (having the least number of bonds) are the dominant ones.

In Fourier space, (8.38) becomes

$$\text{LDH} \Rightarrow \widetilde{w}(k) = n \left[\widetilde{f}(k) \right]^2 + n^2 \left[\widetilde{f}(k) \right]^3 + n^3 \left[\widetilde{f}(k) \right]^4 + \cdots = \frac{n \left[\widetilde{f}(k) \right]^2}{1 - n\widetilde{f}(k)} . \tag{8.39}$$

The conventional Debye–Hückel theory is obtained from (8.39) by assuming that (i) $\ln y(r) \approx w(r)$ and (ii) $f(r) \approx -\beta\phi(r)$. In that case (7.64) yields $\beta\widetilde{\psi}(k) \approx \beta\widetilde{\phi}(k) - \widetilde{w}(k) \approx \beta\widetilde{\phi}(k)/[1 + n\beta\widetilde{\phi}(k)]$.

Another approximation closely related to the linearized Debye–Hückel theory (8.39) is the mean spherical approximation (MSA). First, we start from the identity $h(r) = f(r)y(r) + y(r) - 1$. Next, in the same spirit as the assumption (i) above, we assume $f(r)y(r) \approx y(r)$, so that $\widetilde{h}(k) \approx \widetilde{f}(k) + \widetilde{w}(k)$. Insertion of (8.39) yields $\widetilde{h}(k) \approx \widetilde{f}(k)/[1 - n\widetilde{f}(k)]$. According to the Ornstein–Zernike relation (8.2), the above approximation is equivalent to $\widetilde{c}(k) = \widetilde{f}(k)$. Going back to real space, $c(r) = f(r)$. Finally, repeating the assumption (ii) above, we get

$$\text{MSA} \Rightarrow c(r) = -\beta\phi(r) \Rightarrow \widetilde{h}(k) = \frac{-\beta\widetilde{\phi}(k)}{1 + n\beta\widetilde{\phi}(k)} . \tag{8.40}$$

It must be noted that in the mean spherical approximation the direct correlation function is independent of density but differs from its correct zero-density limit $c(r) \to f(r)$ [see (8.20)].

The mean spherical approximation (8.40) has usually been applied to bounded and soft potentials [85]. For potentials with a hard core at $r = \sigma$ plus an attractive tail for $r \geq \sigma$, the mean spherical approximation (8.40) is replaced by the double

Fig. 9.1 Scheme of the relationship between the functions $\gamma_k(r)$ and the virial coefficients B_k.

$$y(r) = 1 + \gamma_3(r)n + \gamma_4(r)n^2 + \gamma_5(r)n^3 + \cdots$$

Thermodynamic routes

$$Z \equiv \frac{p}{nk_BT} = 1 + B_2n + B_3n^2 + B_4n^3 + B_5n^5 + \cdots$$

condition

$$\begin{cases} g(r) = 0\,, & r < \sigma\,, \\ c(r) = -\beta\phi(r)\,, & r > \sigma\,. \end{cases} \tag{8.41}$$

This version of the mean spherical approximation is exactly solvable for Yukawa fluids [86, 87].

9 Some Thermodynamic Consistency Relations in Approximate Theories

As sketched in Fig. 5.3, an approximate $g(r)$ does not guarantee thermodynamic consistency among the different routes. However, there are a few cases where either a partial consistency or a certain relationship may exist.

9.1 Are $B_4^{(HNC,v)}$ and $B_4^{(PY,c)}$ Related?

As summarized in Fig. 9.1, the knowledge of the coefficients $\gamma_k(r)$ in the density expansion of the cavity function allows one to obtain the virial coefficients B_k. In general, unless the functions $\gamma_k(r)$ are exact, the virial coefficients B_k will depend on the thermodynamic route followed. Here, we will focus on the compressibility route [see (5.1)] and the virial route [see (5.13)], denoting the corresponding virial coefficients by $B_k^{(c)}$ and $B_k^{(v)}$, respectively.

As shown before [see (7.75)], the virial route yields

$$B_k^{(v)} = \frac{1}{2d}\int d\mathbf{r}\,\gamma_k(r)r\frac{\partial f(r)}{\partial r}\,. \tag{9.1}$$

As for the compressibility route, from (5.1) one has

$$\chi = 1 + n \int d\mathbf{r} \left\{ [f(r)+1] y(r) - 1 \right\}$$
$$= 1 + \chi_2 n + \chi_3 n^2 + \chi_4 n^3 + \cdots , \tag{9.2}$$

where

$$\chi_2 = \int d\mathbf{r} \, f(r) , \quad \chi_k = \int d\mathbf{r} \, [f(r)+1] \, \gamma_k(r) , \quad k \geq 3 . \tag{9.3}$$

Then, taking into account that $\chi \equiv [\partial (nZ)/\partial n]^{-1}$, we obtain

$$B_2^{(c)} = -\frac{1}{2}\chi_2 , \quad B_3^{(c)} = -\frac{1}{3}\left(\chi_3 - \chi_2^2\right) , \quad B_4^{(c)} = -\frac{1}{4}\left(\chi_4 - 2\chi_2\chi_3 + \chi_2^3\right) . \tag{9.4}$$

9.1.1 HNC and Percus–Yevick Theories

Let us now particularize to the HNC and Percus–Yevick theories. Since $\gamma_3^{(PY)}(r) = \gamma_3^{(HNC)}(r) = \gamma_3^{(exact)}(r)$ (see Fig. 8.4), it follows that

$$B_3^{(PY,v)} = B_3^{(PY,c)} = B_3^{(HNC,v)} = B_3^{(HNC,c)} = B_3^{(exact)} . \tag{9.5}$$

On the other hand, $\gamma_4^{(PY)}(r) \neq \gamma_4^{(HNC)}(r) \neq \gamma_4^{(exact)}(r)$ (see again Fig. 8.4). Therefore, it can be expected that

$$B_4^{(PY,v)} \neq B_4^{(PY,c)} \neq B_4^{(HNC,v)} \neq B_4^{(HNC,c)} \neq B_4^{(exact)} . \tag{9.6}$$

However, interestingly enough, $B_4^{(PY,c)}$ and $B_4^{(HNC,v)}$ turn out to be closely related. More specifically, our aim is to prove that [88]

$$\boxed{B_4^{(HNC,v)} = \frac{3}{2} B_4^{(PY,c)}} \tag{9.7}$$

for any potential $\phi(r)$ and dimensionality d.

9.1.2 A "Flexible" Function $\gamma_4(r)$

The exact function $\gamma_4(r)$ is given by (7.61). As shown by Fig. 8.4, the HNC approximation neglects the last diagram and the Percus–Yevick approximation neglects the two last diagrams. In order to account for all of these possibilities, let us construct the function

$$\gamma_4 = \frac{1}{2}\left(2 \; \rule{0pt}{0pt}\vcenter{\hbox{⬡}} \; + 4 \; \vcenter{\hbox{◹}} \; + \lambda_1 \; \vcenter{\hbox{▢}} \; + \lambda_2 \; \vcenter{\hbox{◺}} \right) . \tag{9.8}$$

The cases $(\lambda_1, \lambda_2) = (1,1)$, $(1,0)$, and $(0,0)$ correspond to the exact, HNC, and Percus–Yevick functions, respectively.

Inserting (9.8) into (9.1), one has

$$B_4^{(v)} = \frac{1}{4d}\left(2\,\square + 4\,\square\!\!\diagup + \lambda_1\,\square\!\!\diagup + \lambda_2\,\boxtimes\right), \tag{9.9}$$

where a dashed line denotes a factor $r\,\partial f(r)/\partial r$. By integrating by parts, the following properties can be proved [88]:

$$\square = -\frac{3d}{4}\,\square\,, \tag{9.10}$$

$$\square\!\!\diagup + \frac{1}{4}\,\square\!\!\diagup = -\frac{3d}{4}\,\square\!\!\diagup\,, \tag{9.11}$$

$$\boxtimes = -\frac{d}{2}\,\boxtimes\,. \tag{9.12}$$

Consequently,

$$B_4^{(v)} = -\frac{3}{8}\,\square - \frac{3}{4}\,\square\!\!\diagup - \frac{\lambda_2}{8}\,\boxtimes + \frac{\lambda_1 - 1}{4d}\,\square\!\!\diagup\,. \tag{9.13}$$

In the case of the compressibility route, (9.3) yields

$$\chi_2 = \circ\!\!-\!\!\bullet\,, \quad \chi_3 = \triangle + \triangle\,, \tag{9.14}$$

$$\chi_4 = \square + \frac{2+\lambda_1}{2}\,\square + 2\,\square\!\!\diagup + \frac{4+\lambda_1+\lambda_2}{2}\,\square\!\!\diagup + \frac{\lambda_2}{2}\,\boxtimes\,, \tag{9.15}$$

where in (9.15) use has been made of the property

$$\square\!\!\diagup = \square\!\!\diagup = V^{-1}\,\square\!\!\diagup\,. \tag{9.16}$$

Noting that

$$\chi_2\chi_3 = \square + \square\!\!\diagup\,, \quad \chi_2^3 = \square\,, \tag{9.17}$$

and using (9.4), we finally obtain

$$B_4^{(c)} = -\frac{2+\lambda_1}{8}\,\square - \frac{4+\lambda_1+\lambda_2}{8}\,\square\!\!\diagup - \frac{\lambda_2}{8}\,\boxtimes\,. \tag{9.18}$$

Fig. 9.2 The diagonal (labeled c) and vertical (labeled v) lines represent the classes of approximations $\lambda_1 = \lambda_2$ and $\lambda_1 = 1$, respectively. The dashed tie lines connect the pairs of approximations whose respective values of $B_4^{(c)}$ and $B_4^{(v)}$ are related by (9.19).
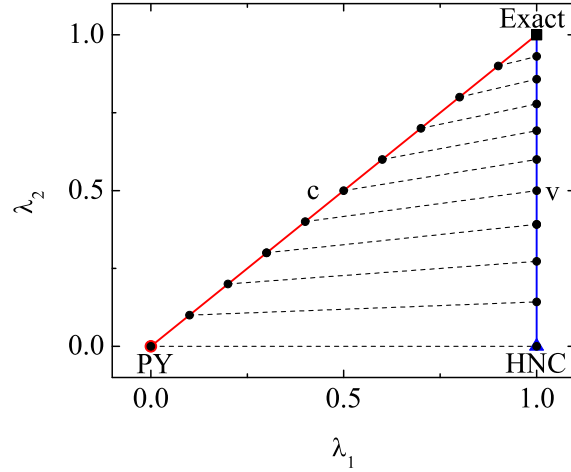
Comparison between (9.13) and (9.18) shows that

$$B_4^{(v)}\left(\text{with } \lambda_1 = 1 \text{ and } \lambda_2 = \frac{3\lambda}{2+\lambda}\right) = \frac{3}{2+\lambda}B_4^{(c)}\left(\text{with } \lambda_1 = \lambda_2 = \lambda\right). \quad (9.19)$$

In the case of the exact $\gamma_4(r)$ we have $\lambda = 1$ in both sides of (9.19) and therefore $B_4^{(\text{exact},v)} = B_4^{(\text{exact},c)}$, as expected. On the other hand, the choice $\lambda = 0$ makes the left- and right-hand sides correspond to the HNC and Percus–Yevick approximations, respectively, and then (9.19) reduces to the sought result (9.7).

More in general, (9.19) implies that for any approximation of the class $\lambda_1 = \lambda_2$ there exists a specific approximation of the class $\lambda_1 = 1$, such that the compressibility and virial values, respectively, of B_4 are proportional to each other. The connection between both classes is schematically illustrated in Fig. 9.2. Interestingly, the largest deviation of the proportionality factor from 1 occurs in the case of the Percus–Yevick and HNC pair. The proof of (9.19) can be easily extended to mixtures [88].

9.2 Energy and Virial Routes in the Linearized Debye-Hückel Theory and in the Mean Spherical Approximation

As said in Sect. 8, the energy and virial routes are equivalent in the HNC approximation. Now we will see that the same property holds in the linearized Debye–Hückel approximation (8.39) [89] and in the mean spherical approximation (8.40) [90].

9.2.1 Linearized Debye–Hückel Theory

We start by recalling the energy and pressure routes (5.6) and (5.13), respectively. In terms of $w(r) = y(r) - 1$, they are given by

$$u^{\text{ex}} \equiv \frac{\langle E \rangle^{\text{ex}}}{N} = -\frac{n}{2} \int d\mathbf{r} \, [1 + w(r)] \frac{\partial f(r)}{\partial \beta} \,, \tag{9.20}$$

$$Z \equiv \frac{\beta p}{n} = 1 + \frac{n}{2d} \int d\mathbf{r} \, [1 + w(r)] \, \mathbf{r} \cdot \nabla f(r) \,. \tag{9.21}$$

The consistency condition between both routes is provided by the Maxwell relation

$$n \frac{\partial u^{\text{ex}}}{\partial n} = \frac{\partial Z}{\partial \beta} \,. \tag{9.22}$$

Given the mathematical identity

$$-\int d\mathbf{r} \, \frac{\partial f(r)}{\partial \beta} = \frac{1}{d} \frac{\partial}{\partial \beta} \left[\int d\mathbf{r} \, \mathbf{r} \cdot \nabla f(r) \right] \,, \tag{9.23}$$

the consistency condition (9.22) becomes

$$-\frac{\partial}{\partial n} \left[n \int d\mathbf{r} \, w(r) \frac{\partial f(r)}{\partial \beta} \right] = \frac{1}{d} \frac{\partial}{\partial \beta} \left[\int d\mathbf{r} \, w(r) \mathbf{r} \cdot \nabla f(r) \right] \,. \tag{9.24}$$

Since the linearized Debye–Hückel approximation (8.39) is formulated in Fourier space, it is convenient to express the spatial integrals in (9.24) as wavevector integrals:

$$\frac{\partial}{\partial n} \left[n \int d\mathbf{k} \, \widetilde{w}(k) \frac{\partial \widetilde{f}(k)}{\partial \beta} \right] = \frac{1}{d} \frac{\partial}{\partial \beta} \left\{ \int d\mathbf{k} \, \widetilde{w}(k) \nabla_{\mathbf{k}} \cdot \left[\mathbf{k} \widetilde{f}(k) \right] \right\} \,. \tag{9.25}$$

We now make use of the mathematical identity

$$\frac{\partial}{\partial \beta} \left\{ \widetilde{w}(k) \, \nabla_{\mathbf{k}} \cdot \left[\mathbf{k} \widetilde{f}(k) \right] \right\} = d \frac{\partial \widetilde{w}(k)}{\partial \beta} \widetilde{f}(k) + \nabla_{\mathbf{k}} \cdot \left[\mathbf{k} \widetilde{w}(k) \frac{\partial \widetilde{f}(k)}{\partial \beta} \right]$$

$$+ \mathbf{k} \cdot \left[\frac{\partial \widetilde{w}(k)}{\partial \beta} \nabla_{\mathbf{k}} \widetilde{f}(k) - \frac{\partial \widetilde{f}(k)}{\partial \beta} \nabla_{\mathbf{k}} \widetilde{w}(k) \right] \tag{9.26}$$

to rewrite (9.25) as

$$\frac{\partial}{\partial n} \left[n \int d\mathbf{k} \, \widetilde{w}(k) \frac{\partial \widetilde{f}(k)}{\partial \beta} \right] = \frac{1}{d} \int d\mathbf{k} \, \mathbf{k} \cdot \left[\frac{\partial \widetilde{w}(k)}{\partial \beta} \nabla_{\mathbf{k}} \widetilde{f}(k) - \frac{\partial \widetilde{f}(k)}{\partial \beta} \nabla_{\mathbf{k}} \widetilde{w}(k) \right]$$

$$+ \int d\mathbf{k} \, \frac{\partial \widetilde{w}(k)}{\partial \beta} \widetilde{f}(k) \,. \tag{9.27}$$

It must be emphasized that no approximations have been carried out so far. Therefore, *any* $\widetilde{w}(k)$ satisfying the condition (9.27) gives thermodynamically consistent results via the energy and virial routes.

Let us suppose a *closure* relation of the form

$$\widetilde{w}(k) = n^{-1}\mathscr{F}\left(n\widetilde{f}(k)\right) , \quad \mathscr{F}(z) = \text{arbitrary} . \tag{9.28}$$

This implies the relations

$$\frac{\partial}{\partial n}[n\widetilde{w}(k)] = \mathscr{F}'\left(n\widetilde{f}(k)\right)\widetilde{f}(k) , \tag{9.29}$$

$$\frac{\partial \widetilde{w}(k)}{\partial \beta} = \mathscr{F}'\left(n\widetilde{f}(k)\right)\frac{\partial \widetilde{f}(k)}{\partial \beta} , \tag{9.30}$$

$$\nabla_{\mathbf{k}}\widetilde{w}(k) = \mathscr{F}'\left(n\widetilde{f}(k)\right)\nabla_{\mathbf{k}}\widetilde{f}(k) . \tag{9.31}$$

It is then straightforward to check that the energy-virial consistency condition (9.27) is identically satisfied.

As a corollary, the linearized Debye–Hückel approximation (8.39) belongs to the scaling class (9.28) with the particular choice $\mathscr{F}(z) = z^2/(1-z)$, what closes the proof.

9.2.2 Mean Spherical Approximation

The proof in the case on the mean spherical approximation (8.40) follows along similar lines [90]. Now, instead of (9.20) and (9.21), we start from the energy and virial routes written in the forms (5.4) and (5.12), namely

$$u^{\text{ex}} = \frac{n}{2}\int d\mathbf{r}\,[1+h(r)]\frac{\partial\,[\beta\phi(r)]}{\partial\beta} , \tag{9.32}$$

$$Z = 1 - \frac{n}{2d}\int d\mathbf{r}\,[1+h(r)]\mathbf{r}\cdot\nabla[\beta\phi(r)] . \tag{9.33}$$

We observe that (9.20) and (9.21) become (9.32) and (9.33), respectively, with the formal changes $w(r) \to h(r)$ and $f(r) \to -\beta\phi(r)$. Since all the steps leading from (9.22) to (9.27) are purely technical, it is clear that we obtain a consistency condition analogous to (9.27), except for the formal changes $\widetilde{w}(k) \to \widetilde{h}(k)$ and $\widetilde{f}(k) \to -\beta\widetilde{\phi}(k)$. Consequently, that consistency condition is automatically satisfied by closures of the form

$$\widetilde{h}(k) = n^{-1}\mathscr{F}\left(-n\beta\widetilde{\phi}(k)\right) , \quad \mathscr{F}(z) = \text{arbitrary} . \tag{9.34}$$

As shown in (8.40), the mean spherical approximation belongs to that class of closures with the particular choice $\mathscr{F}(z) = z/(1-z)$.
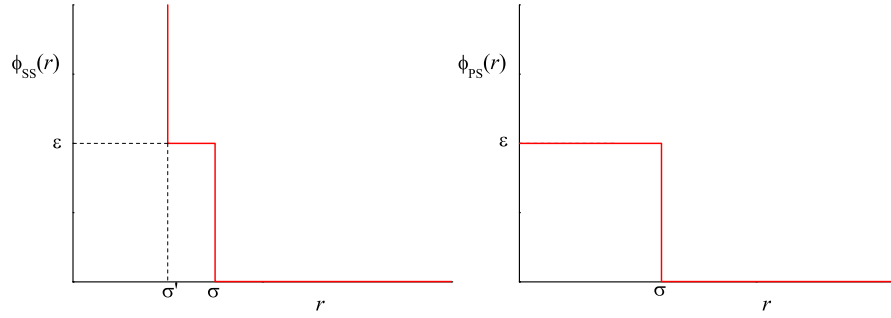
Fig. 9.3 Left panel: Square-shoulder potential. Right panel: Penetrable-sphere potential

9.3 Energy Route in Hard-Sphere Liquids

We saw in (5.34) that the energy route is *useless* for hard spheres. In fact, the consistency condition (9.22) is *trivially* satisfied since

$$n\frac{\partial u_{\text{HS}}^{\text{ex}}}{\partial n} = 0\,, \qquad \frac{\partial Z_{\text{HS}}}{\partial \beta} = 0\,. \tag{9.35}$$

The last equality expresses the fact that the hard-sphere compressibility factor

$$Z_{\text{HS}}(\eta) = 1 + 2^{d-1}\eta y_{\text{HS}}(\sigma;\eta) \tag{9.36}$$

is independent of temperature. Thus, there is no possibility of extracting thermodynamic information from $u_{\text{HS}}^{\text{ex}}$.

However, a physical meaning can be allocated to the energy route for hard spheres if *first* it is applied to a non-hard-sphere system that includes the hard-sphere system as a special case and *then* the hard-sphere limit is taken.

9.3.1 A "Core-Softened" Potential. The Square-Shoulder Interaction

Let us take the square-shoulder (SS) potential

$$\phi_{\text{SS}}(r) = \begin{cases} \infty\,, & r < \sigma'\,, \\ \varepsilon\,, & \sigma' < r < \sigma\,, \\ 0\,, & r > \sigma \end{cases} \tag{9.37}$$

as a convenient choice of a non-hard-sphere potential (see Fig. 9.3, left panel). The square-shoulder potential is the simplest example of a core-softened potential, i.e., a potential with a two-length scale repulsive part exhibiting a softening region where the slope changes dramatically [91].

The square-shoulder potential has the interesting property of reducing to the hard-sphere potential in three independent limits:

$$\lim_{\beta\varepsilon\to 0}\phi_{\mathrm{SS}}(r)=\phi_{\mathrm{HS}}(r)\ (\text{diameter }\sigma')\,, \tag{9.38}$$

$$\lim_{\beta\varepsilon\to\infty}\phi_{\mathrm{SS}}(r)=\phi_{\mathrm{HS}}(r)\ (\text{diameter }\sigma)\,, \tag{9.39}$$

$$\lim_{\sigma'\to\sigma}\phi_{\mathrm{SS}}(r)=\phi_{\mathrm{HS}}(r)\ (\text{diameter }\sigma'=\sigma)\,. \tag{9.40}$$

It also reduces to the so-called penetrable-sphere (PS) potential (see Fig. 9.3, right panel) in the limit $\sigma'\to 0$:

$$\lim_{\sigma'\to 0}\phi_{\mathrm{SS}}(r)=\phi_{\mathrm{PS}}(r)\,. \tag{9.41}$$

9.3.2 Equation of State from the Energy Route

Suppose an *approximate* cavity function $y_{\mathrm{SS}}(r;n,\beta)$ is known (for instance, as the solution to an integral equation) for the square-shoulder fluid. Then, the energy route (5.6) gives

$$u_{\mathrm{SS}}^{\mathrm{ex}}(n,\beta)=d2^{d-1}v_d n\varepsilon\,\mathrm{e}^{-\beta\varepsilon}\int_{\sigma'}^{\sigma}\mathrm{d}r\,r^{d-1}y_{\mathrm{SS}}(r;n,\beta)\,. \tag{9.42}$$

Then, the energy-route equation of state is obtained from (9.22) as

$$\begin{aligned}
Z_{\mathrm{SS}}(n,\beta)&=Z_{\mathrm{HS}}(n\sigma'^{d})+n\frac{\partial}{\partial n}\int_{0}^{\beta}\mathrm{d}\beta'\,u_{\mathrm{SS}}^{\mathrm{ex}}(n,\beta')\\
&=Z_{\mathrm{HS}}(n\sigma'^{d})+d2^{d-1}v_d n\varepsilon\frac{\partial}{\partial n}n\int_{0}^{\beta}\mathrm{d}\beta'\,\mathrm{e}^{-\beta'\varepsilon}\int_{\sigma'}^{\sigma}\mathrm{d}r\,r^{d-1}y_{\mathrm{SS}}(r;n,\beta')\,,
\end{aligned} \tag{9.43}$$

where in the first step we have fixed the integration constant by the physical condition (9.38), while in the second step we have used (9.42).

As a second step, we now, take the limit $\beta\varepsilon\to\infty$ on both sides of (9.43), apply (9.39), and divide both sides by $n\sigma^{d}-n\sigma'^{d}$. The result is

$$\frac{Z_{\mathrm{HS}}(n\sigma^{d})-Z_{\mathrm{HS}}(n\sigma'^{d})}{n\sigma^{d}-n\sigma'^{d}}=\frac{d2^{d-1}v_d\varepsilon}{\sigma^{d}-\sigma'^{d}}\frac{\partial}{\partial n}n\int_{0}^{\infty}\mathrm{d}\beta\,\mathrm{e}^{-\beta\varepsilon}\int_{\sigma'}^{\sigma}\mathrm{d}r\,r^{d-1}y_{\mathrm{SS}}(r;n,\beta)\,. \tag{9.44}$$

Finally, we take the limit $\sigma'\to\sigma$. The left-hand side of (9.44) becomes

$$\lim_{\sigma'\to\sigma}\frac{Z_{\mathrm{HS}}(n\sigma^{d})-Z_{\mathrm{HS}}(n\sigma'^{d})}{n\sigma^{d}-n\sigma'^{d}}=\sigma^{-d}\frac{\partial}{\partial n}Z_{\mathrm{HS}}(n\sigma^{d})\,. \tag{9.45}$$

Moreover, the spatial integral on the right-hand side of (9.44) reduces to

Fig. 9.4 Scheme of the steps followed to derive (9.36) starting from (9.42).
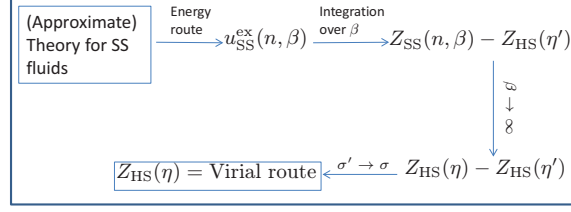
$$\lim_{\sigma' \to \sigma} \frac{1}{\sigma^d - \sigma'^d} \int_{\sigma'}^{\sigma} \mathrm{d}r\, r^{d-1} y_{\mathrm{SS}}(r; n, \beta) = \frac{1}{d} y_{\mathrm{HS}}(\sigma; n\sigma^d)\,, \qquad (9.46)$$

where the third limit (9.40) has been used. Taking into account (9.45) and (9.46) in (9.44), one gets

$$\frac{\partial}{\partial n} Z_{\mathrm{HS}}(n\sigma^d) = 2^{d-1} v_d \frac{\partial}{\partial n} n\sigma^d y_{\mathrm{HS}}(\sigma; n\sigma^d)\,. \qquad (9.47)$$

Integration over density and application of the ideal-gas boundary condition $Z_{\mathrm{HS}}(0) = 1$ yields (9.36), which is not but the virial equation of state! The generalization to mixtures follows essentially the same steps [92].

In summary, the ill definition of the energy route to the equation of state of hard spheres can be avoided by first considering a square-shoulder fluid and then taking the limit of a vanishing shoulder width. The resulting equation of state coincides exactly with the one obtained through the virial route. *From that point of view*, the energy and virial routes to the equation of state of hard-sphere fluids can be considered as equivalent. Figure 9.4 presents a scheme of the energy route $\to$ virial route path.

It must be emphasized that the application of the three limits (9.38)–(9.40) is *essential* to derive (9.36) from (9.42) [93]. For instance, if the limit $\sigma' \to 0$ (instead of $\sigma' \to \sigma$) is taken in (9.44), the result is

$$Z_{\mathrm{HS}}(n\sigma^d) = 1 + d2^{d-1} n v_d \varepsilon \frac{\partial}{\partial n} n \int_0^{\infty} \mathrm{d}\beta\, \mathrm{e}^{-\beta\varepsilon} \int_0^{\sigma} \mathrm{d}r\, r^{d-1} y_{\mathrm{PS}}(r; n, \beta)\,, \qquad (9.48)$$

where the change $y_{\mathrm{SS}} \to y_{\mathrm{PS}}$ is a consequence of (9.41). Equation (9.48) is an alternative recipe to obtain the hard-sphere equation of state from the energy route applied to penetrable spheres. In general, it gives a result different from (9.36) when an approximate y_{PS} is used. For instance, in the Percus–Yevick approximation for three dimensional systems, (9.36) gives a (reduced) fourth virial coefficient $b_4 = 16$, while (9.48) gives $b_4 = 1814/175 \simeq 10.37$ [93].

10 Exact Solution of the Percus–Yevick Equation for Hard Spheres ... and Beyond

As said in Sect. 8, one of the milestones of the statistical-mechanical theory of liquids in equilibrium was the exact analytical solution of the Percus–Yevick integral equation (8.30) for three-dimensional hard spheres [18, 70, 71, 72].

The statement of the problem is as follows. Particularized to $d = 3$, the Ornstein–Zernike relation (8.1) can be written as

$$h(r) = c(r) + \frac{2\pi n}{r} \int_0^\infty \mathrm{d}r' \, r' c(r') \int_{|r-r'|}^{r+r'} \mathrm{d}r'' \, r'' h(r'') \,, \qquad (10.1)$$

where bipolar coordinates have been used. In the hard-sphere case, one necessarily has $g(r) = 0$ for $r < \sigma$. Moreover, the Percus–Yevick closure (8.28) implies that $c(r) = 0$ for $r > \sigma$. Thus, the mathematical problem consists in solving (10.1) subject to the boundary conditions

$$\begin{cases} g(r) = 0, & r < \sigma \text{ (exact hard-core condition)}, \\ c(r) = 0, & r > \sigma \text{ (Percus–Yevick approximation for hard spheres)}. \end{cases} \qquad (10.2)$$

The solution relies on the use of Laplace transforms, as suggested by the structure of (10.1), and stringent analytical properties of *entire functions* of complex variable.

Here, however, we will follow an alternative method [3, 94, 95, 96] that does not make explicit use of (10.2) and lends itself to extensions and generalizations.

10.1 An Alternative Approach. The Rational-Function Approximation

The main steps we will follow are the following ones:

  (I) Introduce the Laplace transform $G(s)$ of $rg(r)$.

 (II) Define an auxiliary function $F(s)$ directly related to $G(s)$.

(III) Find the exact properties of $F(s)$ for small s and for large s.

(IV) Propose a rational-function *approximation* (RFA) for $F(s)$ satisfying the previous exact properties.

As will be seen, the *simplest* approximation (i.e., the one with the least number of parameters) yields the Percus–Yevick solution. Furthermore, the next-order approximation contains two free parameters which can be determined by prescribing

a given equation of state and thermodynamic consistency between the virial and compressibility routes.

The same approach can be extended to mixtures, to other related systems with piece-wise constant potentials, and to higher dimensionalities with $d = \text{odd}$.

We now proceed with the four steps described above.

(I) Introduction of $G(s)$

Let us introduce the Laplace transform of $rg(r)$:

$$G(s) = \mathscr{L}\left[rg(r)\right](s) = \int_0^\infty dr\, e^{-sr} rg(r)\,. \tag{10.3}$$

The choice of $rg(r)$ instead of $g(r)$ as the function to be Laplace transformed is suggested by the structure of (10.1) and also by the link of $G(s)$ to the *Fourier transform* $\widetilde{h}(k)$ of $h(r) = g(r) - 1$ and hence to the structure function $S(k) = 1 + n\widetilde{h}(k)$:

$$\widetilde{h}(k) = -2\pi \left[\frac{H(s) - H(-s)}{s}\right]_{s=ik} = -2\pi \left[\frac{G(s) - G(-s)}{s}\right]_{s=ik}\,, \tag{10.4}$$

where $H(s) = G(s) - s^{-2}$ is the Laplace transform of $rh(r)$. Had we defined $G(s)$ as the Laplace transform of $g(r)$, (10.4) would have involved the derivative $G'(s)$, what would be far less convenient.

In the more general case of $d = \text{odd} \geq 3$, it can be seen that the right choice for $G(s)$ is [78]

$$G(s) = \int_0^\infty dr\, e^{-sr} \theta_{(d-3)/2}(sr) rg(r)\,, \tag{10.5}$$

where

$$\theta_k(x) = \sum_{j=0}^k \frac{(2k-j)!}{2^{k-j}(k-j)!j!} x^j \tag{10.6}$$

are the so-called *reverse Bessel polynomials* [97]. In this more general case, (10.4) becomes

$$\widetilde{h}(k) = (-2\pi)^{(d-1)/2} \left[\frac{H(s) - H(-s)}{s^{d-2}}\right]_{s=ik} = (-2\pi)^{(d-1)/2} \left[\frac{G(s) - G(-s)}{s^{d-2}}\right]_{s=ik}\,, \tag{10.7}$$

where $H(s) = G(s) - (d-2)!!s^{-2}$ is defined as in (10.5), except for the replacement $g(r) \to h(r)$.

(II) Definition of $F(s)$

Henceforth we return to the three-dimensional case ($d = 3$) and, for simplicity, we take $\sigma = 1$ as the length unit. Taking (7.62) and (7.68) into account, the hard-sphere radial distribution function to first order in density is

$$g(r) = \Theta(r-1) \left[1 + \Theta(2-r)(r-2)^2 \left(\frac{r}{2} + 2 \right) \eta + \cdots \right] . \tag{10.8}$$

To that order, the Laplace transform of $rg(r)$ is given by

$$s^{-1}G(s) = [F_0(s) + F_1(s)\eta]\,e^{-s} - 12\eta\,[F_0(s)]^2 e^{-2s} + \cdots , \tag{10.9}$$

where

$$F_0(s) = s^{-2} + s^{-3} , \quad F_1(s) = \frac{5}{2}s^{-2} - 2s^{-3} - 6s^{-4} + 12s^{-5} + 12s^{-6} . \tag{10.10}$$

The exact form (10.9) of $G(s)$ to order η *suggests* the *definition* of an auxiliary function $F(s)$ through

$$s^{-1}G(s) = F(s)e^{-s} - 12\eta\,[F(s)]^2 e^{-2s} + (12\eta)^2\,[F(s)]^3 e^{-3s} - \cdots$$
$$= \frac{F(s)e^{-s}}{1 + 12\eta F(s)e^{-s}} . \tag{10.11}$$

Equivalently,

$$\boxed{F(s) \equiv e^s \frac{s^{-1}G(s)}{1 - 12\eta s^{-1}G(s)}} . \tag{10.12}$$

Of course, $F(s)$ depends on η. To first order,

$$F(s) = F_0(s) + F_1(s)\eta + \cdots . \tag{10.13}$$

In analogy with the one-dimensional case [see (6.47)], the introduction of $F(s)$ allows one to express $g(r)$ as a succession of *shells* ($1 < r < 2$, $2 < r < 3$, $\dots$) in a natural way. First, according to (10.11),

$$G(s) = \sum_{\ell=1}^{\infty} (-12\eta)^{\ell-1} s\,[F(s)]^\ell\, e^{-\ell s} . \tag{10.14}$$

Then, Laplace inversion term by term gives

$$g(r) = \frac{1}{r} \sum_{\ell=1}^{\infty} (-12\eta)^{\ell-1} \Psi_\ell(r-\ell)\Theta(r-\ell) , \tag{10.15}$$

where

$$\Psi_\ell(r) = \mathscr{L}^{-1}\left[s\,[F(s)]^\ell \right](r) . \tag{10.16}$$

(III) Exact Properties of $F(s)$ for Small s and Large s

In order to derive the exact behavior of $G(s)$ for large s, and in view of (10.15), we need to start from the behavior of $g(r)$ for $r \gtrsim 1$:

$$g(r) = \Theta(r-1) \left[g(1^+) + g'(1^+)(r-1) + \frac{1}{2}g''(1^+)(r-1)^2 + \cdots \right] . \quad (10.17)$$

In Laplace space,

$$s e^s G(s) = g(1^+) + \left[g(1^+) + g'(1^+) \right] s^{-1} + \mathcal{O}(s^{-2}) . \quad (10.18)$$

Therefore, according to (10.12),

$$\boxed{\lim_{s \to \infty} s^2 F(s) = g(1^+) = \text{finite}} . \quad (10.19)$$

Thus, we see that $F(s)$ must necessarily behave as s^{-2} for large s.
Now we turn to the small-s behavior. Let us expand the Laplace transform of $rh(r)$ in powers of s:

$$H(s) = H^{(0)} + H^{(1)}s + \cdots , \quad (10.20)$$

where

$$H^{(0)} \equiv \int_0^\infty dr\, rh(r) , \quad H^{(1)} \equiv - \int_0^\infty dr\, r^2 h(r) . \quad (10.21)$$

In particular, $H^{(1)}$ is directly related to the isothermal compressibility [see (5.1)]:

$$\chi = 1 + n\widetilde{h}(0) = 1 - 24\eta H^{(1)} . \quad (10.22)$$

Since χ must be finite, and recalling that $H(s) = G(s) - s^{-2}$, we find

$$s^2 G(s) = 1 + 0 \times s + H^{(0)}s^2 + H^{(1)}s^3 + \mathcal{O}(s^4) . \quad (10.23)$$

Therefore, from (10.12) the small-s behavior of $F(s)$ is found to be

$$\frac{e^s}{F(s)} = -12\eta + \frac{s}{G(s)}$$
$$= -12\eta + 0 \times s + 0 \times s^2 + 1 \times s^3 + 0 \times s^4 - H^{(0)}s^5 - H^{(1)}s^6 + \mathcal{O}(s^7) . \quad (10.24)$$

Thus, just the condition $\chi = $ finite univocally fixes the first *five* coefficients in the power series expansion of $F(s)$. More specifically,

$$\boxed{F(s) = -\frac{1}{12\eta} \left[1 + s + \frac{s^2}{2} + \frac{1+2\eta}{12\eta}s^3 + \frac{1+\eta/2}{12\eta}s^4 \right] + \mathcal{O}(s^5)} . \quad (10.25)$$

(IV) Construction of the Approximation

Thus far, all the results are formally exact. To summarize, we have defined the Laplace transform $G(s)$ in (10.3) and the auxiliary function $F(s)$ in (10.12). This latter function must comply with the two basic requirements (10.19) and (10.25). A simple way of satisfying both conditions is by means of a *rational-function* form:

$$F(s) = \frac{\text{Polynomial in } s \text{ of degree } k}{\text{Polynomial in } s \text{ of degree } k+2} \qquad (10.26)$$

with $2k+3 \geq 5 \Rightarrow k \geq 1$. The *simplest* rational-function approximation corresponds to $k = 1$:

$$\boxed{F(s) = -\frac{1}{12\eta} \frac{1 + L^{(1)}s}{1 + S^{(1)}s + S^{(2)}s^2 + S^{(3)}s^3}}, \qquad (10.27)$$

where the coefficients are determined from (10.25). They are

$$L^{(1)} = \frac{1 + \eta/2}{1 + 2\eta}, \qquad (10.28)$$

$$S^{(1)} = -\frac{3}{2}\frac{\eta}{1+2\eta}, \quad S^{(2)} = -\frac{1}{2}\frac{1-\eta}{1+2\eta}, \quad S^{(3)} = -\frac{1}{12\eta}\frac{(1-\eta)^2}{1+2\eta}. \qquad (10.29)$$

10.2 Structural Properties

Once $F(s)$ and hence $G(s)$ have been completely determined by the approximation (10.27), it is easy to go back to real space and obtain the corresponding $g(r)$. Three alternative ways are possible. First, one can invert numerically the Laplace transform $G(s)$ by means of efficient algorithms [98]. A second method consists of obtaining $\widetilde{h}(k)$ from (10.4) and then performing a numerical Fourier inversion. The third method is purely analytical and is based on (10.15) and (10.16). From a practical point of view, one is interested in determining $g(r)$ up to a certain distance $r_{\max}$ since $g(r) \to 1$ for large distances. In that case, the summation in (10.15) can be truncated for $\ell > r_{\max}$. In obtaining $\Psi_\ell(r)$ from (10.16) and (10.27) one only needs the roots of the cubic equation $1 + S^{(1)}s + S^{(2)}s^2 + S^{(3)}s^3$ and to apply the residue theorem. This latter method is the one employed in [99]

As for the structure function, application of (4.17) and (10.4) yields the explicit expression
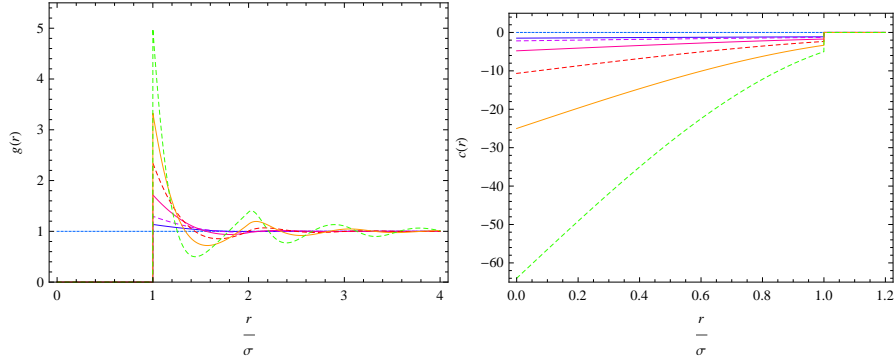
Fig. 10.1 Radial distribution function (left panel) and direct correlation function (right panel) of a three-dimensional hard-sphere fluid, as obtained from the Percus–Yevick approximation. at several values of the packing fraction $\eta \equiv (\pi/6)n\sigma^3 = 0.05, 0.1, 0.2, 0.3, 0.4$, and 0.5, in increasing order of complexity.

$$
\frac{1}{S(k)} = 1 + \frac{72\eta^2(2+\eta)^2}{(1-\eta)^4}k^{-4} + \frac{288\eta^2(1+2\eta)^2}{(1-\eta)^4}k^{-6} - \cos k\left[\frac{12\eta(2+\eta)}{(1-\eta)^2}k^{-2}\right.
$$
$$
\left. + \frac{72\eta^2(2-4\eta-7\eta^2)}{(1-\eta)^4}k^{-4} + \frac{288\eta^2(1+2\eta)^2}{(1-\eta)^4}k^{-6}\right]
$$
$$
+ \sin k\left[\frac{24\eta(1-5\eta-5\eta^2)}{(1-\eta)^3}k^{-3} - \frac{288\eta^2(1+2\eta)^2}{(1-\eta)^4}k^{-5}\right]. \qquad (10.30)
$$

To complete the description of the structural properties stemming from the approximation (10.27), let us consider the direct correlation function. Its Fourier transform can be obtained from $\widetilde{h}(k)$ via the Ornstein–Zernike relation (8.2). The inverse Fourier transform can be performed analytically with the result

$$
c(r) = \begin{cases} -\frac{(1+2\eta)^2}{(1-\eta)^4} + \frac{6\eta(1+\eta/2)^2}{(1-\eta)^4}r - \frac{\eta(1+2\eta)^2}{2(1-\eta)^4}r^3, & r < 1, \\ 0, & r > 1. \end{cases} \qquad (10.31)
$$

We observe that $c(r) = 0$ for $r > 1$. But this is the *signature* of the Percus–Yevick approximation for hard spheres [see (10.2)]. This shows that the *simplest* realization (10.27) of the rational-function approximation (10.26) turns out to coincide with the exact Percus–Yevick solution.

Figure 10.1 displays the Percus–Yevick functions $g(r)$ and $c(r)$ at several densities. The corresponding structure factor curves were plotted in Fig. 4.3.

10.3 Equation of State

Once $G(s)$ is fully determined, one can obtain the equation of state. As expected, the result depends on the thermodynamic route employed. Let us start with the virial route. According to (9.36), the virial route in the three-dimensional case is

$$Z^{(v)} = 1 + 4\eta g(1^+) . \tag{10.32}$$

The contact value is obtained from (10.19) as

$$g(1^+) = -\frac{1}{12\eta} \frac{L^{(1)}}{S^{(3)}} = \frac{1+\eta/2}{(1-\eta)^2} . \tag{10.33}$$

Thus,

$$\boxed{Z_{PY}^{(v)} = \frac{1+2\eta+3\eta^2}{(1-\eta)^2}} . \tag{10.34}$$

In the case of the compressibility route, (10.22) shows that we need $H^{(1)}$. This quantity is evaluated from the coefficient of s^6 in the Taylor expansion of $e^s/F(s)$, as shown in (10.24). The result is

$$H^{(1)} = \frac{8-2\eta+4\eta^2-\eta^3}{24(1+2\eta)^2} . \tag{10.35}$$

Insertion into (10.22) yields

$$\boxed{\chi_{PY} = \frac{(1-\eta)^4}{(1+2\eta)^2}} . \tag{10.36}$$

The associated compressibility factor is obtained upon integration as

$$\boxed{Z_{PY}^{(c)} = \frac{1}{\eta} \int_0^\eta \frac{d\eta'}{\chi_{PY}(\eta')} = \frac{1+\eta+\eta^2}{(1-\eta)^3}} . \tag{10.37}$$

Finally, we consider the chemical-potential equation of state. In the three-dimensional one-component case, (5.42) gives

$$\beta\mu^{ex} = -\ln(1-\eta) + 24\eta \int_{\frac{1}{2}}^1 d\sigma_{01} \sigma_{01}^2 g_{01}(\sigma_{01}^+) . \tag{10.38}$$

We see that the contact value (10.33) is not enough to compute μ^{ex}. We need to "borrow" the solute-solvent contact value $g_{01}(\sigma_{01}^+)$ from the Percus–Yevick solution for mixtures [73]:

$$g_{01}(\sigma_{01}^+) = \frac{1}{1-\eta} + \frac{3}{2} \frac{\eta}{(1-\eta)^2} \left(2 - \frac{1}{\sigma_{01}}\right) . \tag{10.39}$$

Table 10.1 First eleven (reduced) virial coefficients b_k as obtained exactly and from several equations of state related to the Percus–Yevick theory.

k	exact	$Z_{\mathrm{PY}}^{(v)}$	$Z_{\mathrm{PY}}^{(c)}$	$Z_{\mathrm{PY}}^{(\mu)}$	Z_{CS}	$Z^{(\mu c,1)}$	$Z^{(\mu c,2)}$
2	4	4	4	4	4	4	4
3	10	10	10	10	10	10	10
4	$18.36476\cdots$	16	19	$\frac{67}{4}=16.75$	18	$\frac{181}{10}=18.1$	$\frac{145}{8}=18.125$
5	$28.2245(3)$	22	31	$\frac{119}{5}=23.8$	28	$\frac{703}{25}=28.12$	$\frac{141}{5}=28.2$
6	$39.8151(9)$	28	46	31	40	40	$\frac{241}{6}\simeq40.2$
7	$53.344(4)$	34	64	$\frac{268}{7}\simeq38.3$	54	$\frac{376}{7}\simeq53.7$	54
8	$68.54(2)$	40	85	$\frac{365}{8}=45.6$	70	$\frac{277}{4}=69.25$	$\frac{1115}{16}\simeq69.7$
9	$85.81(9)$	46	109	53	88	$\frac{433}{5}=86.6$	$\frac{785}{9}\simeq87.2$
10	$105.8(4)$	52	136	$\frac{302}{5}=60.4$	108	$\frac{2644}{25}=105.76$	$\frac{533}{5}=106.6$
11	$128(5)$	58	166	$\frac{746}{11}\simeq67.8$	130	$\frac{1394}{11}\simeq126.7$	$\frac{1406}{11}\simeq127.8$

This expression is exact if $\sigma_{01}=\frac{1}{2}$ [30] and reduces to (10.33) if $\sigma_{01}=1$. Performing the integration in (10.38) one finds

$$\beta\mu_{\mathrm{PY}}^{\mathrm{ex}} = -\ln(1-\eta)+\eta\frac{7+\eta/2}{(1-\eta)^2}. \tag{10.40}$$

The excess free energy F^{ex} consistent with (10.40) is obtained taking into account the thermodynamic relation (2.9), i.e., $\mu^{\mathrm{ex}}=\partial(F^{\mathrm{ex}}/V)/\partial n$, as

$$\frac{\beta F_{\mathrm{PY}}^{\mathrm{ex}}}{N} = \frac{1}{\eta}\int_0^\eta \mathrm{d}\eta'\,\beta\mu_{\mathrm{PY}}^{\mathrm{ex}}(\eta') = \frac{9-\eta}{\eta}\ln(1-\eta)+\frac{3}{2}\frac{6-\eta}{1-\eta}. \tag{10.41}$$

Then, the equation of state is derived from the thermodynamic relation (2.9), i.e., $Z=1+n\partial(\beta F^{\mathrm{ex}}/N)/\partial n$. The result is

$$Z_{\mathrm{PY}}^{(\mu)} = -9\frac{\ln(1-\eta)}{\eta}-8\frac{1-31\eta/16}{(1-\eta)^2}. \tag{10.42}$$

Surprisingly, while the virial and compressibility equations of state (10.34) and (10.37), respectively, are known since 1963 [71], the chemical-potential equation of state (10.42) has remained hidden until recently [30].

The reduced virial coefficients b_k [see (7.89)] predicted by the three equations of state (10.34), (10.37), and (10.42) are

$$b_k^{(\mathrm{PY},v)} = 2(3k-4)\,, \quad b_k^{(\mathrm{PY},c)} = \frac{3k^2-3k+2}{2}\,, \quad b_k^{(\mathrm{PY},\mu)} = \frac{15k^2-31k+18}{2k}\,. \tag{10.43}$$

Those virial coefficients are compared with the exact values [51, 53, 54] in Table 10.1. We observe that (10.37) overestimates the known coefficients, while (10.34)

Fig. 10.2 Plot of $Z_{CS}(\eta) - Z_{MD}(\eta)$ (circles), $Z^{(\mu c,1)}(\eta) - Z_{MD}(\eta)$ (triangles), and $Z^{(\mu c,2)}(\eta) - Z_{MD}(\eta)$ (squares).
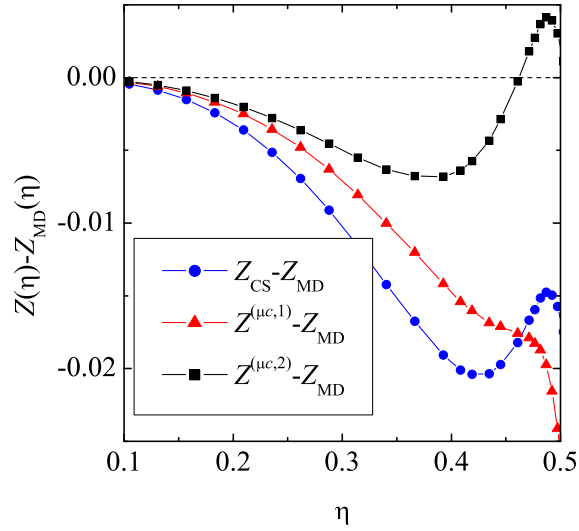
and (10.42) underestimate them, the chemical-potential route being slightly more accurate than the virial one.

Interestingly, the Carnahan–Starling equation of state [see (7.95) and (7.96)] can be recovered as an *interpolation* between the Percus–Yevick virial and compressibility equations:

$$Z_{CS} = \frac{1}{3}Z_{PY}^{(v)} + \frac{2}{3}Z_{PY}^{(c)} . \tag{10.44}$$

As shown by Fig. 7.9, Z_{CS} is an excellent equation of state. On the other hand, since $Z_{PY}^{(\mu)}$ is more reliable than $Z_{PY}^{(v)}$, one may wonder whether a similar interpolation formula, this time between $Z_{PY}^{(\mu)}$ and $Z_{PY}^{(c)}$, i.e.,

$$Z^{(\mu c)} = \lambda Z_{PY}^{(\mu)} + (1 - \lambda)Z_{PY}^{(c)} , \tag{10.45}$$

might be even more accurate. From an analysis of the virial coefficients one can check that the optimal value of the interpolation parameter is $\lambda \approx 0.4$. In particular, the two choices

$$\lambda = \frac{2}{5} \Rightarrow Z^{(\mu c,1)} , \quad \lambda = \frac{7}{18} \Rightarrow Z^{(\mu c,2)} \tag{10.46}$$

are analyzed in Table 10.1 at the level of the virial coefficients, where

$$b_k^{(\mu c,1)} = \frac{9k^3 + 21k^2 - 56k + 36}{10k} , \quad b_k^{(\mu c,2)} = \frac{11k^3 + 24k^2 - 65k + 42}{12k} . \tag{10.47}$$

A better performance than that of the Carnahan–Starling coefficients is clearly observed (except in the cases of b_6 and b_7).

The good quality of $Z^{(\mu c,1)}$ and $Z^{(\mu c,2)}$, even better than that of Z_{CS}, is confirmed by Fig. 10.2, where the deviations of those three compressibility factors from molec-

ular dynamics simulation values (Z_{MD}) [64] are plotted as functions of the packing fraction.

It is worth mentioning that (10.33), (10.34), (10.36), (10.37), (10.40), (10.41), and (10.42) are extended to additive hard-sphere mixtures as [31, 73]

$$g_{\alpha\gamma}(\sigma_{\alpha\gamma}^+) = \frac{1}{1-\eta} + \frac{3}{2}\frac{\eta}{(1-\eta)^2}\frac{\sigma_\alpha\sigma_\gamma}{\sigma_{\alpha\gamma}}\frac{M_2}{M_3} , \tag{10.48}$$

$$Z_{\mathrm{PY}}^{(v)} = \frac{1}{1-\eta} + \frac{3\eta}{(1-\eta)^2}\frac{M_1M_2}{M_3} + \frac{3\eta^2}{(1-\eta)^2}\frac{M_2^3}{M_3^2} , \tag{10.49}$$

$$\chi_{\mathrm{PY}}^{-1} = \frac{1}{(1-\eta)^2} + \frac{6\eta}{(1-\eta)^3}\frac{M_1M_2}{M_3} + \frac{9\eta^2}{(1-\eta)^4}\frac{M_2^3}{M_3^2} , \tag{10.50}$$

$$Z_{\mathrm{PY}}^{(c)} = \frac{1}{1-\eta} + \frac{3\eta}{(1-\eta)^2}\frac{M_1M_2}{M_3} + \frac{3\eta^2}{(1-\eta)^3}\frac{M_2^3}{M_3^2} , \tag{10.51}$$

$$\beta\mu_{\mathrm{PY},v}^{\mathrm{ex}} = -\ln(1-\eta) + \frac{3\eta}{1-\eta}\frac{M_2}{M_3}\sigma_v + \frac{3\eta}{1-\eta}\left(\frac{M_1M_2}{M_3} + \frac{3}{2}\frac{\eta}{1-\eta}\frac{M_2^3}{M_3^2}\right)\frac{\sigma_v^2}{M_2}$$
$$+ \frac{\eta}{1-\eta}\left(1 + 3\frac{\eta}{1-\eta}\frac{M_1M_2}{M_3}\right)\frac{\sigma_v^3}{M_3} , \tag{10.52}$$

$$\frac{\beta F_{\mathrm{PY}}^{\mathrm{ex}}}{N} = -\ln(1-\eta) + \frac{3\eta}{1-\eta}\frac{M_1M_2}{M_3} + \frac{3\eta^2}{2(1-\eta)^2}\frac{M_2^3}{M_3^2}$$
$$+ \frac{3M_2^3}{2M_3^2}\left[\frac{6-9\eta+2\eta^2}{(1-\eta)^2} + 6\frac{\ln(1-\eta)}{\eta}\right] , \tag{10.53}$$

$$Z_{\mathrm{PY}}^{(\mu)} = \frac{1}{1-\eta} + \frac{3\eta}{(1-\eta)^2}\frac{M_1M_2}{M_3} + \frac{3\eta^2}{(1-\eta)^3}\frac{M_2^3}{M_3^2} - \frac{9M_2^3}{M_3^2}\left[\frac{1-\frac{3}{2}\eta}{(1-\eta)^2} + \frac{\ln(1-\eta)}{\eta}\right] , \tag{10.54}$$

where

$$M_q \equiv \sum_\alpha x_\alpha\sigma_\alpha^q . \tag{10.55}$$

10.4 Beyond the Percus–Yevick Solution

Once we have obtained the exact solution of the Percus–Yevick integral equation for hard spheres as the simplest application of the rational-function approximation methodology, let us go beyond it either by improving the approximation or by considering other interaction models.

10.4.1 Next-Order Approximation for Hard-Sphere Fluids

In the spirit of the rational-function approximation (10.26), the next-order approximation is obtained with $k = 2$, i.e.,

$$F(s) = -\frac{1}{12\eta} \frac{1 + L^{(1)}s + L^{(2)}s^2}{1 + S^{(1)}s + S^{(2)}s^2 + S^{(3)}s^3 + S^{(4)}s^4} \ . \tag{10.56}$$

From the exact series expansion (10.25) one can obtain

$$L^{(1)} = L^{(1)}_{PY} + \frac{12\eta}{1 + 2\eta} \left[\frac{1}{2}L^{(2)} - S^{(4)} \right] , \tag{10.57}$$

$$S^{(1)} = S^{(1)}_{PY} + \frac{12\eta}{1 + 2\eta} \left[\frac{1}{2}L^{(2)} - S^{(4)} \right] , \tag{10.58}$$

$$S^{(2)} = S^{(2)}_{PY} + \frac{12\eta}{1 + 2\eta} \left[\frac{1 - 4\eta}{12\eta}L^{(2)} + S^{(4)} \right] , \tag{10.59}$$

$$S^{(3)} = S^{(3)}_{PY} - \frac{12\eta}{1 + 2\eta} \left[\frac{1 - \eta}{12\eta}L^{(2)} + \frac{1}{2}S^{(4)} \right] , \tag{10.60}$$

where $L^{(1)}_{PY}$, $S^{(1)}_{PY}$, $S^{(2)}_{PY}$, and $S^{(3)}_{PY}$ are given by (10.28) and (10.29).

So far, the two coefficients $L^{(2)}$ and $S^{(4)}$ remain free. They can be fixed by imposing any desired contact value $g(1^+)$ (or compressibility factor Z) and the corresponding consistent isothermal susceptibility $\chi = [\partial(\eta Z)/\partial\eta]^{-1}$. First, the exact condition (10.19) fixes the ratio $L^{(2)}/S^{(4)}$, so that

$$L^{(2)} = -3(Z - 1)S^{(4)} \ . \tag{10.61}$$

Next, the expansion (10.24) allows us to identify $H^{(1)}$ and, by means of (10.22), relate χ, $L^{(2)}$, and $S^{(4)}$. Using (10.61), one gets a quadratic equation for $S^{(4)}$ [95], whose physical solution is

$$S^{(4)} = \frac{1 - \eta}{36\eta(Z - \frac{1}{3})} \left[1 - \sqrt{1 + \frac{Z - \frac{1}{3}}{Z - Z^{(v)}_{PY}}\left(\frac{\chi}{\chi_{PY}} - 1 \right)} \right] , \tag{10.62}$$

where $Z^{(v)}_{PY}$ and χ_{PY} are given by (10.34) and (10.36), respectively.

Figure 10.3 compares computer simulations results of $g(r)$ at $\eta = 0.471$ [64] with the predictions obtained from the Percus–Yevick solution (10.27) and from the next-order rational-function approximation (10.56). In the latter, Z and χ have been chosen as given by the Carnahan–Starling equation of state [see (7.96) and (7.97)]. We observe that both theories describe quite well the behavior of $g(r)$ but the Percus–Yevick approximation underestimates the contact value and then decays by crossing the simulation data. Both features are satisfactorily corrected by the rational-function approximation.
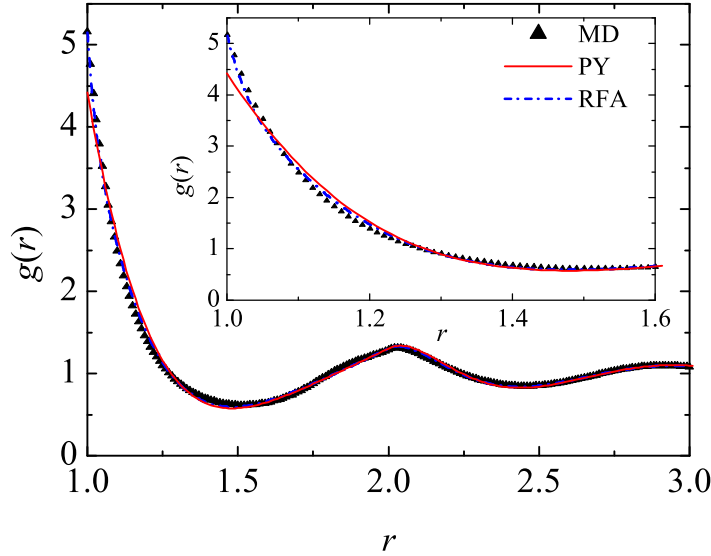
Fig. 10.3 Radial distribution function $g(r)$ of a hard-sphere fluid at a packing fraction $\eta = 0.471$ as obtained by molecular dynamics simulations [64] and from the Percus–Yevick and rational-function approximation approaches.

It is interesting to note that the rational-function approximation (10.56) coincides with the solution of the so-called generalized mean-spherical approximation (GMSA) [86, 100, 101], where the direct correlation function $c(r)$ outside the hard core ($r > 1$), which vanishes in the Percus–Yevick theory, is assumed to be given by a Yukawa form. The rational-function approximation method, however, is mathematically much more economical and open to applications to other systems.

10.5 Non-Hard-Sphere Systems

The rational-function approximation methodology has been applied to systems different from one-component three-dimensional hard spheres. Those systems can be classified into two categories: (i) systems amenable to an exact solution of the Percus–Yevick equation and (ii) systems non-amenable to an exact solution of the Percus–Yevick equation. The first class includes sticky hard spheres (see Fig. 6.3, right panel) [39], additive hard-sphere mixtures [73], additive sticky-hard-sphere mixtures [74, 75], and hard hyperspheres [76, 77]. In that class of systems, the rational-function approximation method recovers the Percus–Yevick solution as the *simplest* possible approach, just as in the hard-sphere case [see (10.27)]. The next-order approach allows one to make contact with empirical equations of state,

thus improving the predictions. The interested reader can consult the references [78, 79, 96, 102, 103, 104, 105, 106, 107] for further details.

The application of the rational-function approximation to systems of the second class includes the penetrable-sphere model (see Fig. 9.3, right panel) [108, 109], the penetrable-square-well model [110], the square-well potential (see Fig. 6.3, left panel) [111, 112, 113], the square-shoulder potential (see Fig. 9.3, left panel) [114], piece-wise constant potentials with more than one step [115, 116], nonadditive hard-sphere mixtures [117, 118], and Janus particles with constrained orientations [119]. In those cases, the *simplest* rational-function approximation is already quite accurate, generally improving on the (numerical) solution of the Percus–Yevick equation.

11 Concluding Remark

These lecture notes are already too long, so let this author conclude just by saying that he will feel fully satisfied if the notes are useful to some of the students who attended the 5th Warsaw School of Statistical Physics, to some of the readers who have had the patience to read them, or to some instructors who might find something profitable for their own courses.

References

1. A. Mulero (ed.), *Theory and Simulation of Hard-Sphere Fluids and Related Systems* (Springer-Verlag, Berlin, 2008), *Lectures Notes in Physics*, vol. 753
2. J.A. Barker, D. Henderson, Rev. Mod. Phys. **48**, 587 (1976)
3. J.R. Solana, *Perturbation Theories for the Thermodynamic Properties of Fluids and Solids* (CRC Press, Boca Raton, 2013)
4. C.N. Likos, Phys. Rep. **348**, 267 (2001)
5. P.N. Pusey, E. Zaccarelli, C. Valeriani, E. Sanz, W.C.K. Poon, M.E. Cates, Phil. Trans. R. Soc. A **367**, 4993 (2009)
6. R. Evans, in *Fundamentals of Inhomogeneous Fluids*, ed. by D. Henderson (Dekker, New York, 1992)
7. P. Tarazona, J.A. Cuesta, Y. Martínez-Ratón, in *Theory and Simulation of Hard-Sphere Fluids and Related Systems*, *Lectures Notes in Physics*, vol. 753, ed. by A. Mulero (Springer-Verlag, Berlin, 2008), *Lectures Notes in Physics*, vol. 753, pp. 247–341
8. R. Evans, in *3rd Warsaw School of Statistical Physics*, ed. by B. Cichocki, M. Napiórkowski, J. Piasecki (Warsaw University Press, Warsaw, 2010), pp. 43–85

9. H. Löwen, in *3rd Warsaw School of Statistical Physics*, ed. by B. Cichocki, M. Napiórkowski, J. Piasecki (Warsaw University Press, Warsaw, 2010), pp. 87–121
10. J.F. Lutsko, in *Advances in Chemical Physics*, vol. 144, ed. by S.A. Rice (John Wiley & Sons, Inc., 2010), vol. 144, pp. 1–92
11. R. Roth, J. Phys.: Cond. Matt. **22**(6), 063102 (2010)
12. G. Parisi, Z. Zamponi, Rev. Mo **82**, 789 (2010)
13. L. Berthier, G. Biroli, Rev. Mod. Phys. **3**, 587 (2011)
14. J. Kurchan, in *4th Warsaw School of Statistical Physics*, ed. by B. Cichocki, M. Napiórkowski, J. Piasecki (Warsaw University Press, Warsaw, 2012), pp. 131–167
15. M.W. Zemansky, *Heat and Thermodynamics* (McGraw-Hill, New York, 1981)
16. H.B. Callen, *Thermodynamics and an Introduction to Thermostatistics* (Wiley, New York, 1985)
17. H. Goldstein, J. Safko, C.P. Poole, *Classical Mechanics* (Pearson Education, 2013)
18. R. Balescu, *Equilibrium and Nonequilibrium Statistical Mechanics* (Wiley, New York, 1974)
19. L.E. Reichl, *A Modern Course in Statistical Physics*, 1st edn. (University of Texas Press, Austin, 1980)
20. C.E. Shannon, W. Weaver, *The Mathematical Theory of Communication* (University of Illinois Press, 1971)
21. A. Ben-Naim, *A Farewell to Entropy: Statistical Thermodynamics Based on Information* (World Scientific, Singapore, 2008)
22. J.P. Hansen, I.R. McDonald, *Theory of Simple Liquids* (Academic Press, London, 2006)
23. M.P. Allen, D.J. Tildesley, *Computer Simulation of Liquids* (Clarendon Press, Oxford, 1987)
24. D. Frenkel and B. Smit, *Understanding Molecular Simulation: From Algorithms to Applications*, 2nd edn. (Academic Press, San Diego, 2002)
25. S. Labík, A. Malijevský, Mol. Phys. **53**, 381 (1984)
26. L. Onsager, Chem. Rev. **13**, 73 (1933)
27. T.L. Hill, *Statistical Mechanics* (McGraw-Hill, New York, 1956)
28. H. Reiss, H.L. Frisch, J.L. Lebowitz, J. Chem. Phys. **31**, 369 (1959)
29. M. Mandell, H. Reiss, J. Stat. Phys. **13**, 113 (1975)
30. A. Santos, Phys. Rev. Lett. **109**, 120601 (2012)
31. A. Santos, R.D. Rohrmann, Phys. Rev. E **87**, 052138 (2013)
32. A.B. Bathia, D.E. Thornton, Phys. Rev. B **8**, 3004 (1970)
33. J.S. Rowlinson, F. Swinton, *Liquids and Liquid Mixtures* (Butterworth, London, 1982)
34. Z.W. Salsburg, R.W. Zwanzig, J.G. Kirkwood, J. Chem. Phys. **21**, 1098 (1953)
35. J.L. Lebowitz, D. Zomick, J. Chem. Phys. **54**, 3335 (1971)
36. M. Heying, D.S. Corti, Fluid Phase Equil. **220**, 85 (2004)
37. A. Santos, Phys. Rev. E **76**, 062201 (2007)
38. A. Ben-Naim, A. Santos, J. Chem. Phys. **131**, 164512 (2009)
39. R.J. Baxter, J. Chem. Phys. **49**, 2770 (1968)
40. See also A. Santos, "Radial Distribution Function for Sticky Hard Rods", `http://demonstrations.wolfram.com/RadialDistributionFunctionForStickyHardRods/`, Wolfram Demonstrations Project
41. E.G.D. Cohen. Einstein and Boltzmann: Determinism and Probability or The Virial Expansion Revisited. `http://arxiv.org/abs/1302.2084` (2013)
42. M. Baus, J.L. Colot, Phys. Rev. A **36**, 3912 (1987)
43. M. Abramowitz, I.A. Stegun (eds.), *Handbook of Mathematical Functions* (Dover, New York, 1972)
44. B.R.A. Nijboer, L. van Hove, Phys. Rev. **85**, 777 (1952)
45. F.H. Ree, N. Keeler, S.L. McCarthy, J. Chem. Phys. **44**, 307 (1966)
46. A. Santos, A. Malijevský, Phys. Rev. E **75**, 021201 (2007)
47. See also A. Santos, "Second Virial Coefficients for the Lennard-Jones ($2n$-n) Potential", `http://demonstrations.wolfram.com/SecondVirialCoefficientsForTheLennardJones2nNPotential/`, Wolfram Demonstrations Project
48. N. Clisby, B. McCoy, J. Stat. Phys. **114**, 1361 (2004)
49. I. Lyberg, J. Stat. Phys. **119**, 747 (2005)

50. N. Clisby, B.M. McCoy, J. Stat. Phys. **114**, 1343 (2004)
51. S. Labík, J. Kolafa, A. Malijevský, Phys. Rev. E **71**, 021105 (2005)
52. N. Clisby, B.M. McCoy, Pramana **64**, 775 (2005)
53. N. Clisby, B.M. McCoy, J. Stat. Phys. **122**, 15 (2006)
54. R.J. Wheatley, Phys. Rev. Lett. **110**, 200601 (2013)
55. M. Luban, A. Baram, J. Chem. Phys. **76**, 3233 (1982)
56. R.D. Rohrmann, M. Robles, M. López de Haro, A. Santos, J. Chem. Phys. **129**, 014510 (2008)
57. A. Mulero, C.A. Galán, M.I. Parra, F. Cuadros, in *Theory and Simulation of Hard-Sphere Fluids and Related Systems*, *Lectures Notes in Physics*, vol. 753, ed. by A. Mulero (Springer-Verlag, Berlin, 2008), *Lectures Notes in Physics*, vol. 753, pp. 37–109
58. C.M. Bender, S.A. Orszag, *Advanced Mathematical Methods for Scientists and Engineers* (McGraw-Hill, Auckland, 1987)
59. D. Henderson, Mol. Phys. **30**, 971 (1975)
60. A. Santos, M. López de Haro, S.B. Yuste, J. Chem. Phys. **103**, 4622 (1995)
61. M. López de Haro, A. Santos, S.B. Yuste, Eur. J. Phys. **19**, 281 (1998)
62. J.J. Erpenbeck, M.J. Luban, Phys. Rev. A **32**, 2920 (1985)
63. N.F. Carnahan, K.E. Starling, J. Chem. Phys. **51**, 635 (1969)
64. J. Kolafa, S. Labík, A. Malijevský, Phys. Chem. Chem. Phys. **6**, 2335 (2004). See also `http://www.vscht.cz/fch/software/hsmd/` for molecular dynamics results of $g(r)$
65. L.A. Fernández, V. Martín-Mayor, B. Seoane, P. Verrocchio, Phys. Rev. Lett. **108**, 165701 (2012)
66. T. Morita, Prog. Theor. Phys. **20**, 920 (1958)
67. J.M.J. van Leeuwen, J. Groeneveld, J. de Boer, Physica **25**, 792 (1959)
68. J.K. Percus, G.J. Yevick, Phys. Rev. **110**, 1 (1958)
69. T. Morita, Prog. Theor. Phys. **23**, 829 (1960)
70. M.S. Wertheim, Phys. Rev. Lett. **10**, 321 (1963)
71. E. Thiele, J. Chem. Phys. **39**, 474 (1963)
72. M.S. Wertheim, J. Math. Phys. **5**, 643 (1964)
73. J.L. Lebowitz, Phys. Rev. **133**, A895 (1964)
74. J.W. Perram, E.R. Smith, Chem. Phys. Lett. **35**, 138 (1975)
75. B. Barboy, Chem. Phys. **11**, 357 (1975)
76. C. Freasier, D.J. Isbister, Mol. Phys. **42**, 927 (1981)
77. E. Leutheusser, Physica A **127**, 667 (1984)
78. R.D. Rohrmann, A. Santos, Phys. Rev. E **76**, 051202 (2007)
79. R.D. Rohrmann, A. Santos, Phys. Rev. E **83**, 011201 (2011)
80. L. Verlet, Mol. Phys. **41**, 183 (1980)
81. G.A. Martynov, G.N. Sarkisov, Mol. Phys. **49**, 1495 (1983)
82. F.J. Rogers, D.A. Young, Phys. Rev. A **30**, 999 (1984)
83. P. Ballone, G. Pastore, G. Galli, D. Gazzillo, Mol. Phys. **59**, 275 (1986)
84. L. Acedo, A. Santos, Phys. Lett. A **323**, 427 (2004)
85. B.M. Mladek, G. Kahl, M. Neuman, J. Chem. Phys. **124**, 064503 (2006)
86. E. Waisman, Mol. Phys. **25**, 45 (1973)
87. Y. Tang, J. Chem. Phys. **118**, 4140 (2003)
88. A. Santos, G. Manzano, J. Chem. Phys. **132**, 144508 (2010)
89. A. Santos, R. Fantoni, A. Giacometti, J. Chem. Phys. **131**, 181105 (2009)
90. A. Santos, J. Chem. Phys. **126**, 116101 (2007)
91. Z. Yan, S.V. Buldyrev, N. Giovambattista, H.E. Stanley, Phys. Rev. Lett. **95**, 130604 (2005)
92. A. Santos, J. Chem. Phys. **123**, 104102 (2005)
93. A. Santos, Mol. Phys. **104**, 3411 (2006)
94. S.B. Yuste, A. Santos, Phys. Rev. A **43**, 5418 (1991)
95. S.B. Yuste, M. López de Haro, A. Santos, Phys. Rev. E **53**, 4820 (1996)

96. M. López de Haro, S.B. Yuste, A. Santos, in *Theory and Simulation of Hard-Sphere Fluids and Related Systems*, *Lectures Notes in Physics*, vol. 753, ed. by A. Mulero (Springer-Verlag, Berlin, 2008), *Lectures Notes in Physics*, vol. 753, pp. 183–245

97. L. Carlitz, Duke Math. J. **24**, 151 (1957)

98. J. Abate, W. Whitt, Queueing Systems **10**, 5 (1992)

99. A. Santos, "Radial Distribution Function for Hard Spheres", `http://demonstrations.wolfram.com/RadialDistributionFunctionForHardSpheres/`, Wolfram Demonstrations Project

100. D. Henderson, L. Blum, Mol. Phys. **32**, 1627 (1976)

101. J.S. Høye, L. Blum, J. Stat. Phys. **16**, 399 (1977)

102. S.B. Yuste, A. Santos, M. López de Haro, J. Chem. Phys. **108**, 3683 (1998)

103. A. Santos, S.B. Yuste, M. López de Haro, J. Chem. Phys. **109**, 6814 (1998)

104. A. Malijevský, A. Malijevský, S.B. Yuste, A. Santos, M. López de Haro, Phy. Rev. E **66**, 061203 (2002)

105. A. Malijevský, S.B. Yuste, A. Santos, M. López de Haro, Phys. Rev. E **75**, 061201 (2007)

106. S.B. Yuste, A. Santos, M. López de Haro, J. Chem. Phys. **128**, 134507 (2008)

107. R.D. Rohrmann, A. Santos, Phys. Rev. E **84**, 041203 (2011)

108. A. Malijevský, A. Santos, J. Chem. Phys. **124**, 074508 (2006)

109. A. Malijevský, S.B. Yuste, A. Santos, Phy. Rev. E **76**, 021504 (2007)

110. R. Fantoni, A. Giacometti, A. Malijevský, A. Santos, J. Chem. Phys. **131**, 124106 (2009)

111. S.B. Yuste, A. Santos, J. Chem. Phys. **101**, 2355 (1994)

112. L. Acedo, A. Santos, J. Chem. Phys. **115**, 2805 (2001)

113. J. Largo, J.R. Solana, S.B. Yuste, A. Santos, J. Chem. Phys. **122**, 084510 (2005)

114. S.B. Yuste, A. Santos, M. López de Haro, Mol. Phys. **109**, 987 (2011)

115. A. Santos, S.B. Yuste, M. López de Haro, Condens. Matter Phys. **15**, 23602 (2012)

116. A. Santos, S.B. Yuste, M. López de Haro, M. Bárcenas, P. Orea, J. Chem. Phys. **139**, 074503 (2013)

117. R. Fantoni and A. Santos, Phys. Rev. E **84**, 041201 (2011). Note that in Eq. (2.12) the hats on the partial correlation functions should be replaced by tildes.

118. R. Fantoni, A. Santos, Phys. Rev. E **87**, 042102 (2013)

119. M.A.G. Maestre, R. Fantoni, A. Giacometti, A. Santos, J. Chem. Phys. **138**, 094904 (2013)